Effects of Injection Pipe Orientation on Mixing Behavior in Contributing to Thermal Fatigue in a T-junction of a Pipe

A thesis presented to the:

Department of NUCLEAR ENGINEERING

UNIVERSITY OF GHANA

By

Afia Boatemaa

Student ID: 10511749

BSc Kumasi, 2013

In partial fulfillment of the requirements for the degree of

MASTER OF PHILOSOPHY

in

NUCLEAR ENGINEERING

July, 2016

DECLARATION

This thesis is the result of research work undertaken by Afia Boatemaa in the Department of Nuclear Engineering, University of Ghana, under the supervision of Dr. Vincent Agbodemegbe and Dr. Seth Kofi Debrah.

Afia Boatemaa

Date:

Vincent Agbodemegbe, PhD.	**Seth Kofi Debrah, PhD.**
Date:	Date
(Principal Supervisor)	(Co-Supervisor)

ABSTRACT

The thesis dealt with the temperature fluctuation in a T-junction with two fluid streams of different temperature. This phenomenon is of crucial importance in many engineering applications such as Nuclear Power Plants, because temperature fluctuation leads to thermal fatigue and subsequently might result in failure of structural material. In mixing areas of a Nuclear Power Plant where piping structure is exposed to unavoidable temperature differences in a bid to maintain plant operational capacity, the effects of the temperature difference on the piping structure at the mixing junctions cannot be neglected. Temperature fluctuation is tightly coupled with flow turbulence, which has attracted extensive attention and been investigated worldwide since several decades. The main target of this thesis is the investigation of the temperature fluctuation with the emphasis on the effect of the injection pipe orientation on the temperature fluctuation. The computational fluid dynamics (CFD) approach was applied using STAR CCM+ code. Due to the limitation in computing efforts, the RANS method was selected instead of LES or DNS method. Four inclination angles were selected. The mixing intensity and the size of the effective mixing zone were investigated. Smaller inclination angle (both injection pipes are perpendicular to each other, in case of zero degree inclination angle) led in one side to a larger turbulence intensity or mixing intensity, and subsequently to larger temperature fluctuation and on the other side the mixing zone is reduced. The simulated temperature fields are employed as thermal boundary conditions in heat transfer analyses of a pipe wall.

The findings gives useful data for the design of devices where attention needs to be paid to thermal fatigue.

DEDICATION

To my family, especially my mum Catherine Cobbinah and Brothers; Jessie and Randy.

ACKNOWLEDGMENTS

Firstly, I would like to thank God for being my strength and guide in the writing of this thesis.

I would like to express my gratefulness to my supervisors Dr. Vincent Agbodemegbe and Dr. Seth Kofi Debrah of the Department of Nuclear Engineering for their support at various stages of my research project and in the writing of this thesis. I would like to thank them for their guidance and supports throughout this work.

I would like to acknowledge CD-adapco for providing the software license used in this project.

I would to take the opportunity to thank Professor J.J Fletcher for his encouragement and kind advices.

I would also like to thank everyone at the Department of Nuclear Engineering for their support and encouragement.

My sincere thanks to my friends Benjamin Decardi-Nelson and Joshua Ayodeji Abey, for their moral supports and sharing many experiences and thoughts with me and helping me face the challenges that lies behind this work.

Lastly, I would like to express my love and respect to my family for educating and encouraging me to pursue my interests.

TABLE OF CONTENTS

LIST OF TABLES

LIST OF FIGURES

LIST OF ABBREVIATIONS

BWR	Boiling Water Reactor
CFD	Computational Fluid Mechanics
DES	Direct Eddy Simulation
DNS	Direct Numerical Simulation
ECCSs	Emergency Core Cooling Systems
EVM	Eddy Viscosity Model
FEM	Finite Element Method
LES	Large Eddy Simulation
LMFBRs	Liquid metal fast breeder reactor
RANS	Reynolds Averaged Navier-Stokes Simulation
RMS	Root Mean Square
NLEVM	Non Linear Eddy Viscosity Model
NPP	Nuclear Power Plant
PISO	Pressure Implicit with Split Operator

PIV	Particle Image Velocimetry
PWR	Pressurized Water Reactor
RSTM	Reynolds Stress Transport Models
SAS	Scale Adaptive Simulation
SOC	Second Order Closure
TKE	Turbulence Kinetic Energy
NPP	Nuclear Power Plant
WALE	Wall Adaptive Local Eddy Viscosity
3D-CAD	3 Dimensional Computer Aided Design

NOMENCLATURE

$D_{1,}$ D_{cold}	Diameter of cold inlet	[m]
$D_{2,}$ D_{hot}	Diameter of hot inlet	[m]
v_b	Branch Fluid Velocity	[m/s]
v_m	Main Pipe Fluid Velocity	[m/s]
l_{te}	Thermal Equilibrium	[-]
l_{he}	Hydraulic Equilibrium	[-]
InCo	Inlet Cold	[-]
InHo	Inlet Hot	[-]
0.6 D_{cold}	0.6 x Diameter of cold inlet	[m]
1.6 D_{cold}	1.6 x Diameter of cold inlet	[m]
2.6 D_{cold}	2.6 x Diameter of cold inlet	[m]
3.5 D_{cold}	3.5 x Diameter of cold inlet	[m]
TI	Turbulent Intensity	[-]
T_{hot}	Temperature of hot water	[K]
T_{cold}	Temperature of cold water	[K]

Q1, Q_{hot}	Flow rate in branch pipe (hot water)	[l/s]
Q2, Q_{cold}	Flow rate in main pipe (cold water)	[l/s]
$\bar{p}$	Mean Component Pressure	[Pa]
p'	Fluctuating Component Pressure	[Pa]
S	modulus of mean rate of strain tensor	[-]
P_b	Buoyancy Effect	[-]
T^*	Dimensionless Temperature	[-]
T^*_{rms}	Root Mean Square Temperature	[-]
K	Thermal conductivity	[W/mK]
Cp	Specific heat capacity	[J/kgK]
A	Thermal expansion coefficient	[K^{-1}]
E	Young's modulus	[GPa]
N	Poisson's ratio	[-]

LIST OF GREEK SYMBOLS

$\boldsymbol{\rho}$	Density	[kg/m^3]
$\overline{u}_i$	Mean Component Velocity	[m/s]
$u_i^{'}$	Fluctuating Component Velocity	[m/s]
μ_t	Turbulent Viscosity	[Pa.s]
β	Coefficient of Thermal Expansion	[K^{-1}]
ε	Turbulence dissipation	[m^2/s^3]
k	Turbulence Kinetic Energy	[m^2/s^2]
ω	Specific Dissipation	[s^{-1}]

CHAPTER ONE

INTRODUCTION

Thermal fatigue phenomena is an issue of growing importance and several researches have been conducted worldwide to better understand the phenomenon and develop evaluation methods aimed at supporting informed decision making in Nuclear Power Plant (NPP) piping system design. When piping structure is exposed to unavoidable temperature differences in other to maintain plant conditions, the effects of the temperature difference on the piping structure at the mixing junctions cannot be neglected. In summary the consequences of the flow parameters on the piping structure can now be predicted with more confidence by accurate characterization of the flow parameters being studied.

1.1. Background to the Study

The basis of this study is the T-junction Benchmark which was initiated by OECD/NEA-Vattenfall, to test how significant parameters affecting high-cycle thermal fatigue in mixing T-junctions can be predicted by Computational Fluid Dynamics (CFD) codes. Interest in the subject first arose in the early 1980s (NEA/CSNI/R, 2011), but then gained significant attention following the 1998 incident in France at the Civaux-1 where several incidents of high-cycle fatigue mainly in T-junctions were observed (Shah, 1999; Jungclaus et al.,1998).

When hot and cold streams meet and mix in a junction, the mixing is often not complete and significant temperature fluctuations can be created close to the pipe walls (Jayaraju et al., 2011).

Cyclical thermal stresses can occur due to these temperature fluctuations near the pipe walls, which may induce fatigue cracking in the structure. Thermal fatigue problem in the1980's in context of Liquid-Metal Fast Breeder Reactors were initially studied when it was considered a significant problem due to the high thermal conductivity of the liquid-metal sodium coolant (NEA/CSNI/R, 2011). The upper core structure and the plenum region were areas of major concern.

The Civaux-1 failure and other related incidents showed that piping system T-junction connections are exposed to thermal fatigue that arises from low and high cycle temperature turbulences (Jhung, 2013). In service experiences showed that thermal fatigue cracks may occur arbitrarily in different locations, example; welds, elbows, base material, straight pipes subjected to diverse loading conditions. Cracks that occurs according to Jhung (2013) are normally attributed to temperature mixing effects and thermal stratification caused by the different mass flows in "run" and "branch" pipes at the T-junction connection.

Experiments on thermal mixing in T-junctions are being carried out in several countries including; Germany, Japan, France, Sweden and Switzerland (NEA/CSNI/R, 2011). In particular, experiments have been performed at the Älvkarleby Laboratory of Vattenfall Research and Development in Sweden since 2006, aimed at providing high quality validation data for CFD calculations (OECD/NEA-Vattenfall T-junction Benchmark).

The European Commission also funded a 3-year project “thermal fatigue evaluation of piping system Tee-connections” with the primary aim of advancing the accuracy and reliability of thermal fatigue load determination and to formulate research oriented approaches and methodologies in managing risks of thermal fatigue (Jhung, 2013).

Failure of materials in T-junction piping system has been associated with variation in flow rate of fluid occurring at different temperatures (Nakamura et al., 2015).This fluctuation in temperature causes deformation in the structural material which in turn causes changes in the boundary conditions of the fluid flow (Velusamy et al., 2006). To predict this phenomenon, models available in software application such as STAR-CCM+ (models for predicting phenomena relating to flow of fluid) are evaluated in the present research. The study adopted STAR-CCM+ Computational Fluid Dynamic (CFD) code version 10.04.011 to predict the effect of varying branch pipe angle of inclination on flow parameters that affect thermal fatigue.

1.2 Research Problem Statement

In an attempt to increase power in Nuclear Power Plant (NPP), higher operating temperatures are utilized. If a piping system is subjected to unavoidable temperature differences in a bid to maintain plant operational capacity conditions, the risk of fatigue cracking by temperature fluctuation is not negligible. At mixing junctions of NPP piping systems, there are possibilities of occurrence of high-cycle thermal fatigue caused by these

temperature fluctuations. Evaluation methods to determine flow and mixing characteristics (e.g. temperature fluctuations) leading to thermal fatigue are therefore important when plant are designed to prevent fatigue cracking.

1.3 Justification for the Study

Thermal fatigue is a major degradation mechanism that needs be considered in Nuclear Power Plant piping system. Thermal fatigue, vis-à-vis ageing and life-management of LWRs is of serious safety concern and hence ought to be investigated. Temperature fluctuation initiated by fluid mixing spreads throughout the pipe wall and generates thermal stress, the pipe cracking may be caused by thermal stress exceeding the fatigue limit.

Thus, it becomes necessary to investigate the development of thermal fatigue due to temperature distribution and methods used in the evaluation of temperature fluctuations contributing to thermal fatigue. The use of computer-based simulations helps to predict temperature fluctuations contributing to thermal fatigue downstream the mixing-junction. This study will therefore focus on determining the thermal and velocity distribution downstream the mixing -junction and the possible effects of the flow characteristics due to varying the angle of inclination of branch pipe to the main pipe.

1.4 Goal

This study is borne out of the fact that power plant design involves the incorporation of high level of safety measures due to operations at extremely high temperatures. Although

the effect of thermal fatigue is material specific, it is largely dependent on several other flow parameters such as the magnitude and propagation of temperature fluctuation in flow channels. Since there is the possibility of structural deformation due to temperature fluctuation, this study sought to characterise such deformation through knowledge of the temperature fluctuation and velocity fields downstream the mixing-junction.

1.4.1 Specific Objectives

The specific objectives of the study are to;

a) perform sensitivity analysis of turbulence models for the experimental results from the Vattenfall research using STAR-CCM+;

b) examine the mean temperature fluctuations recorded at various locations along the tube downstream the mixing-junction and comparative analysis of temperature fluctuation for varying angles of inclination of branch pipe to the mixing-junction domain;

c) determine the velocity fields downstream the mixing-junction and comparative analysis of velocity fields for varying angles of inclination of branch pipe to the mixing-junction domain;

d) ascertain the trends of other mean and turbulent flow parameters (turbulence intensity, pressure) downstream the mixing-junction and the effects of angle of inclination.

1.5 Turbulent Modelling Options

The transfer of heat, momentum and mass in most flows is influenced by turbulent motions and therefore influences the distribution of velocity and temperature over the flow field (Rodi, 1993). The selection of a suitable turbulent model depends on the specific problem since no turbulence model is suited for every case. Spalart-Allmaras model is a 1-equation model, which is used mainly for aerospace industrial application; while, k-omega and k-epsilon, (2-equation models) are semi analytic models. K-epsilon model is suitable for predicting far from the wall boundaries while k-omega model predicts well near wall boundaries, though it depends on y+. There is also the Menter's Shear Stress Transport (SST) model which is a combination of both, k-omega and k-epsilon models but requiring fine tuning is required. SST model used with good mesh at boundary and wall treatment usually works in most cases but again it is problem specific. It is possible to use suitable numerical procedures, by solving the flow equation with appropriate boundary conditions to simulate any turbulent flow.

1.6 Scope of the Study

This study is limited to the application of specific models in STAR-CCM+ to investigate the distribution of mean and turbulent flow fields of T-junction geometry. Comparative analysis of trends of these parameters was carried out at varying change in temperature between the hot and cold inlet of the T-junction geometry.

1.7 Structure of Thesis

The orientation to the research study has been explained in this chapter. The mechanisms of thermal fatigue and the computational methods applied in thermal fatigue analysis are discussed in chapter two. Chapter three then explains The methodology used in the research, presenting the most suitable approach to provide the best result that replicates the experimental data. The results are presented and discussed in Chapter four, based on that, a conclusion is established in the last chapter.

CHAPTER TWO

LITERATURE REVIEW

2.1 INTRODUCTION

Chapter two offers insights on what has been published on thermal fatigue mechanism in relation to nuclear reactor material as well as Computational Fluid Dynamic methods used in predicting the phenomenon by researchers in the field, which includes the current knowledge in thermal fatigue analysis, substantive findings, as well as theoretical and methodological contributions.

This section presents a review of literature on the mechanism of thermal fatigue, the characteristic flow parameters associated with the mechanism and its effects on T-junction pipes, as well as Computational Fluid Dynamic (CFD) methods used in predicting fatigue phenomenon in pipes. The main problem which is thermal effect and its frequency are reviewed. An overview of thermal fatigue problems in T-junction pipes and some recent techniques for predicting thermal fatigue in T-junction of piping systems are also reviewed.

2.2 Thermal Fatigue Failure Mechanism

Thermal loads and cracking failure mechanism at mixing zone of hot and cold fluids can be decomposed into elemental processes as indicated in Figure 2.1;

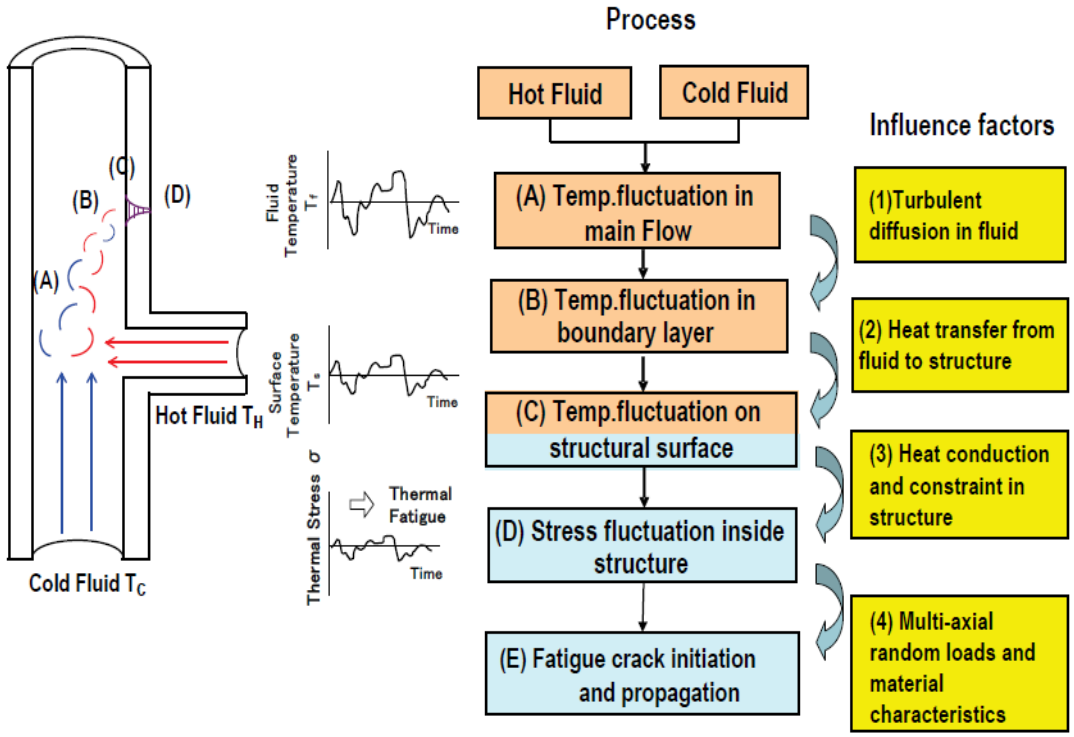

Figure 2.1: Thermal load and cracking mechanism at a mixing zone of hot and cold fluids (Nakamura et. al., 2015)

Mechanisms at mixing zones of hot and cold fluids shown in the Figure 2.4 as proposed by Nakamura et al. (2015) are described as follows;

A. Vortices generate temperature fluctuations in the main flow

B. Fluctuation propagates to the boundary layer of flow

C. The fluctuations in the layer is transferred to the structure surface

D. Fluctuations on the surface then propagate through the pipe wall by heat conduction and generates thermal stress by the constraint of pipe structure.

E. The recurrence of thermal stress instigates high cycle fatigue cracking.

2.3 Navier-Stokes Equation

The basis of Navier-Stokes equation is the conservation law of physical properties of fluid. Navier-Stokes equation is 3-dimensional partial differential equation (Sodja, 2007), it is nonlinear (rotational) and fully time dependent. Interactions between non-linear inertial terms and viscous terms in the Navier-Stokes equation account for the turbulent flow instabilities.

The four main components in solving CFD problems are: preprocessing which includes geometry and grid generation, setting up a physical model, which is; setting boundary names and types, defining the models in the continua and applying them to the regions, solving it (running the simulation) and post-processing the computed data.

2.4 Thermal Fatigue

Thermal fatigue has been a topic of great interest for many years and researchers have been working for decades with regards to understanding and solving fatigue problems related to several spheres of thermal hydraulics and reactor management.

Thermal fatigue is a phenomenon that occurs frequently in thermal hydraulics systems such as reheat systems, turbines, emergency core cooling systems (ECCS) of nuclear power plants (NPP) and as such ought to be studied to comprehend the mechanisms behind the phenomenon. The understanding of these phenomena and the development of evaluation methods of thermal fatigue are important from the viewpoint of design, operation and safety of the plants. It is an important factor in ageing management of nuclear power (Tipping, 1996). Thermal fatigue mechanisms need to be monitored to ensure safety and continuous operation of nuclear power systems (Saito & Sawada, 2002). Roos et al., (2006) considered thermal fatigue as an important safety issue in primary piping system of nuclear power plants. The degradation mechanism of thermal fatigue is induced by temperature fluctuations that result from mixing hot and cold flows. Ayhan & Sökmen (2013) suggested that these fluctuations occur when a fluid meeting at different temperatures arrives at the pipe wall before reaching thermal equilibrium.

2.4.1 Temperature Variation Induced Fatigue

Possible phenomena that can occur as a result of temperature fluctuations include; thermal stripping, thermal stratification, turbulent mixing, and thermal fatigue. Temperature fluctuations observed at interfaces between two non-isothermal components or mixing T-junction components in heat transport systems is referred to as thermal stripping (Velusamy et al., 2006). This suggests that heat is readily transferred to the material, thereby subjecting

it to a repetitive cycle of temperature fluctuations that could potentially lead to fatigue and crack initiation. Thermal fluctuation becomes prominent and is observed more frequently when the temperature increases and decreases. Such temperature differentials can produce stresses high enough to cause fatigue failure in pipes, thereby limiting its lifespan. Since materials function usefully at different temperatures, different materials have different fatigue limit. Tensile and compressive stress may be caused by restricting thermal expansion. This situation occurs in complex piping systems such as welded joints, elbows, and T-junctions which are commonly found in nuclear power plant.

Nakamura et al., (2015) pointed out that temperature fluctuation caused by fluid mixing at T-junctions generates thermal stress which upon exceeding fatigue limit leads to pipe cracking. Prawoto (2013) suggested that a material subjected to stresses in a cyclic pattern will suffer from fatigue cracking when the induced stress is below the ultimate tensile stress of the material. This implies that the material fails at a stress level below its nominal strength. Figure 2.2 shows typical representation of fatigue failure in a pipe.

Figure 2.2: Thermal fatigue failures (Jayaraju et. al., 2011)

Failures related to thermal fatigue have occurred in several nuclear power plants around the world, including; Genkail (Japan), Tihange (Belgium), Farley (USA), Lovilsa (Finland), PFR (UK), Forsmark (Sweden), Tsuruga (Japan), Tomari (Japan), Civaux (France) (Jayaraju et al., 2011; Qian et al., 2010). Although installation of static mixers enhances mixing process which is a possible way of reducing the risk of thermal fatigue related problems, static mixers according to Ndombo & Howard (2011) have been developed and installed in nuclear power plants at Vattenfall Utveckling AB since the early 1980s, however these static mixing devices are expensive to install. This cost can be avoided if simulations can accurately predict thermal fatigue. Computational fluid dynamic methods such as Reynolds Averaged Navier-Stokes (RANS) equations, Large Eddy Simulation (LES), Scale-Adaptive Simulation (SAS) can be used to compute the flow in the component to predict the thermal load (Egorov et al., 2010). Codes available for performing these simulations include; Fluent, STAR-CCM+, CFX, CABARET, OpenFOAM, NEK5000, and TransAT.

A methodology used to predict thermal fatigue as proposed by Kucza et al., (2010) involves the determination of the temperature fluctuations using Computational Fluid Dynamics simulations. The temperature fluctuations are imposed as thermal loads in the FEM (Finite Element Method) model of the structure; the thermal stresses are then determined by means of mechanical analysis. Based on the thermal stresses determined, the fatigue lifetime of the structure is predicted using a fatigue curve from a design code.

A coupled CFD-FEM approach to predict thermal fatigue in mixing T-junction connections of nuclear reactor have been reported by Hannink et. al., (2008). In the report, a description of strategy applicable to specific test case was presented. The demonstrated test case shown in Table 2.1 was based on an experiment set up with a temperature difference of 80 °C between the hot and cold flow, while Table 2.2 shows the pipe material properties.

Table 2.1: The properties of cold and hot flow

	Temperature (°C)	**Diameter (m)**	**Velocity (m/s)**
Cold flow	10	0.14	0.78
Hot flow	90	0.10	0.76

Source: (Hannink et. al., 2008)

Table 2.2: Material properties of the pipe

Property	**Symbol**	**Value**
Density	ρ	7.9×10^{3} kg/m^{3}
Thermal conductivity	*K*	15.29 W/mK
Specific heat capacity	C_p	493 J/kgK
Thermal expansion coefficient	A	15.67×10^{-6} K^{-1}

Young's modulus	*E*	193 GPa
Poisson's ratio	N	0.3

Source: (Hannink et al., 2008)

The CFD simulation method used was LES, which is highly accurate but will require a high computational efforts and the simulation package used was FLUENT with 2nd order implicit non iterative time advancement scheme. Wall-adopting local eddy viscosity (WALE) model was used for LES. Bounded central difference was used for the convective term in momentum equation with 2nd order upwind scheme for the energy equation and a standard PISO (Pressure Implicit with Split Operator) algorithm for coupling pressure and velocity.

The initial conditions were taken from a well-developed case and the simulation performed for 6s of physical time with a time step of 0.001s. Only 2.5s of the flow was used for the structural analysis. The results showed snapshots of the fluid temperature and velocity fields to visualize the important flow phenomena associated with turbulent mixing.

The magnitude of the velocity field was also presented. The temperature profile was observed as a smooth curve, meaning that the mesh of the structure was fine enough to describe the penetration of the temperature fluctuations in the pipe wall properly. The temperature fluctuations at the interface were in line with the temperature fluctuations in the rest of the wall as shown in Figure 2.2.

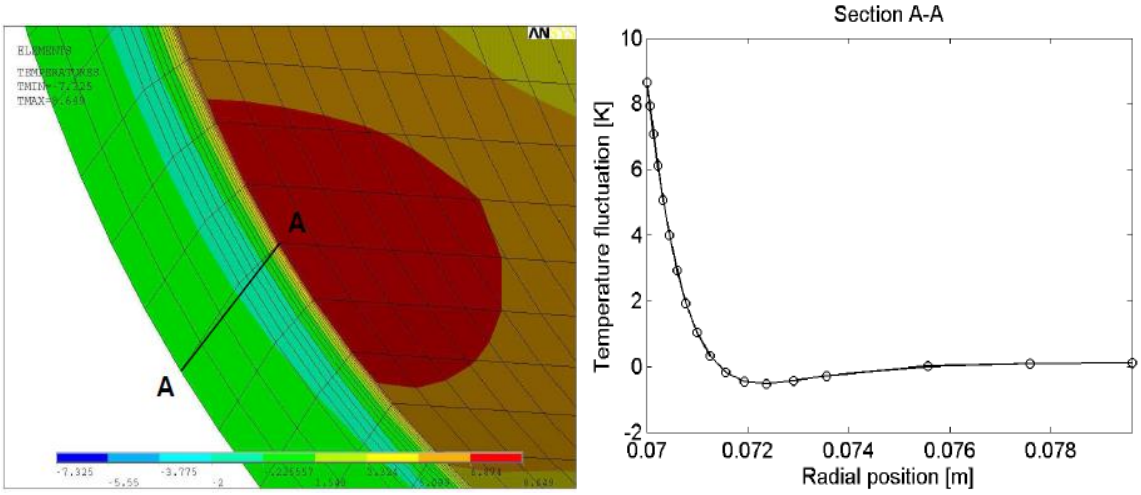

Figure 2.3: Temperature fluctuations at the interface and temperature fluctuations in the rest of the wall (Hannink et. al., 2008)

2.4.2 Computational Tools and Methods for Analyzing Thermal Fatigue

Temperature fluctuations are imposed as thermal loads in the FEM-model of the structure. The coupled CFD-FEM presented by Hannink et al., (2008) was established by user written interface between FLUENT and ANSYS to determine the stresses induced in the pipe. Temperatures from the CFD simulation was used as thermal loads in the FEM analysis using the FEM program ANSYS. The stress calculation was carried out for the part of the pipe in the mixing region which is important for the fatigue analysis. The stress calculation was performed with a time step of 0.020 s and for a total simulation time of 2.5 s. The temperature fluctuation in the structure for the simulation period varied between -11.8 °C and 11.4 °C. The stress intensity distribution was similar to that of the temperature since

they are both connected by a linear relation. Based on the stresses determined in FEM, a fatigue analysis was carried out which was referenced to ASME Boiler and Pressure Vessel Code (Hannink et al., 2008).

Jhung (2013) pointed out the need to study thermal fatigue evaluation of piping system's T-Junction connections using CFD models. An example is Fluid Structure Interaction (FSI), which was used in his analysis. Though common fatigue related problems are understood and controlled by plant instrumentation at fatigue susceptible locations, incidents that indicate that certain T- Junction piping system connections are susceptible to temperature mixing effects are not well monitored by common thermocouple instrumentations. Hence the need to use numerical analysis and algorithms in computing problems associated with fluid flow in a component and further predicting the thermal load. Numerical simulations of thermal fatigue in a mixing Tee has been studied by Aulery et al., (2010) where the Phoenix Tee configuration has been evaluated through thermal hydraulic simulations using both RANS and LES methodology. The simulation was performed using Fluent coupled between liquid and solid heat equation on mesh with 4.8 million tetrahedral prism cells. Flow rate of 800 kgs^{-1} and Reynolds number (Re) of $6x10^6$ was used for the main cold sodium inlets of 610 K temperature and flow rate of 7 kgs^{-1} and Re of $5x10^5$ was used for the second hot branch inlet at temperature of 700 K. The behavior of the hot jet within the main branch was well captured by both RANS and LES simulations. The mean temperature profiles at the wall past the hot injection pipe was well

represented by the calculations with a very close agreement with the LES calculations as shown in Figure 2.4:

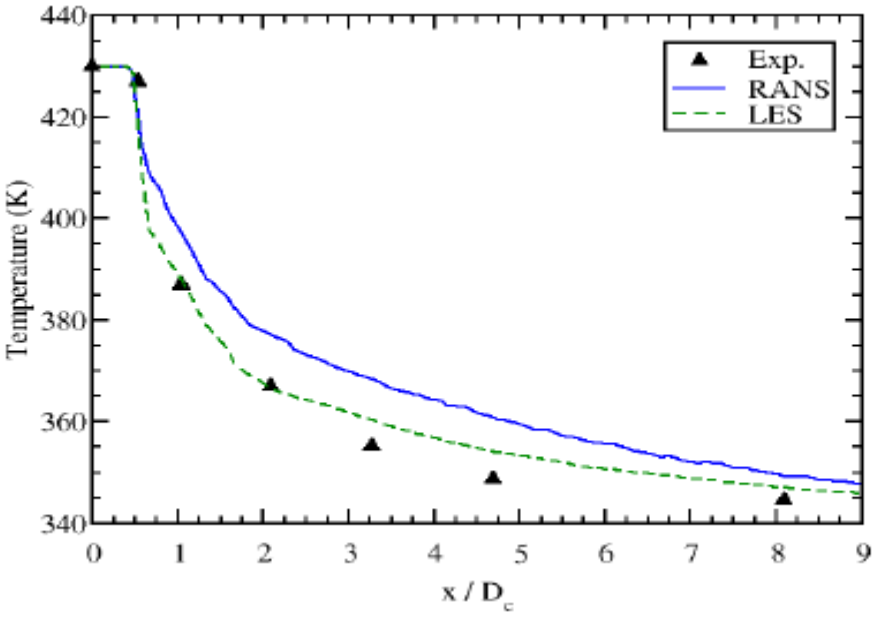

Figure 2.4: Mean temperature at wall past the hot injection pipe (Aulery et al., (2010)

It was concluded that, the simulation calculations was able to correctly reproduce the main characteristics of the turbulent mixing of two flows in a Tee junction of the Phoenix reactor and it demonstrates the ability of turbulent flow simulations to give valuable information for the evaluation of the thermal fatigue risk.

Tawade et al., (2015) reviewed thermal stress in mixing junction using Fluid Structure Interaction (FSI). The study was performed using FSI analysis and the temperature distribution at different zone determined using thermal hydraulic system analysis. Two bodies were created for the analysis; a solid body that is the pipe created in modeling

software and a second body which is the fluid flowing through the pipe. The meshed model was transferred into CFD software and the inlet and velocity constraint were imposed and the model was then solved for the transient analysis. Based on temperature transient in the piping walls obtained from the CFD computations, the thermal stress was calculated. The pipe geometry model created is transferred into the structural analysis. The pipe was meshed using structural meshing and the transfer of the thermal results from the CFD computation was done through FSI analysis mapping of nodes and elements. The results was directly imported and imposed on the pipe body. The corresponding stress analysis and the response characteristics of the T-junction subjected to the mixing effects investigated were found maximum at the joint contact.

The effect of branch pipe diameter in thermal mixing of a T-junction pipe has also been studied by Ayhan & Sökmen (2013). They studied the need to characterize temperature fluctuation in order to estimate the lifetime of pipe material. Several experiments and computational study conducted showed the most likely distance that thermal fatigue can occur in the two main pipe diameters at downstream after mixing. The study described the effects of branch pipe when the main pipe was constant in the geometry. Calculations were performed using different pipe diameters with the same flow rate conditions. The hot branch hydraulic diameter was changed, whilst the mass flow rate and the cold branch hydraulic diameter was held constant. Analysis was done to determine the effects of these conditions on the frequency and magnitude of the temperature fluctuations. Comparative

analysis was done for all cases. Detailed analysis was performed based on a previous work which showed the most probable distance of the two main diameters of 20 m at downstream after the junction where thermal fatigue occurs. LES turbulence model was chosen for turbulence calculation with filtered Navier-Stokes equation being used to solve the turbulence in Large Eddy Simulation (LES) as unsteady turbulent approach. Small eddies were modelled using the sub grid-scale (SGS) model and the large scale eddies solved by using the filtered Navier-Stokes equation. Three different test cases were simulated; the geometry and boundary conditions are shown in Table 2.3.

Table 2.3: Simulated test cases, geometry and test conditions.

	Hydraulic Diameter	**Temperature (°C)**	**Volumetric Flow Rate (l/s)**	**Re (x10^5)**
Main Duct	140	19	9	0.622
Branch Duct	80	36	6	1.055
	100	36	6	0.842
	120	36	6	0.704

Source: (Ayhan & Sökmen, 2013)

The non-dimensional (normalized) and root mean square (rms) values reported in the study were calculated from equation 2.1 (Ayhan & Sökmen, 2013);

$$T^* = \frac{T - T_{cold}}{T_{hot} - T_{cold}} \quad \text{and} \quad T^*_{rms} = \left[\frac{1}{N} \sum_{1}^{N} \left(T_i^* - T_{avg}^* \right)^2 \right]^{1/2} \tag{2.1}$$

where N: is the number of instantaneous temperature at a given location and T is the local and instantaneous fluid temperature. The normalized (T^*) and rms (T^*rms) values obtained from 3 cases were presented. For each test case, information about thermal fatigue were obtained from the magnitude and intensity of thermal load represented by the frequency of temperature fluctuation. The mean and vertical velocity distribution gave information about the hydraulic conditions of the flow. It was concluded that as the branch duct hydraulic diameter increases, the velocity or momentum ratio decreases, magnitude of thermal load decreases, on the other hand, intensity of thermal load does not change, the length required to reach hydraulic equilibrium l_{he} decreases but the length required to reach thermal equilibrium l_{te} increases. The magnitude of thermal load is dependent on temperature difference between the fluids. Temperature fluctuation becomes considerably important if their magnitude is high. The results also provided information about the lifetime of mixing T-junction connection exposed to the thermal load.

Recent models such as LES, Scale Adaptive Simulation (SAS) and combined models have been examined to assess fluid temperature fluctuations by Nakamura et al (2015). Numerical simulation evaluation methods and influencing factors such as turbulence models, computational meshes and inlet conditions have been reviewed. Knowing which turbulence model is applicable to represent temperature fluctuation is important because it affects the flow patterns related to the flow mechanisms.

2.4.4 Parameters Influencing Thermal Fatigue

Thermal fatigue is dependent on both mean and turbulent flow parameters such as; velocity, temperature, turbulent kinetic energy and turbulent dissipation rate.

Flow velocity is a vector field quantity used to express the motion of continuum. Mean horizontal and vertical velocity distributions give information about hydraulic conditions of flow. According to Ayhan & Sökmen (2013), heat transfer area increases as the velocity of branch inlet flow increase due to rapid mixing. Thermal mixing therefore takes place at a relatively short distance after meeting of streams on increasing velocity. Hence after the T-Junction, the fully developed condition is disturbed.

Stress and stress intensity factors are analysed under fluid temperature fluctuations. The magnitude of temperature fluctuations gives information about the magnitude of thermal load and subsequently, the thermal fatigue related failure (Ayhan & Sökmen, 2013).

In turbulent flow, the mean kinetic energy associated with eddies is known as Turbulent kinetic energy (TKE). Methods of resolving TKE is dependent on the turbulence model used. TKE is a fundamental flow property required for fluid turbulence modeling.

2.5 Turbulence models

Turbulence is characterized by chaotic property changes (Babiano et al., 1994). Turbulent flows are computed using different approaches. It can be computed either by using suitable

models for turbulent quantities using Reynolds Averaged Navier-Stokes equations or by computing them directly. The main approaches using Reynolds Averaged Navier-Stokes equation are EVM, NLEVM, DSM, LES DNS and RANS.

2.5.1 Eddy-viscosity Model (EVM)

The eddy viscosity model is developed from the turbulent transport equation (k + one other quantity). The turbulent stress for EVM is proportional to the mean rate of strain (Sodja, 2007). EVM assumes a Boussinesq relationship between the turbulent stresses and mean strain rate tensor through the use of isotropic eddy viscosity (Rumsey & Gatski, 2003).

2.5.2 Non Linear Eddy Viscosity Model (NLEVM)

For NLEVM, the turbulent stress is modeled as a nonlinear function of mean velocity gradient. The turbulent scales are derived from the transport equation (k + one other quantity). NLEVM models assumes a higher order tensor representation comprising of powers of the mean velocity gradient or combinations of the mean strain rate and rotation rate (Rumsey & Gatski, 2003).

2.5.3 Differential Stress Models (DSM)

DSM is composed second order closure models (SOC) or Reynolds-stress transport models (RSTM). DSM requires that transport equations be solved for all turbulent stresses (Sodja, 2007).

2.5.4 Large eddy simulation (LES)

With LES, time varying flow is computed while sub-grid-scale motions are modeled thus Large eddies are computed directly, while small scale eddies are modeled (Sodja, 2007).

2.5.5 Direct numerical simulation (DNS)

No modelling is applied in DNS and it is required to resolve the smallest flow as well (Sodja, 2007). DNS is numerical solving of Navier-Stokes and continuity equation.

The time steps and space grid and time steps in LES may be longer than in DNS. Therefore in terms of computational power requirement, LES is more economical in than DNS (Sodja, 2007). Using models by computing fluctuation quantities have the ability to provide better results because they resolve shorter length scales than models using RANS equations. However they have a demand of much greater computer power than those models applying RANS methods (Sodja, 2007).

2.5.6 Reynolds Averaged Navier-Stokes (RANS)

The RANS equations are time averaged of motion for fluid flow. Based on the properties of the flow turbulence, the RANS equations, can be used with approximations to give approximate averaged solutions to the Navier-Stokes equations (Pope, 2000). The basic requirement for deriving the RANS equation from instantaneous Navier-Stokes equations is the Reynolds decomposition, which is the separation of the flow variables into mean and fluctuating component.

All variables describing flow, fluid's density (ρ), velocity components (v), pressure (p) and components of viscous stress tensor (τ_{ij}) are decomposed into their mean and fluctuating components and integration over time (time-averaging) is performed.

The RANS equation is given in eq. (2.3) (Pope, 2000);

$$\frac{\partial \bar{u}_i}{\partial x_i} = 0 \tag{2.2}$$

$$\bar{u}_j \frac{\partial \bar{u}_i}{\partial x_j} = -\frac{1}{\rho}\frac{\partial \bar{p}}{\partial x_i} + \upsilon \frac{\partial^2 \bar{u}_i}{\partial {x_j}^2} - \frac{\partial \overline{u_i' u_j'}}{\partial x_j} \tag{2.3}$$

This equation describes the effects of turbulence on mean flow characteristics.

The instantaneous velocity and pressure is expressed in equation (2.4) and (2.5) respectively as (Pope, 2000);

$$u = \bar{u}_i + u_i' \tag{2.4}$$

$$p = \bar{p} + p' \tag{2.5}$$

where; u is the instantaneous velocity, $\bar{u}_i$ is the mean component velocity, u_i' is the fluctuating component velocity, P is the instantaneous pressure, $\bar{p}$ is the mean component pressure and p' is the fluctuating component pressure.

$\bar{u}_i = \bar{u}_i(x, t)$, $\bar{p} = \bar{p}(x, t)$ and $\overline{u_i' u_j'} = \overline{u_i' u_j'}(x, t)$; are dependent variables which are function of space and time. **x** = (x, y, z), where **x** is the position vector.

The last term in equation (2.3) is known as Reynolds stress tensor, it represents the correlation between fluctuating velocities. Turbulence effects on the mean flow are lumped into this single term by the process of averaging, this enables a great savings in terms of computational power requirements (Narasimhamurthy, 2004).

The difference between RANS and URANS is that an additional unsteady term is present in the URANS momentum equation (Salim et al., 2011).

The URANS equation is given in eq. (2.7); (Salim et al., 2011).

$$\frac{\partial \bar{u}_i}{\partial x_i} = 0 \tag{2.6}$$

$$\frac{\partial \bar{u}_i}{\partial t} + \bar{u}_j \frac{\partial \bar{u}_i}{\partial x_j} = -\frac{1}{\rho}\frac{\partial \bar{p}}{\partial x_i} + \upsilon \frac{\partial^2 \bar{u}_i}{\partial x_j{}^2} - \frac{\partial \overline{u_i' u_j'}}{\partial x_j} \tag{2.7}$$

It is known as Unsteady-RANS since the transient term is retained during computation. Therefore the results from the URANS are unsteady (Narasimhamurthy, 2004).

The time-averaged velocity is denoted as; $\langle \overline{u}_i \rangle$ which means that the results from URANS can be decomposed as a time averaged part $\langle \overline{u}_i \rangle$, a resolved fluctuation $u_i^{''}$, and the modelled turbulent fluctuation $u_i^{'}$. Equation (2.4) therefore becomes equation (2.8).

$$u = \overline{u}_i + u_i^{'} = \langle \overline{u}_i \rangle + u_i^{''} + u_i^{'} \qquad (2.8)$$

Appropriate models used for solving both mean and turbulent flow properties is selected. Turbulence sensitivity analysis is necessary to arrive at a suitable turbulence model to be used. The two possible turbulence models considered for the URANS models were be, k-epsilon model and k-omega models.

2.5.6.1 K-epsilon model

The K-epsilon model is a two equation turbulence model with two extra transport equations which represent the turbulent flow properties. This accounts for history properties such as diffusion of energy (Schatz, 2004). It is a commonly used turbulence models, though it doesn't perform well in large adverse pressure gradients (Bakker, 2002).

Standard K-epsilon model solves the transport equations for turbulent kinetic energy (*k*) and its dissipation (ε). The turbulent kinetic energy equation is given in equation (2.9) and

turbulent dissipation expressed in eq. (2.10); (Wilcox, 1998; Bardina et al., 1997; Lauder et al., 1974; Jones et al., 1972)

$$\frac{\partial}{\partial t}(\rho k)+\frac{\partial}{\partial x_i}(\rho k u_i)=\frac{\partial}{\partial x_j}\left[\left(\mu+\frac{\mu_t}{\sigma_k}\right)\frac{\partial k}{\partial x_j}\right]+P_k+P_b-\rho\varepsilon-Y_M+S_k \tag{2.9}$$

The turbulent dissipation equation is expressed as;

$$\frac{\partial}{\partial t}(\rho \varepsilon)+\frac{\partial}{\partial x_i}(\rho \varepsilon u_i)=\frac{\partial}{\partial x_j}\left[\left(\mu+\frac{\mu_t}{\sigma_\varepsilon}\right)\frac{\partial \varepsilon}{\partial x_j}\right]+C_{1\varepsilon}\frac{\varepsilon}{k}(P_k+C_{3\varepsilon}P_b)-C_{2\varepsilon}\rho\frac{\varepsilon^2}{k}+S_\varepsilon \tag{2.10}$$

where;

$$P_k=-\rho\overline{u_i'u_j'}\frac{\partial u_j}{\partial x_i} \tag{2.11}$$

u_i represents the velocity component in corresponding direction

$$P_k=-\mu_t S^2 \tag{2.12}$$

where S is the modulus of the mean rate of strain tensor and is given in equation (8);

$$S\equiv\sqrt{2S_{ij}S_{i,j}} \tag{2.13}$$

The effect of buoyancy is defined as;

$$P_b=\beta g_i\frac{\mu_t}{\mathrm{Pr}_t}\frac{\partial T}{\partial x_i} \tag{2.14}$$

Where Pr_t is turbulent Prandtl number for energy and g_i is the component of the gravitational vector in that direction.

The coefficient of thermal expansion β, is defined as;

$$\beta = -\frac{1}{\rho}\left(\frac{\partial \rho}{\partial T}\right)_P \tag{2.15}$$

Model constants are given as;

$C_{1\varepsilon} = 1.44$, $C_{2\varepsilon} = 1.92$, $C_{\mu} = 0.09$, $\sigma_k = 1.0$ and $\sigma_{\varepsilon} = 1.3$

$C_{3\varepsilon}$ depends on the literature reference and is meant to be used only with P_b term.

The scale of the turbulence is determined by; turbulent dissipation (ε), whereas *k,* determines the energy in the turbulence (Schatz, 2004).

K-epsilon model is known to be useful for free-shear layer flows with relatively small pressure gradients, it has been proven experimentally that, accuracy is reduced for flows with large pressure gradients (Bardina et al., 1997).

2.5.6.2 K-ω model

The K-omega (K-ω) model is also a two equation model, ω is an inverse time scale associated with the turbulence (Bakker 2002 & Fluent Inc. 2002). The first and second transport variables are turbulent kinetic energy *k* and specific dissipation, ω respectively. The scale of turbulence is determined by the specific dissipation, whereas the energy in the turbulence is determined by the kinetic energy.

The specific dissipation ω, is related to *k* through the kinematic viscosity by the equation;

$$\nu_T = \frac{k}{\omega} \tag{2.16}$$

where the turbulence kinetic energy equation is given in eq. (2.17) and specific dissipation rate expressed in eq. (2.18); (Wilcox, 988)

$$\frac{\partial k}{\partial t} + U_j \frac{\partial k}{\partial x_j} = \tau_{ij} \frac{\partial U_i}{\partial x_j} - \beta * k\omega + \frac{\partial}{\partial x_j}\left[\left(\nu + \sigma * \nu_T\right) \frac{\partial k}{\partial x_j} \right] \tag{2.17}$$

The specific dissipation rate is also expressed as;

$$\frac{\partial \omega}{\partial t} + U_j \frac{\partial \omega}{\partial x_j} = \alpha \frac{\omega}{k} \tau_{ij} \frac{\partial U_i}{\partial x_j} - \beta \omega^2 + \frac{\partial}{\partial x_j}\left[\left(\nu + \sigma \nu_T\right) \frac{\partial \omega}{\partial x_j} \right] \tag{2.18}$$

where; $\alpha = \frac{5}{9}$, $\beta = \frac{3}{40}$, $\beta^* = \frac{9}{100}$, $\sigma = \frac{1}{2}$, $\sigma^* = \frac{1}{2}$ and $\varepsilon = \beta^* \omega k$

The turbulent viscosity (μ_t) is then calculated by equation (2.19):

$$\mu_t = \rho \frac{k}{\omega} \tag{2.19}$$

where is ρ the density of fluid.

Both K-ω model and k-ε model assumes μ_t to be isotropic. (Bakker 2002 & Fluent Inc. 2002).

2.5.6.3 SST k-ω Turbulence Model

SST k-ω turbulence model (Menter, 1993) is an eddy-viscosity turbulence model with two extra transport equations. The model uses k-ω formulation in the inner parts of the boundary layer which enables the model to be directly used down to the wall through the viscous sub-layer. SST k-ω model can therefore be used without any extra damping functions in low Reynolds number turbulence modeling. The model switches to a k-ε behaviour in the free-stream hence it is not sensitive to the inlet free-stream turbulence properties which is a major k-ω problem. According to Schatz (2008), SST k-ω model is often merited for its good behaviour in adverse pressure gradients and separating flow. In regions with large normal strain for instance, stagnation regions and regions with strong acceleration, SST k-ω model produces large turbulence levels which is less pronounced compared to a normal k-ε model.

The specific dissipation ω, is related to *k* through the kinematic eddy viscosity by equation (2.20);

$$\nu_T = \frac{a_1 k}{\max\left(a_1 \omega, SF_2\right)} \tag{2.20}$$

The turbulence kinetic energy equation is given by equation (2.21) and the specific dissipation expressed in eq. (2.22); (Menter, 1994 & 1993)

$$\frac{\partial k}{\partial t} + U_j \frac{\partial k}{\partial x_j} = P_k - \beta * k\omega + \frac{\partial}{\partial x_j}\left[\left(\nu + \sigma_k \nu_T\right) \frac{\partial k}{\partial x_j} \right] \tag{2.21}$$

The specific dissipation rate is also expressed as equation (2.22);

$$\frac{\partial \omega}{\partial t} + U_j \frac{\partial \omega}{\partial x_j} = \alpha S^2 - \beta \omega^2 + \frac{\partial}{\partial x_j}\left[\left(\nu + \sigma_\omega \nu_T\right) \frac{\partial \omega}{\partial x_j} \right] + 2\left(1 - F_1\right)\sigma_{\omega 2} \frac{1}{\omega} \frac{\partial k}{\partial x_i} \frac{\partial \omega}{\partial x_i} \tag{2.22}$$

where F_1 is defined as;

$$F_1 = \tanh\left\{ \left\{ \min\left[\max\left(\frac{\sqrt{k}}{\beta * \omega y}, \frac{500\nu}{y^2 \omega} \right), \frac{4\sigma_{\omega 2} k}{CD_{k\omega} y^2} \right] \right\}^4 \right\} \tag{2.23}$$

and $CD_{k\omega}$ is expressed as;

$$CD_{k\omega} = \max\left(2\rho\sigma_{\omega 2} \frac{1}{\omega} \frac{\partial k}{\partial x_i} \frac{\partial \omega}{\partial x_i}, 10^{-10} \right) \tag{2.24}$$

$$\phi = \phi_1 F_1 + \phi_2 \left(1 - F_1\right) \tag{2.25}$$

$\alpha_1 = \frac{5}{9}$, $\alpha_2 = 0.44$, $\beta_1 = \frac{3}{40}$, $\beta_2 = 0.0828$, $\beta^* = \frac{9}{100}$,

$\sigma_{k1} = 0.85$, $\sigma_{k2} = 1$, $\sigma_{\omega 1} = 0.5$, $\sigma_{\omega 1} = 0.856$

The quality of numerical simulation is increased by successful modeling of the turbulence. The complex nature of the different turbulence models vary depending on the parameters being observed or investigated. These complex behaviors of the turbulence models are as a result of the nature of the Navier-Stokes equation (Sodja, 2007).

2.6 RANS methods for computing parameters affecting thermal fatigue

In an attempt to predict temperature fluctuations using steady-state RANS simulations, Manera et al., (2009) presented a study on using RANS for prediction of temperature fluctuations in the estimation of thermal fatigue. The study was validated against a T-junction experiment performed at the Paul Scherrer Institute. Mixing pattern between water streams was measured, which served as transport scalar fluctuations for validating the theoretical model. The Reynolds stress was solved and the advantage of the approach used was the significant lower computational power requirements compared to LES and unsteady RANS. For a more complex geometry, alternate methods based on efficient steady state RANS models needs to be considered. The application of temperature fluctuation transport model, coupled to a Reynolds stress model is a promising approach. The basis of this model is the second averaging of the scalar transport equation resulting in an additional transport equation for the RMS of the scalar. For comparison with experimental data, a dimensionless scalar was defined from both calculated temperature and measured conductivities assuming that both physical quantities behaved similarly vis-

à-vis turbulent mixing. The simulation was performed in ANSYS CFX 11.0 with the SSG and the Baseline (BSL) Reynolds stress models adopted.

The advantage of BSL model is the accurate near-wall treatment, which is of importance for wall-bounded flows as the one being investigated. SSG and BSL Reynolds stress models combined with a transport equation for the scalar fluctuations were presented and compared. It was clear from the 2D velocity distribution that both models reproduced the scalar distributions and the RMS profiles correctly, however the axial extension of the recirculation region, where the two vortexes were present were over predicted, though the BSL model led to slightly better prediction of the velocity profile.

Turbulent diffusion were under predicted in both transport scalar and momentum. For the effects of turbulent dissipation, the calculated scalar profiles for both models indicated an underestimation of the turbulent mixing. The underestimation of the turbulent mixing was due to a too low turbulent kinetic energy. Modification of the turbulent Schmidt number improves predictions of the scalar distribution by means of RANS and URANS simulations since it has a direct influence on the turbulent diffusion coefficient.

In the assessment of thermal fatigue of large components, Reynolds stress turbulent models combined with scalar fluctuation transport equations offers great advantage over LES simulations or unsteady RANS. Combining the fluctuations scalar transport equation with a suitable equation for the turbulence dissipation is necessary to yield satisfactory results.

Frank et al., (2010) carried out simulation of turbulent and thermal mixing in T-junction using URANS and scale resolving turbulence models in ANSYS CFX. Turbulent

isothermal and thermal phenomena were investigated in two different scenarios. The first test case scenario was based on what was proposed by ETHZ, Prasser et al., (2002), the setup comprised of turbulent mixing of two water streams of equal temperature in a T-junction of 5-mm pipes in the horizontal plane, thereby excluding buoyancy effects. The objective of the research was to investigate grid independent CFD solutions for RANS/URANS approaches using SST and BSL RSM turbulent models. The second test case was based on the Vattenfall test facility in the Alvkarleby laboratory and as proposed by Westin et al., (2007), water of 15º temperature difference flow in and mix in a T-junction in vertical plane triggering thermal stripping phenomena. The main parameters for the test case was given as shown in Table 2.4;

Table 2.4: Test case parameters

Parameter	**Value**
Flow rate in branch pipe (Q_1, hot water)	12 [l/s]
Flow rate in main pipe (Q_2, cold water)	24 [l/s]
Mean bulk velocity in branch pipe	1.53 [m/s]
Mean bulk velocity in main pipe	1.56 [m/s]
Reynolds number for hot leg	$1.9x10^5$

Reynolds number for cold leg	$1.9x10^5$
Hot water temperature	30.0 [°C]
Cold water temperature	15.0 [°C]

Source: (Frank et al., 2010)

For both test cases, ANSYS CFX 11.0 with Reynolds averaged based URANS turbulent models (SST, BSL, RSM) with scale resolving SAS-SST turbulent was applied. The simulations were carried out with time step Δt of 0.001s, using second order backward Euler time discretization for the transient URANS SST and SST-SAS simulation. The convergence criterion was based on maximum residuals of 10^{-4} at every time step with 3-5 coefficient loops. High resolution advection scheme was applied for the spatial discretization of momentum equation. The solutions obtained with the URANS SST model was used as an initialization for the further transient investigations using the scale resolving SST-SAS turbulence model. This approach has the advantage of considerable lower computational requirement compared to LES therefore allows application to more complex and lager geometries.

2.7 Recent techniques for predicting thermal fatigue.

Early Researchers in the field, (Westin et al., 2008; Manera et al., 2009) were emphatic about the fact that, the most widely used Reynolds Averaged Navier-Stokes (RANS) methodology exhibits difficulties in predicting accurately turbulent mixing in T-junctions. Recently used numerical tools such as LES and DES which shows fairly good predictions of mean and the wall temperature.

The status of LES CFD for Nuclear Reactor Safety (NRS) Analysis has been reviewed by Kerntechnik (2011) where it has been stated that, provided best practices are observed, LES predicts bulk thermal mixing with good accuracy. Jayaraju et al., (2010) performed LES on a T-Junction to analyze the possiblity of wall functions to accurately predict thermal fluctuations acting on pipe walls. The model used in the LES solver was validated by the OECD/NEA T-junction benchmark test case. There was a good agreement of wall function based simulation with the wall resolved approach for the bulk velocity and temperature field. Corresponding root mean square (RMS) components were consistently under estimated close to the wall boundaries. LES with very fine meshes to capture turbulent eddies near the wall or direct numerical simulation may show good result however their calculation time and power are unrealistic.

2.8 STAR-CCM+ simulation for predicting parameters affecting thermal fatigue

Codes available for performing simulations includes STAR-CCM+. STAR-CCM+ has been used in the OECD/NEA T-Junction Blind Benchmark exercise to test the capabilities of state of the art CFD codes in accurately predicting important parameters affecting thermal fatigue as reported by Jayaraju et al., (2011) in the STAR European conference. Conditions at the inlets boundary were provided in the benchmark as flow rate, Q_{hot} = 6 l/s, T_{hot} = 36 °C, turbulence intensity (TI) = 0 % and Q_{cold} = 9 l/s, T_{cold} = 19 °C, TI = 0 %. Data at locations downstream the mixing T-Junction were presented. The turbulence model used was Large Eddy Simulation, Wall-adopting local eddy viscosity (WALE) model was used for LES with 2nd order implicit temporal discretization.

Bounded central difference formula was used for the spatial discretization with upwind blending factor of 0.1. The snapshots of the fluid instantaneous temperature are shown in Figure 2.5. Mean and rms temperatures at 2.6 diameters downstream of mixing zone and velocity (Mean and rms velocities at 2.6 diameters) fields to visualize the important flow phenomena associated with turbulent mixing. The magnitude of the velocity field is also presented in Figure 2.6.

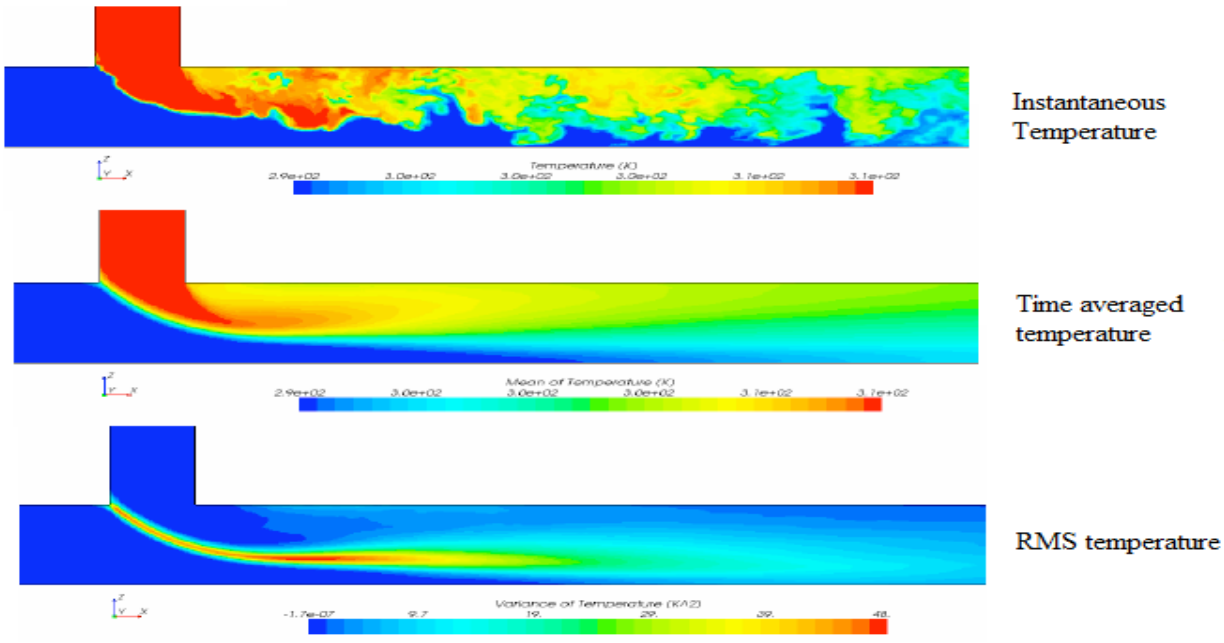

Figure 2.1: Fluid temperature distribution (Jayaraju et. al., 2011).

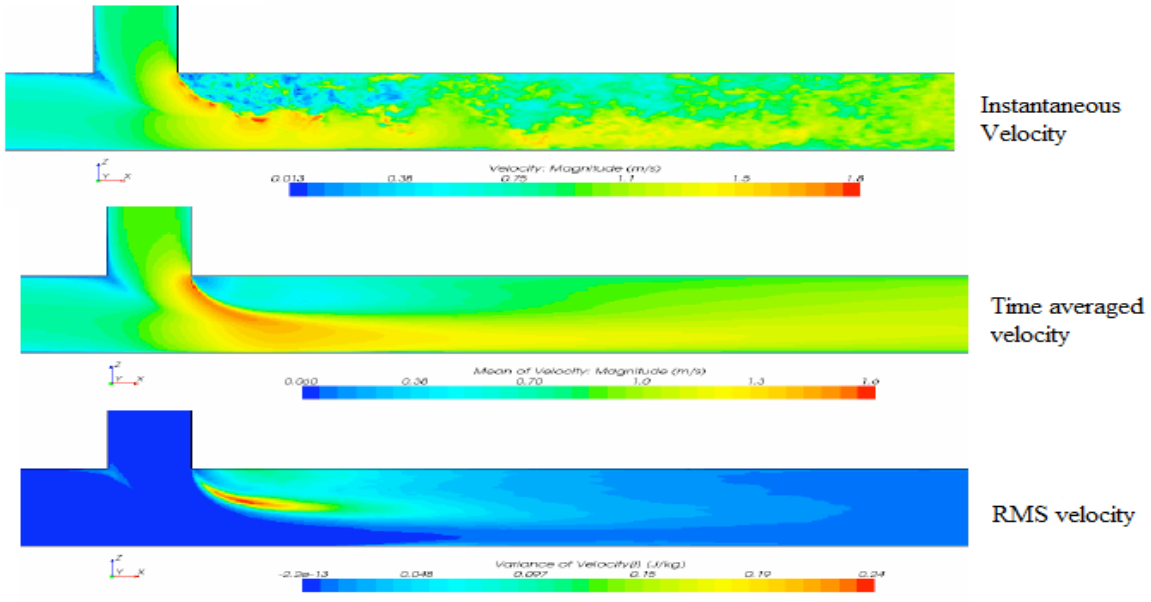

Figure 2.2: Fluid velocity distribution (Jayaraju et. al., 2011).

The study showed generally good agreement between experiments and LES predictions, LES was very much suitable for thermal fatigue predictions and were very pleased with the capabilities of STAR-CCM+. It is clear, that models computing fluctuation quantities have the ability to provide better results because it resolves shorter length scales than models solving RANS equations, hence demand greater computer power.

2.9 Numerical Approach

The method used follows that employed for all computational fluid dynamic simulations, namely: Pre-processing, Solution and Post-processing.

During the pre-processing stage, geometry generation, mesh generation and physics set-up were considered.

2.9.1 Geometry / Meshing Models

The geometry model can be created in STAR-CCM+ or any third party software and imported into STAR-CCM+. The modified model of the geometry used in the experimental analysis is generated using 3D-CAD (3Dimensional-Computer Aided Design) tools in STAR-CCM+.To be able to compute, the software needs to discretize the 3-dimensional geometry model into very small pieces called cells. Converting the 3-dimensional model in to these cells is called meshing (Garlapati, 2012).There are different meshing strategies,

and each one is suited for one or other application (CD-adapco, 2008&User Guide STAR-CCM+, 2013). The domain will be discretized by the application of surface meshing model, polyhedral meshing model and extruder meshing model. Meshing feature in STAR-CCM+ is explained in subsequent sub-sections;

2.9.1.1 Surface Meshing Model

A surface mesh that is imported from a CAD package or some other third party pre-processing software is the starting point for all the mesh models in STAR-CCM+. Quality of surface mesh can vary greatly from one package to another. Typical problems that can be encountered include: Holes and gaps, multiple edges, Poor triangulation (needles cells), Mismatched edges, Self-intersection and Sharp angle folds (Garlapati, 2012).

Small number of problems can be manually repaired whereas more extensive problems, will require the two automatic tools that are available to eliminate the above problems and improve the overall quality of the starting surface mesh imported into STAR-CCM+ (Garlapati, 2012). The two tools are; surface wrapper and surface remesher. The initial surface is wrapped to provide a closed surface mesh from a complex geometry using surface wrapper and it comes with a tool for leak detection and is usually used in conjunction with the surface remesher (CD-adapco, 2008; User Guide STAR-CCM+, 2013). The initial surface is remeshed using Surface Remesher to provide a quality

discretized mesh that is suitable for CFD based on a target edge length that the user specifies (CD-adapco, 2008&User Guide STAR-CCM+, 2013).

Volume mesh is generated using polyhedral meshing model which is composed of polyhedral-shaped cells. Polyhedral meshing model compared to an equivalent tetrahedral mesh is numerically more stable, less diffusive and more accurate than (CD-adapco, 2008).

2.9.1.2 Optional Meshing Model

An optional Meshing Model is the prism layer mesher, which adds prismatic cell layers next to wall boundaries. The core mesh is projected back to the wall boundaries to create prismatic cells. According to CD-adapco (2008), the prismatic cell layers help capture the boundary layer, turbulence effects, and heat transfer near wall boundaries. These layers of prismatic cells are generated next to wall boundaries to enhance the accurateness of flow solution. Prediction of flow characteristics, for instance, drag or pressure drop is dependent on resolving the velocity and temperature gradients normal to the wall.

2.9.1.3 Extruder Meshing Model

Extruder meshing model is normally used for inlet and outlet boundaries, to extend the volume mesh beyond the original dimensions of the starting surface, so that a more

representative computational domain is obtained (CD-adapco, 2008 & User Guide STAR-CCM+, 2013).

After a working mesh based on the limits of the computational resource available is obtained, the appropriate physics models will be selected. Taking a critical look at the existing research, the strategy and selection criteria adopted for this work is presented in the next chapter.

CHAPTER THREE

RESEARCH METHODOLOGY

3.1 Introduction

Chapter three outlines the procedures adopted to achieve the aims spelled out in chapter one. The meshing and physics models explained in the section three were applied and the geometries for this study presented. This research work is accomplished by performing numerical simulation using STAR-CCM+ based on an experimentation performed in Älvkarleby Laboratory of Vattenfall Research and Development. The experimental set up and the simulation approach are presented.

3.2 Experimental Setup by Älvkarleby Laboratory of Vattenfall Research and Development

Although the experimental analysis will not be carried out in this research, simulation data obtained in the present work will be validated with data obtained from the Vattenfall experimental test rig shown in Figure 3.1.

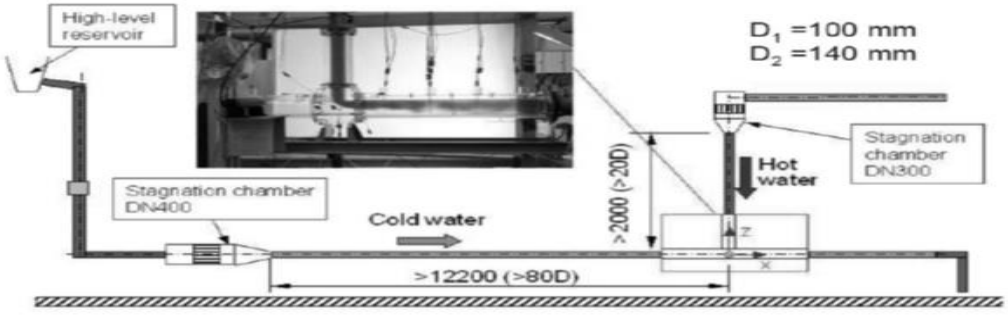

Figure 3.1: Side View of Vattenfall test rig (Westin, 2007).

Temperature fluctuations were recorded using thermocouples (TCs) located 1 mm from the wall at seven positions downstream of the T-junction as shown in Figure 3.2.

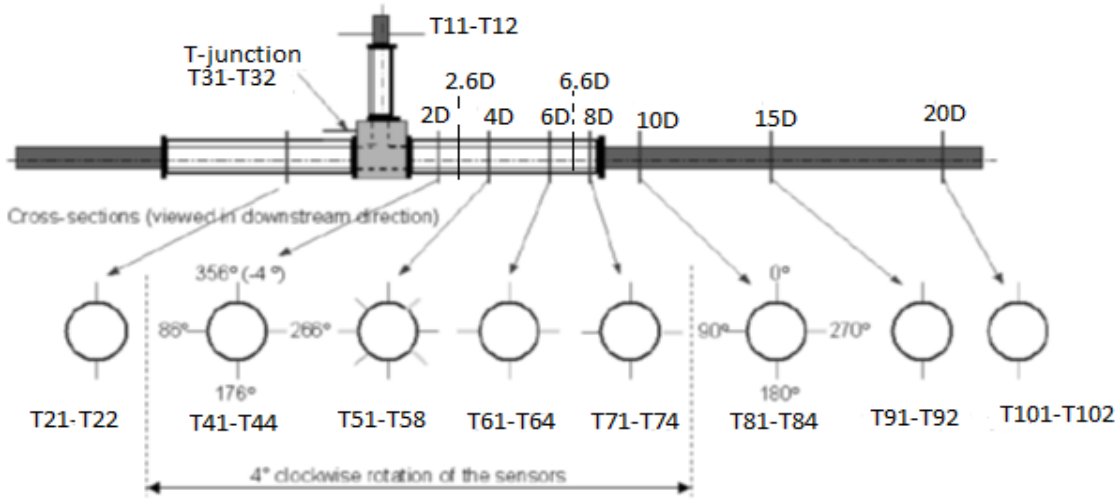

Figure 3.2 Thermocouple locations of the experimental rig (Westin, 2007).

From the data obtained, the normalized temperature was determined by equation 2.1.

3.2.1 Upstream Measuring Boundary Conditions

The working fluid in this test is de-ionized tap water at cold temperature of 19 °C and hot temperature of 36 °C. The volumetric flow rates used in the benchmark tests are shown in Table 3.1 together with the locations where the temperature and velocity distributions over the pipe cross-sections were measured.

Table 3.1: Inlet Temperature and Flow Rates

Inlet/Designation	Temperature (°C)	Pipe diameter (mm)	Measuring location (mm)	Volumetric flow (litres/s)
Main/InCo	19	140(D_2)	-420 (-3D_2)	9.0
Branch/InHo	36	100(D_1)	-310 (-3.1D_1)	6.0

3.2.2 Downstream Measurements

With reference to Figure 3.2, the inside diameter of the main pipe was 140 mm (D_2). Thermocouples of 0.13 mm diameter were placed approximately 1 mm from the inner pipe wall at position x = 2 D_2, 4 D_2, 6 D_2, 8 D_2, 10 D_2, 15 D_2 and 20 D_2.Velocities were measured using Particle Image Velocimetry (PIV) at position x = 1.6 D_2, 2.6 D_2, 3.6 D_2, and 4.6 D_2 along two lines perpendicular to the flow. Mean flow, Root Mean Square (RMS) fluctuations and Reynolds stresses were computed at all four downstream locations. The downstream data obtained were used for comparison against numerical predictions performed in the research work.

3.3 STAR-CCM+ Simulation of Thermal Mixing

The major activity to be conducted in this work is the numerical solution of the research problem by using computational fluid dynamics code STAR-CCM+. The solution will then be monitored and steered until convergence. Finally, data obtained will be plotted using various visualization techniques and vivid analysis to trends will be presented.

3.3.1 Geometry Model

The geometry used in the experimental analysis was modified and generated using the 3D-CAD (Three Dimensional-Computer Aided Design) tools in STAR-CCM+. The dimensions of the computational flow domain considered are shown in Figures 3.3, 3.4, 3.5 and 3.6.

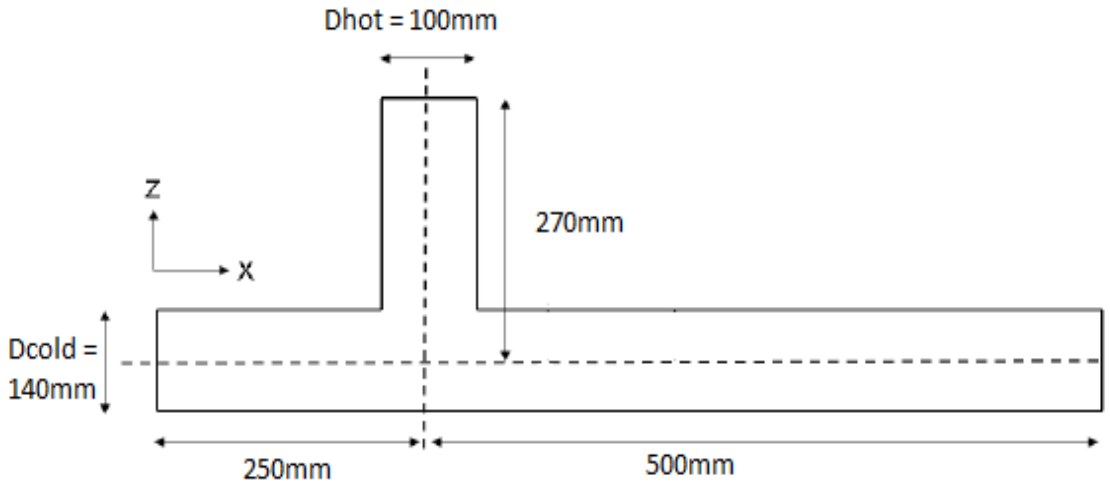

Figure 3.3: 0^{o} Junction Pipe Geometry model

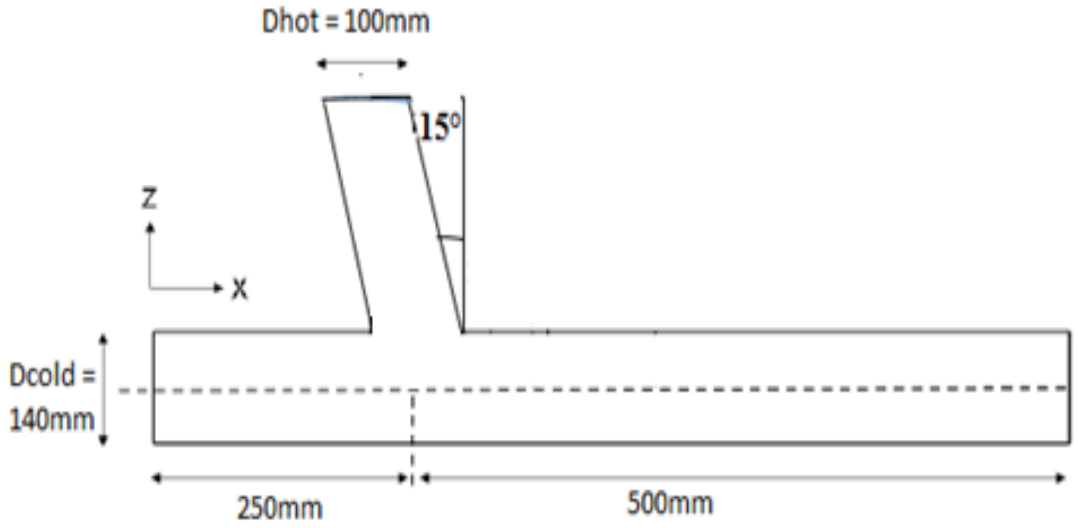

Figure 3.4: -15° Junction Pipe Geometry model

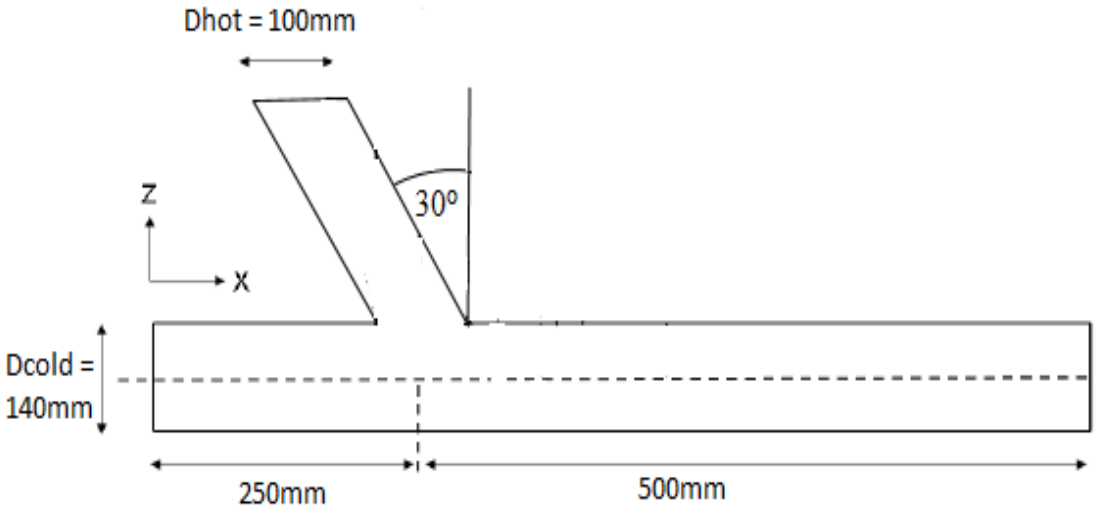

Figure 3.5: -30° Junction Pipe Geometry model

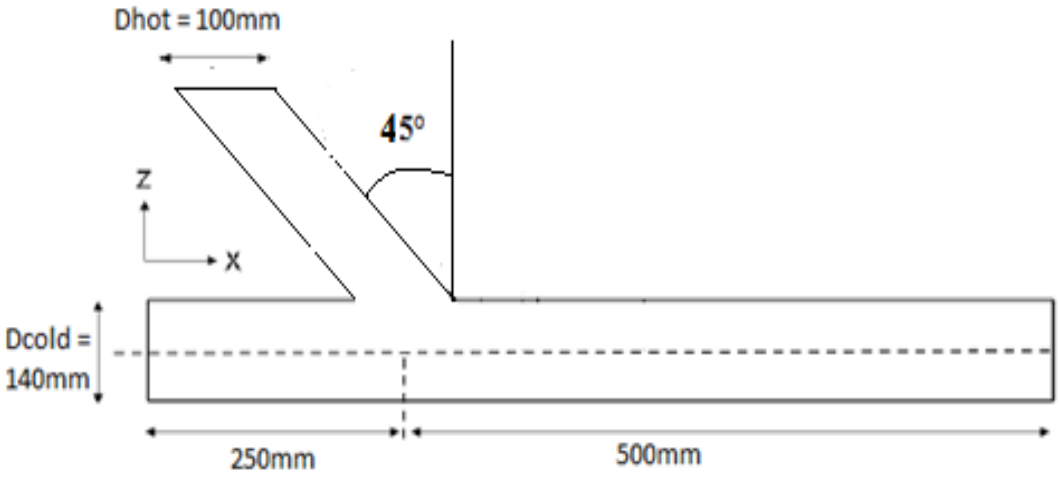

Figure 3.6: -45^{o} Junction Pipe Geometry model

3.3.2 Discretization of the domain

The 3-dimensional geometry model was discretized into very small pieces called cells by the application of surface remesher meshing model, trimmer meshing model and prism layer meshing model.

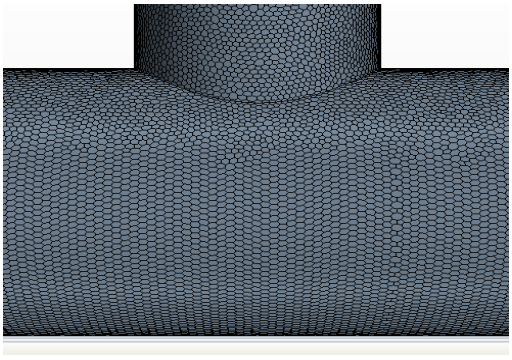

(a)

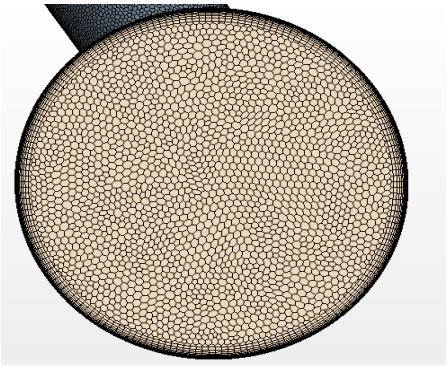

(b)

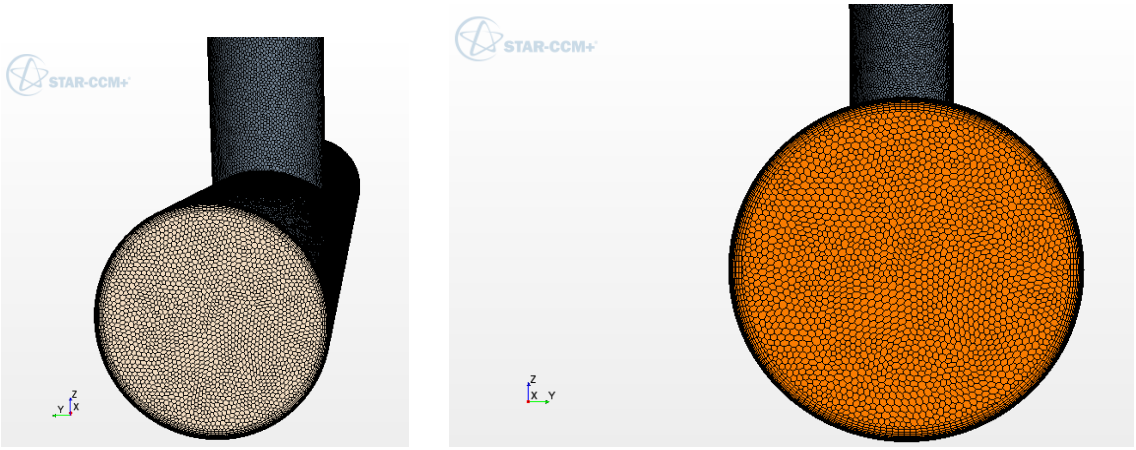

(c) **(d)**

Figure 3.7: Meshed Domain; Mixing-Junction **(a)**, inlet **(b)** & **(c)**, outlet **(d)**

3.3.3 Physics Models

Appropriate models used for solving both mean and turbulent flow properties for the problem considered were selected from a list of models available in STAR-CCM+. Thermal striping is intrinsically unsteady and hence not accessible to steady state simulation approaches such as steady state Reynolds-averaged Navier-Stokes (RANS) models. Consequently, unsteady RANS was considered. Turbulence model is one of the important factors influencing the reproduction of the temperature fluctuation caused by the vortices downstream from a T-junction (Tawade & Suryavanshi, 2015) and as such, a turbulence sensitivity analysis was performed to arrive at an appropriate turbulence model that would accurately predict the experimental data. The two turbulence models to be

considered for the URANS models were, k-epsilon model and k-omega models. Table 2.2 shows the potential physics models that would be considered for a flow problem.

Table 3.3: Physics model Equations considered for the flow problem – Analysis Equations

URANS	$\frac{\partial \overline{u}_i}{\partial t} + \overline{u}_j \frac{\partial \overline{u}_i}{\partial x_j} = -\frac{1}{\rho}\frac{\partial \overline{p}}{\partial x_i} + \upsilon \frac{\partial^2 \overline{u}_i}{\partial x_j{}^2} - \frac{\partial \overline{u_i' u_j'}}{\partial x_j}$ **(2.6)**
K-ω model	
Turbulent kinetic energy, k	$\frac{\partial k}{\partial t} + U_j \frac{\partial k}{\partial x_j} = \tau_{ij} \frac{\partial U_i}{\partial x_j} - \beta * k\omega + \frac{\partial}{\partial x_j}\left[\left(\nu + \sigma * \nu_T\right) \frac{\partial k}{\partial x_j} \right]$ **(2.17)**
Specific dissipation, ω	$\frac{\partial \omega}{\partial t} + U_j \frac{\partial \omega}{\partial x_j} = \alpha \frac{\omega}{k} \tau_{ij} \frac{\partial U_i}{\partial x_j} - \beta \omega^2 + \frac{\partial}{\partial x_j}\left[\left(\nu + \sigma \nu_T\right) \frac{\partial \omega}{\partial x_j} \right]$ **(2.18)**
Kinematic Eddy Viscosity	$\nu_T = \frac{k}{\omega}$ **(2.16)**
SST k-ω model	

Turbulent kinetic energy	$\frac{\partial k}{\partial t} + U_j \frac{\partial k}{\partial x_j} = P_k - \beta * k\omega + \frac{\partial}{\partial x_j}\left[\left(\nu + \sigma_k \nu_T\right) \frac{\partial k}{\partial x_j} \right]$ **(2.2)**
Specific dissipation Rate	$\frac{\partial \omega}{\partial t} + U_j \frac{\partial \omega}{\partial x_j} = \alpha S^2 - \beta \omega^2 + \frac{\partial}{\partial x_j}\left[\left(\nu + \sigma_\omega \nu_T\right) \frac{\partial \omega}{\partial x_j} \right] + 2\left(1 - F_1\right)\sigma_{\omega 2} \frac{1}{\omega} \frac{\partial k}{\partial x_i} \frac{\partial \omega}{\partial x_i}$ **(2.22)**
Kinematic Eddy Viscosity	$\nu_T = \frac{a_1 k}{\max\left(a_1 \omega, SF_2\right)}$ **(2.20)**

Table 3.4: Model specifications used in the flow Problem

MODEL	**MODEL SPECIFICATION**
Space Model	3-Dimensional
Time Model	Implicit Unsteady
Energy of State Model	Constant Density
Flow Model	Segregated Flow
Energy Model	Segregated Fluid Isothermal

Viscous Regime Model	Turbulent
Turbulent Model	K-epsilon model/K-Omega
Wall Function	High y + wall Model
Convection Scheme	2nd Order Upwind

3.3.4 Initial and Boundary Conditions

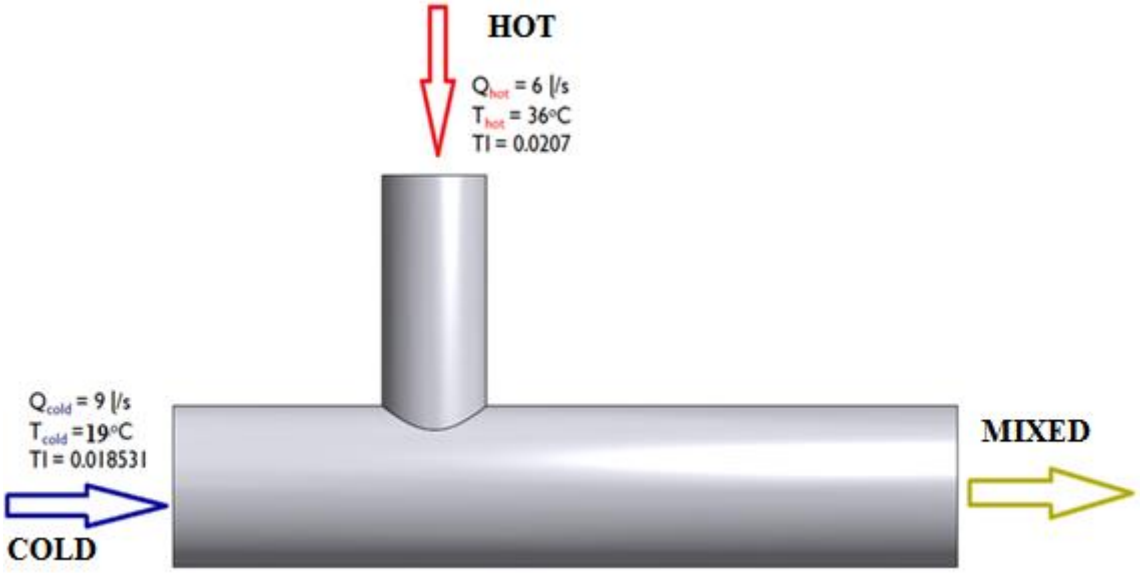

Figure 3.8: Initial and Boundary Conditions

Average values of turbulent intensity data used for the experimentation were adopted for the inlets. The inlet conditions were specified as;

- Hot fluid inlet Volumetric flow rate : 6 l/s

- Cold fluid inlet Volumetric flow rate : 9 l/s
- Hot fluid inlet temperature : 36 ^{o}C
- Cold fluid inlet temperature : 19 ^{o}C

A mass flow boundary condition were be imposed at both cold and hot inlet of the mixing-junction and a pressure boundary condition imposed at the outlet. Adiabatic condition was imposed on the wall surfaces. A non-slip condition was adopted for all the walls.

The temperature specification at both inlets were varied as indicated in Table 3.5.

Table 3.5: Test case Parameters

$T_{HOT,}$ (°C)	$T_{COLD,}$ (°C)	Temperature difference, (ΔT)	Angle of inclination	T_{HOT} (TI)	T_{COLD} (TI)	Case
36	19	17	0˚	0.0207	0.0185	1
36	19	17	15˚	0.0207	0.0185	2
36	19	17	30˚	0.0207	0.0185	3
36	19	17	45˚	0.0207	0.0185	4

The hot pipe will then be inclined at angle -15˚ and -30˚ to the vertical. For all the test cases, the flow rate at both hot and cold inlet will remain unchanged from that applied in case 1 (for the experiment).

After simulating all the test cases presented for a physical time of 10 seconds, the results are presented and discussed in the chapter that follows. The numerical simulation of flow parameters contributing to thermal fatigue at the mixing junction of the different pipes was performed for a physical time of 10s with a time step of 0.001 s. In order to ensure a fully developed flow conditions in both hot and cold legs prior to mixing, separate simulation were conducted for the flow of water in a vertical and horizontal tube (diameter of 0.1 m and 0.14 m respectively) having boundary conditions as that of the hot and the cold legs respectively.

CHAPTER FOUR

RESULTS AND DISCUSSION

4.1 Flow Temperature Fields

The results from the exit of the vertical and horizontal tubes shown in Figure 4.1 were extracted and imposed as inlets conditions for the varying angles of inclination of the flow geometry.

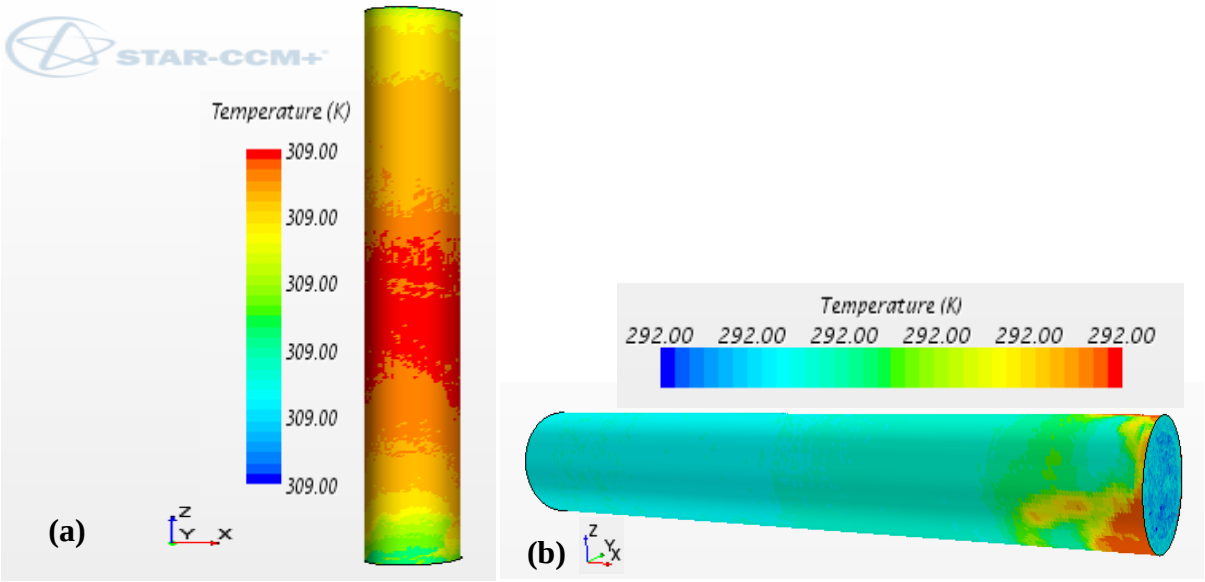

Figure 4.1: 3-D Flow Temperature Fields of vertical and horizontal tube; **(a)** hot leg, **(b)** cold leg

Data was extracted at 0.6, 1.6, 2.6 and 3.5D_{cold} along the downstream of the mixing junction. Figure 4.2 shows a representation of the segments where the data was retrieved.

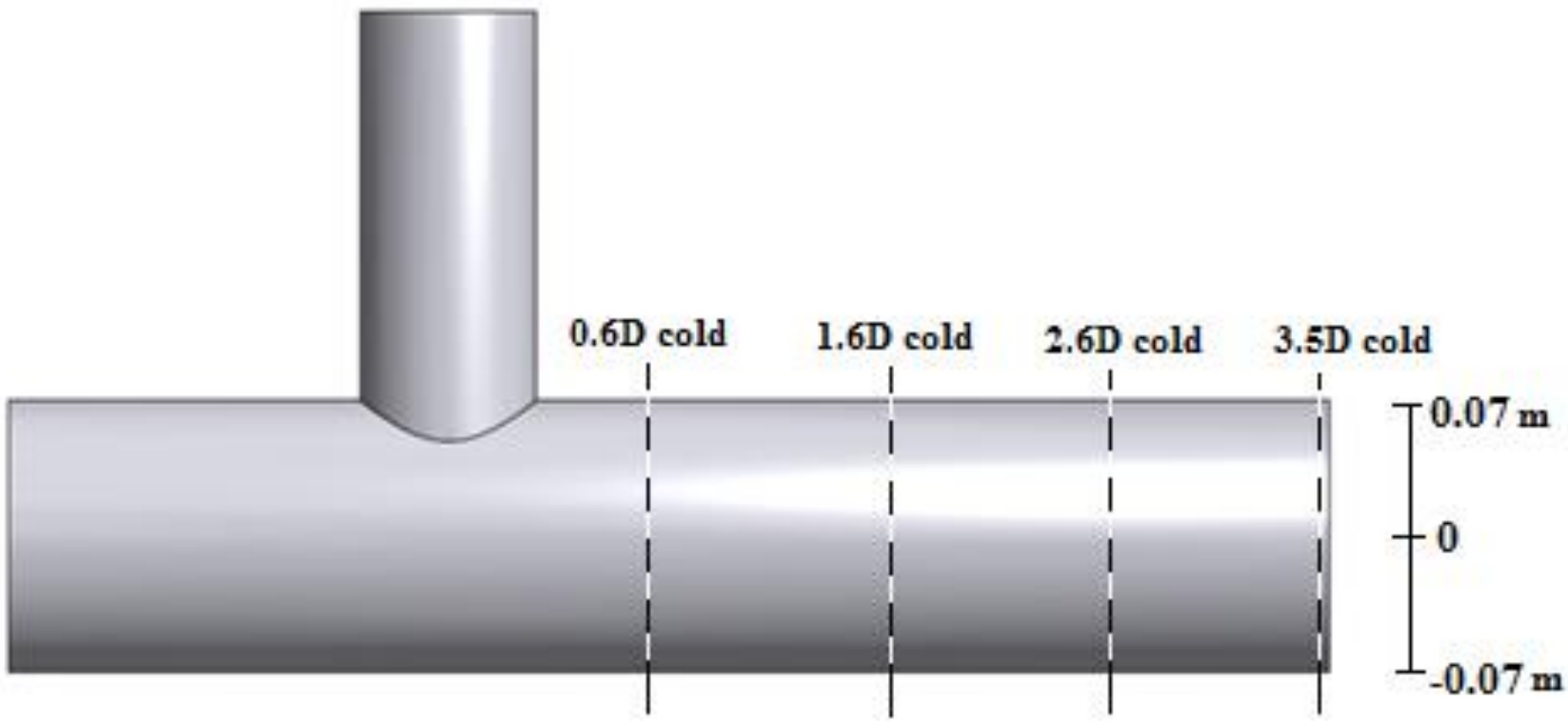

Figure 4.2: Radial positions at which data was extracted

4.2 Modeling Verification with Experimental Data

The turbulence models adopted for simulations were the k-omega turbulence model, the k-epsilon (k- ε) turbulence model and the V_2F turbulence model. In order to arrive at a suitable turbulence model that better predict the experimental results, a sensitivity analysis was conducted.

The results, from the sensitivity analysis as presented in Figure 4.3 shows a comparison of radial velocity distribution obtained at $x = 2.6D_{cold}$ for both experimental data and STAR-CCM+ data. As could be observed, there is an overall good agreement between the experiment and STAR-CCM+ predictions.

From the plot, k-ε turbulence model profile showed a close prediction to the experimental at $2.6D_{cold}$, the model prediction was better away from the wall boundaries. Its prediction in the main flow was in agreement with the experimental but deviated after radial position 0.01m from the center of the pipe. Relative to the prediction by the other turbulence models (SST k-ω model.) considered, the k-ε turbulence model poorly predicted the experimental results at the wall region.

The V_2F turbulence model prediction also agrees well with the prediction by the k-ε turbulence model. In the main flow, the V_2F model appreciably predicted the experimental data than the k-omega model. However nearer the wall boundary, the V_2F turbulence model poorly predicted the experimental data than the SST k-omega (k-ω) model.

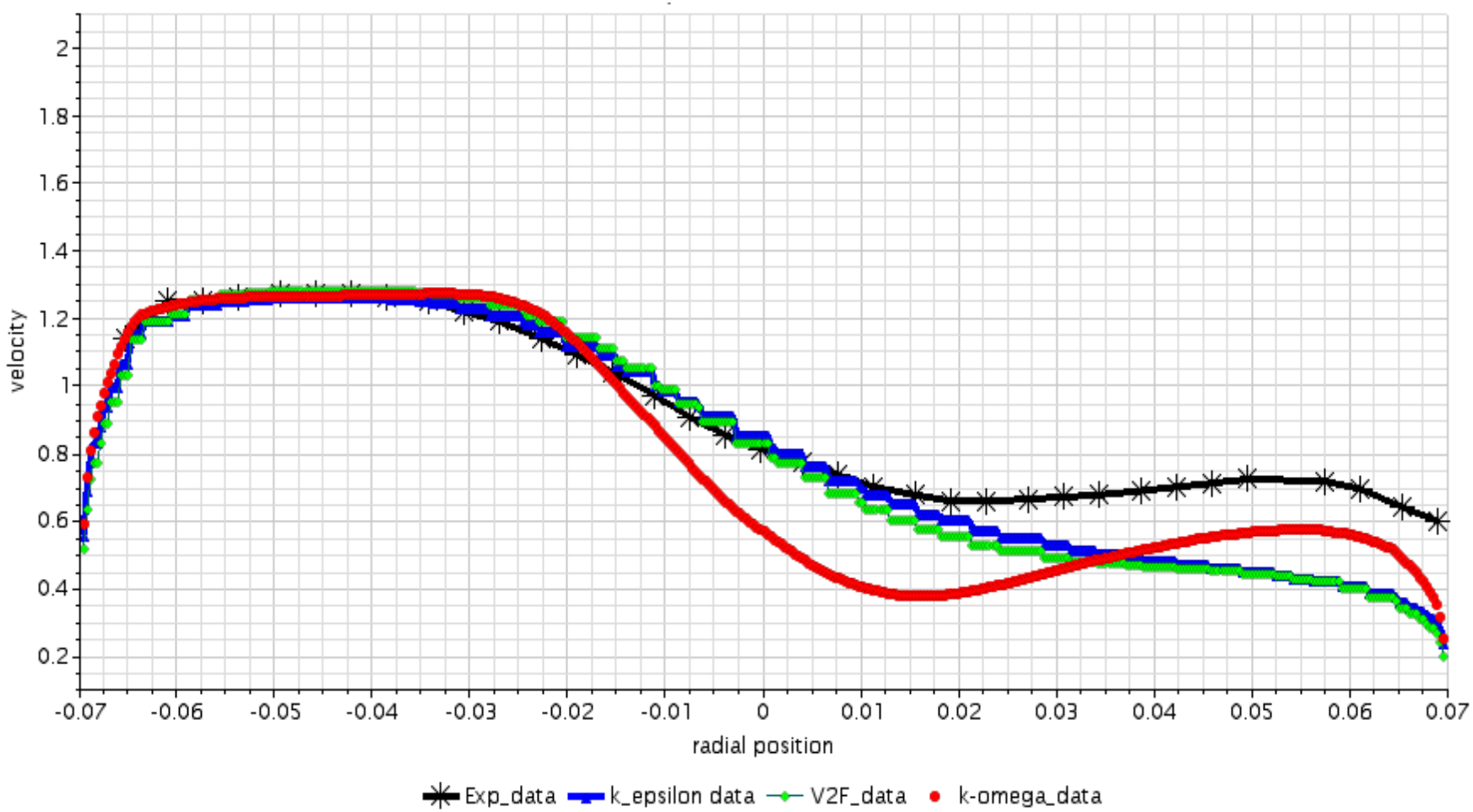

Figure 4.3: Plots of velocity distribution at 2.6 D cold for different turbulence models

In the main flow the k-ω turbulence model prediction at the $2.6D_{cold}$ deviated slightly from the experimental data when compared with the V_2F and k-ε turbulence models. Its prediction in the lower section of the pipe agrees with the experimental observation and the prediction by the other models but gradually deviated after radial position -0.02m. In the upper section of the pipe close to the wall boundary, the model appreciably predicted the experimental data than the V_2F and the k-ε turbulence models. Fluid temperature fluctuation caused by mixing are easily transferred to the structure when mixing takes place near the pipe wall boundary and this detail is important in fatigue analysis. For thermal fatigue, the main objective is to accurately predict significant fluctuation of flow variable near to the wall boundary. SST K- ω turbulent model prediction in the neighborhood of the wall boundary as observed was appreciable in relation to the experimental observation. Therefore the SST k- ω turbulent model was considered as the suitable model for the solution of the physical problem under consideration.

4.3 Effect of angle of Inclination

One of the aims of this study was to investigate the impact of angle of inclination on flow parameters that contribute to thermal fatigue at the mixing junction. This was achieved by inclining the angle of the branch pipe at 0, negative 15, 30 and 45 degrees anticlockwise to the vertical. The temperature results are shown in Figure 4.4 suggests that, the highest temperatures were observed at the sharp corner of the mixing junction and propagates

downstream the upper section of the main pipe as was similarly observed and reported by Timperi (2014).

The various flow inclinations were graphically evaluated and was observed that the branch angle affected the flow distribution. The influence of the branch angle temperature (inlet = 309 K) on the boundary wall downstream the mixing junction was more pronounced in Figure 4.4 (c) and (d) when compared to temperature (302 K) recorded at the wall boundary shown in Figure4.4 (a) and (b). Hence reducing the angle of inclination of branch pipe increased the range of the branch pipe to main pipe velocity (v_b/v_m). Hence there is no sufficient time for mixing to take place.

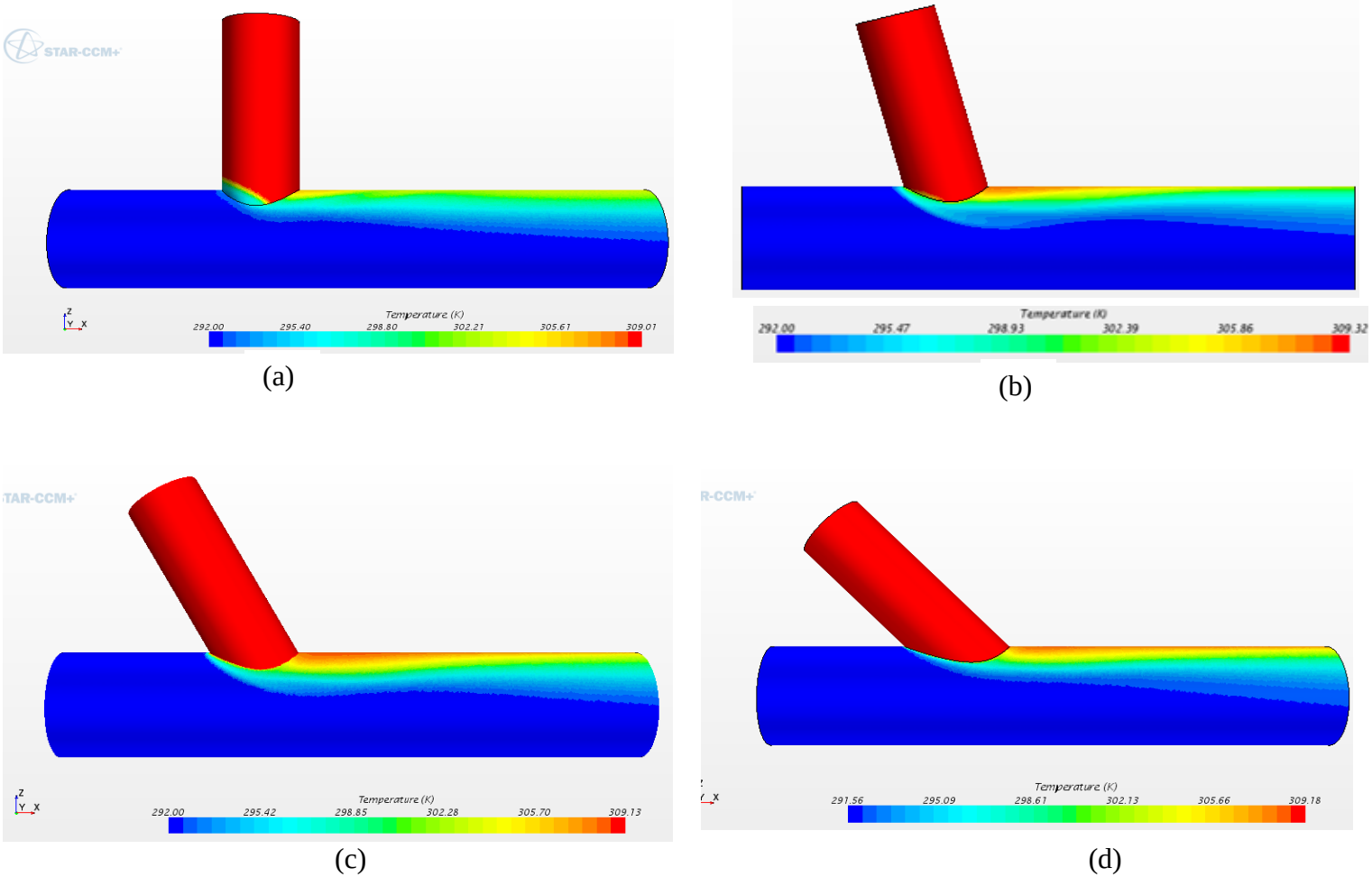

Figure 4.4: Scalar plots for temperature distribution at varying branch pipe inclination angle **(a)** 0 degree, **(b)** 15 degrees, **(c)** 30 degrees, **(d)** 45 degrees

4.3.1 Temperature Distribution

Figure 4.5 shows temperature distribution obtained at position $0.6D_{cold}$ cross section for varying angle of inclination of the branched pipe to the vertical axis. There existed temperature gradient between the upper section of the pipe and the lower section. Thermal stratification was therefore evident in the four diagrams.

However with the increase in angle of the branch pipe inclination, the hot flow from the branched pipe were swept by the cold fluid towards the upper boundary of the horizontal pipe downstream especially at 30 and 45 degrees inclination. At 0 degrees, the upper boundary registered lower temperature than what was observed at 15, 30 and 45 degrees. This implied more effective flow mixing at 0 degrees inclination of the branched pipe than at 15, 30 and 45 degrees.

The comparatively low temperature recorded at the upper section of the pipe at 0 degrees indicates low stress propagation through the structural material of the pipe when compared to temperatures recorded at 15, 30 and 45 degrees.

Observations made in Figure 4.5 were confirmed by the comparison of normalized temperature at $0.6D_{cold}$ for the varying angles of 0, 15, 30 and 45 degrees as shown in Figure 4.6. At 30 and 45 degrees the instantaneous temperature recorded at the upper boundary of the horizontal pipe are very close in magnitude to the hot leg temperature, ($T \approx T_{hot}$). Hence there is negligible mixing of the cold and hot fluid at these mixing of the cold and hot fluid at these inclinations.

At the inclination angle of 15 degrees of the branched pipe (hot leg), higher instantaneous temperature is recorded at the upper boundary of the horizontal pipe downstream when compared to 0 degree inclination of the branched pipe. It could therefore be stated that effective mixing of cold fluid with the hot fluid is achieved at 0 degrees inclination to the vertical (i.e. 90^{o} to the horizontal). This effective mixing will lead to reduced and uniform temperature field at the pipe wall boundary and hence lower thermal stress levels in the structural material.

The effectiveness of the mixing of the cold fluid and the hot fluid along the mean flow can be observed in Figure 4.5 and graphically illustrated in Figure 4.6. Similar observations were made in the 1.6, 2.6 and $3.5D_{cold}$ (See *Appendix I).*

.

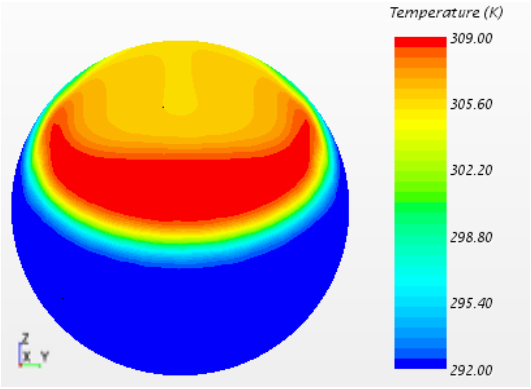

Fig. (a): 0 degree inclination

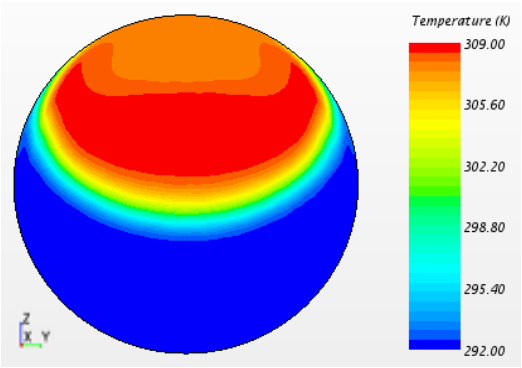

Fig. (b): 15 degree inclination

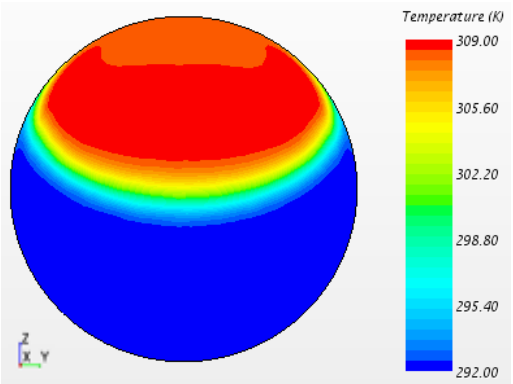

Fig. (c): 30 degree inclination

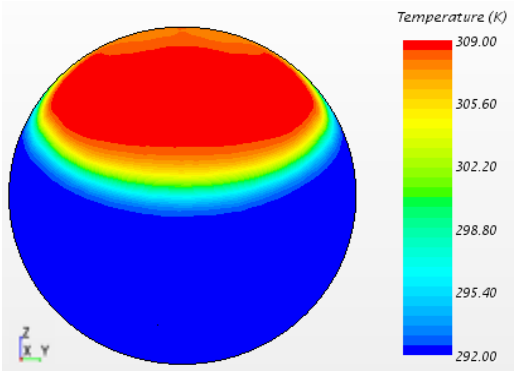

Fig. (d): 45 degree inclination

Figure 4.5: Temperature distribution at 0.6D cold

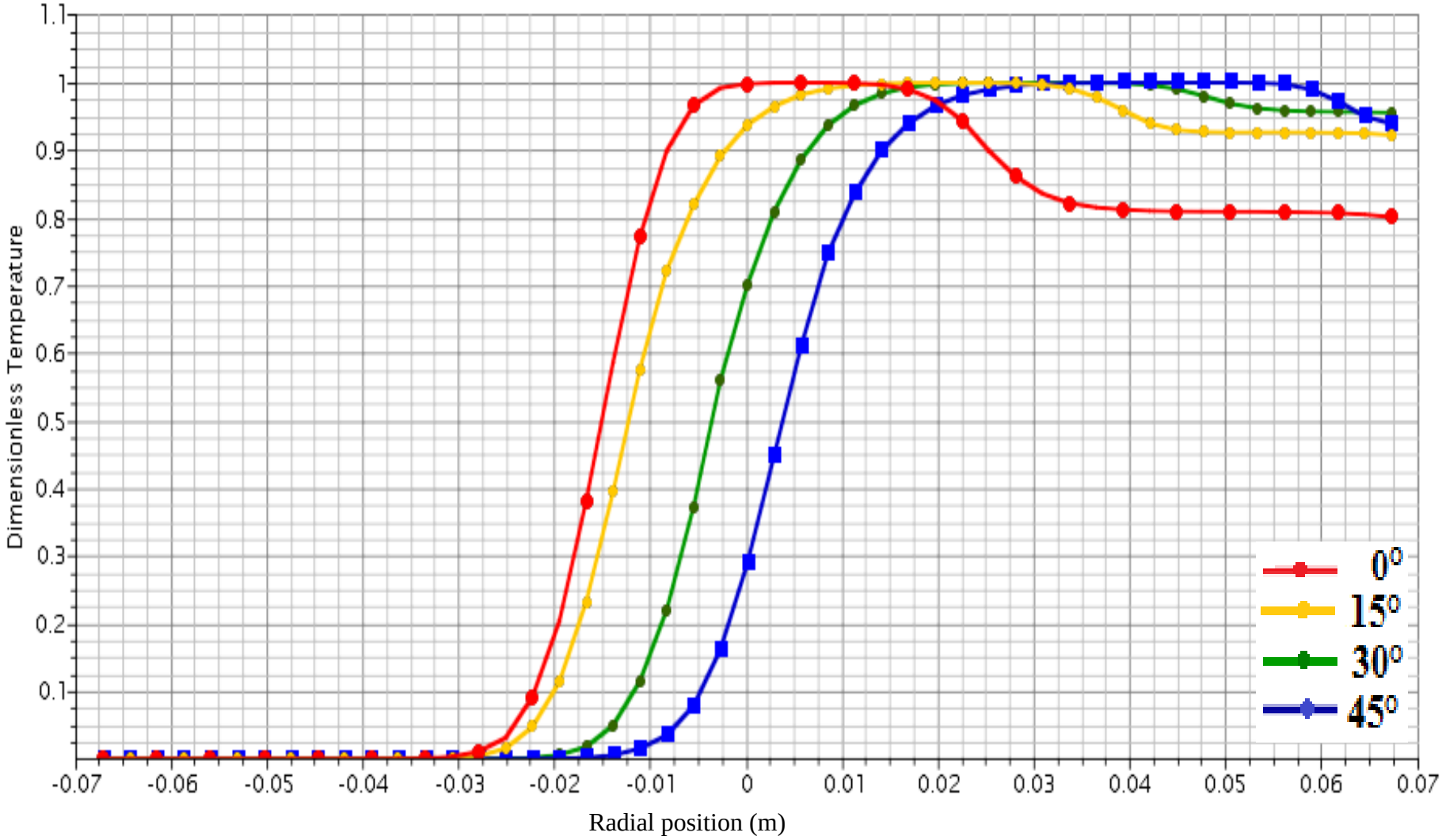

Figure 4.6: Dimensionless temperature distribution at 0.6D cold

4.3.1.1 Thermal Equilibrium

In thermal mixing, both the magnitude of thermal load and length required to reach thermal equilibrium are significant. Information about thermal fatigue related failure can be obtained from the magnitude and intensity of thermal load (Ayhan & Sökmen, 2013).

With increase in the angle of inclination of the branch pipe from 0 degree to 45 degrees anticlockwise, the radial length at which thermal equilibrium was reached decreases. This is because the vortex (area of effective mixing) that was generated after the hot and cold streams meet increases with increase in angle of inclination of the branch pipe.

While the radial length at which thermal equilibrium is reached for 0 degree to 45 degrees decreases, the magnitude of temperature field increases. This can be observed in Figure 4.7. The magnitude of temperature fluctuations gives information about the magnitude of induced thermal load. It is evident that while branch angle decreases, the magnitude of thermal load increases but, at the same time, the radial length at which thermal equilibrium is reached decreases. The magnitude of the fluid temperature at equilibrium is propagated through the material as thermal loads.

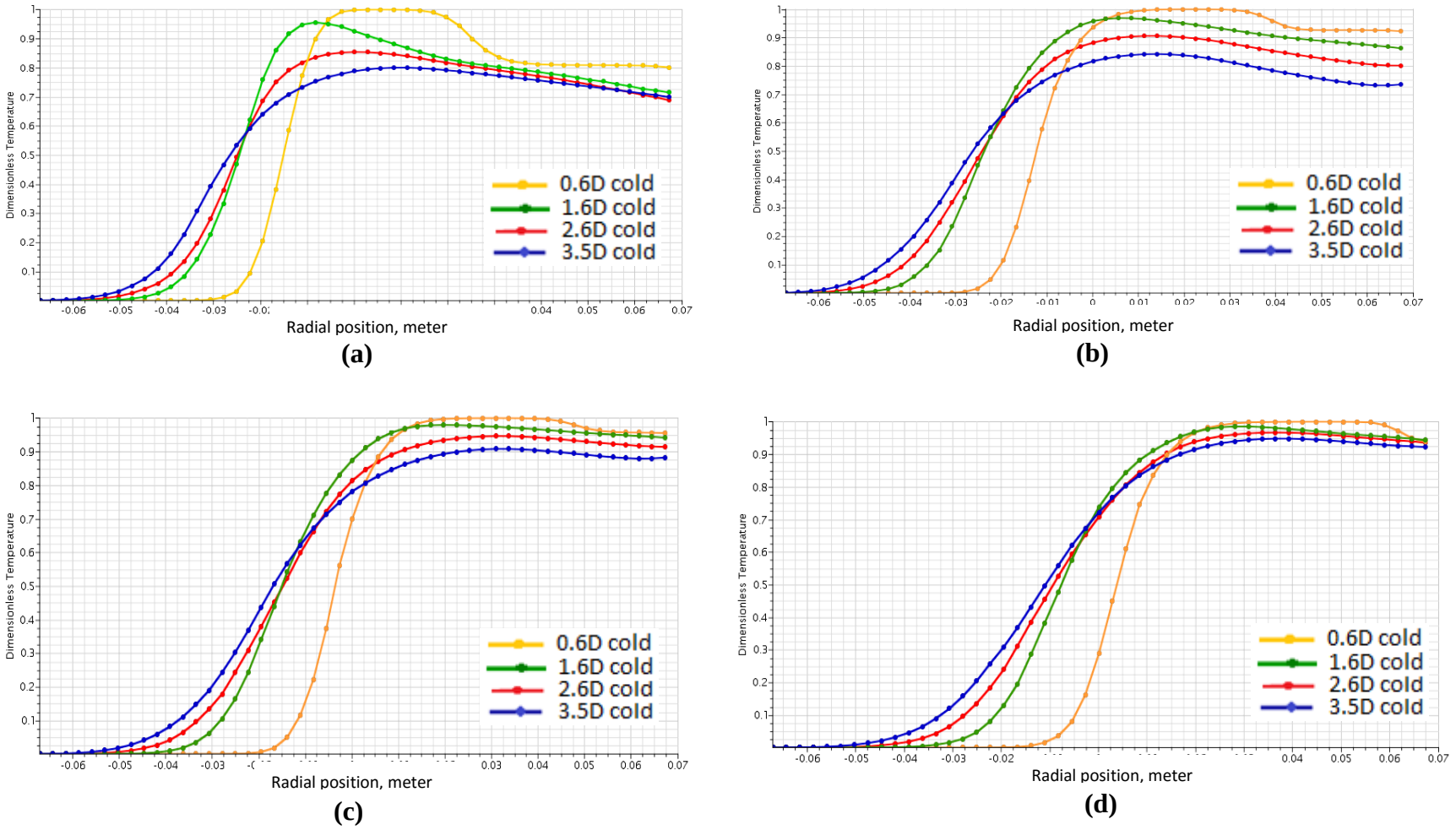

Figure 4.7: Comparison of dimensionless temperature distribution for; 0 degrees (a), 15 degrees (b), 30 degrees (c), 45 degrees (d)

4.3.2 Turbulence Intensity

Figures 4.8 shows a scalar scene of turbulence distribution and Figure 4.9 shows plots of turbulent intensity at position $0.6D_{cold}$ for varying angle of 15, 30 and 45 degrees to the vertical.

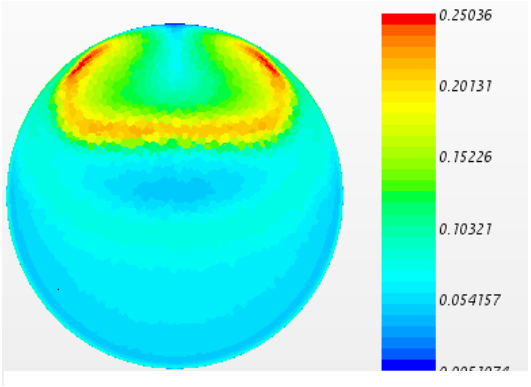

Fig.(a): 0 degree inclination

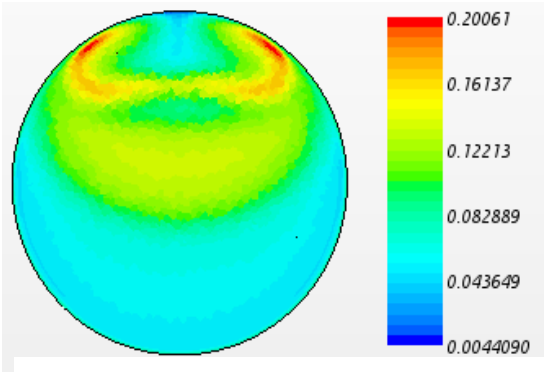

Fig.(b): 15 degree inclination

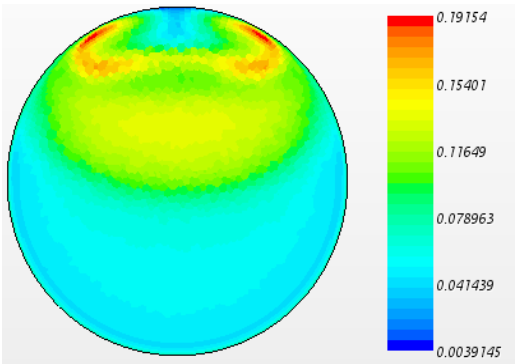

Fig.(c): 30 degree inclination

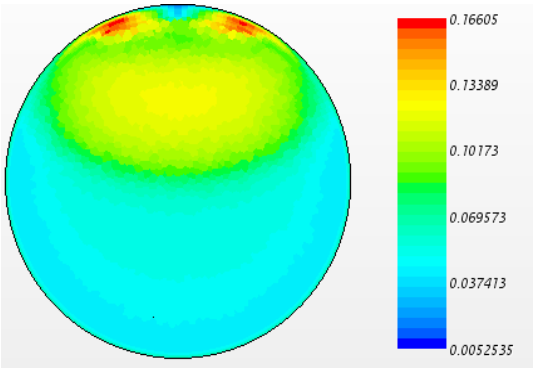

Fig.(d): 45 degree inclination

Figure 4.8: Scalar scene of Turbulence Intensity distribution at 0.6D cold

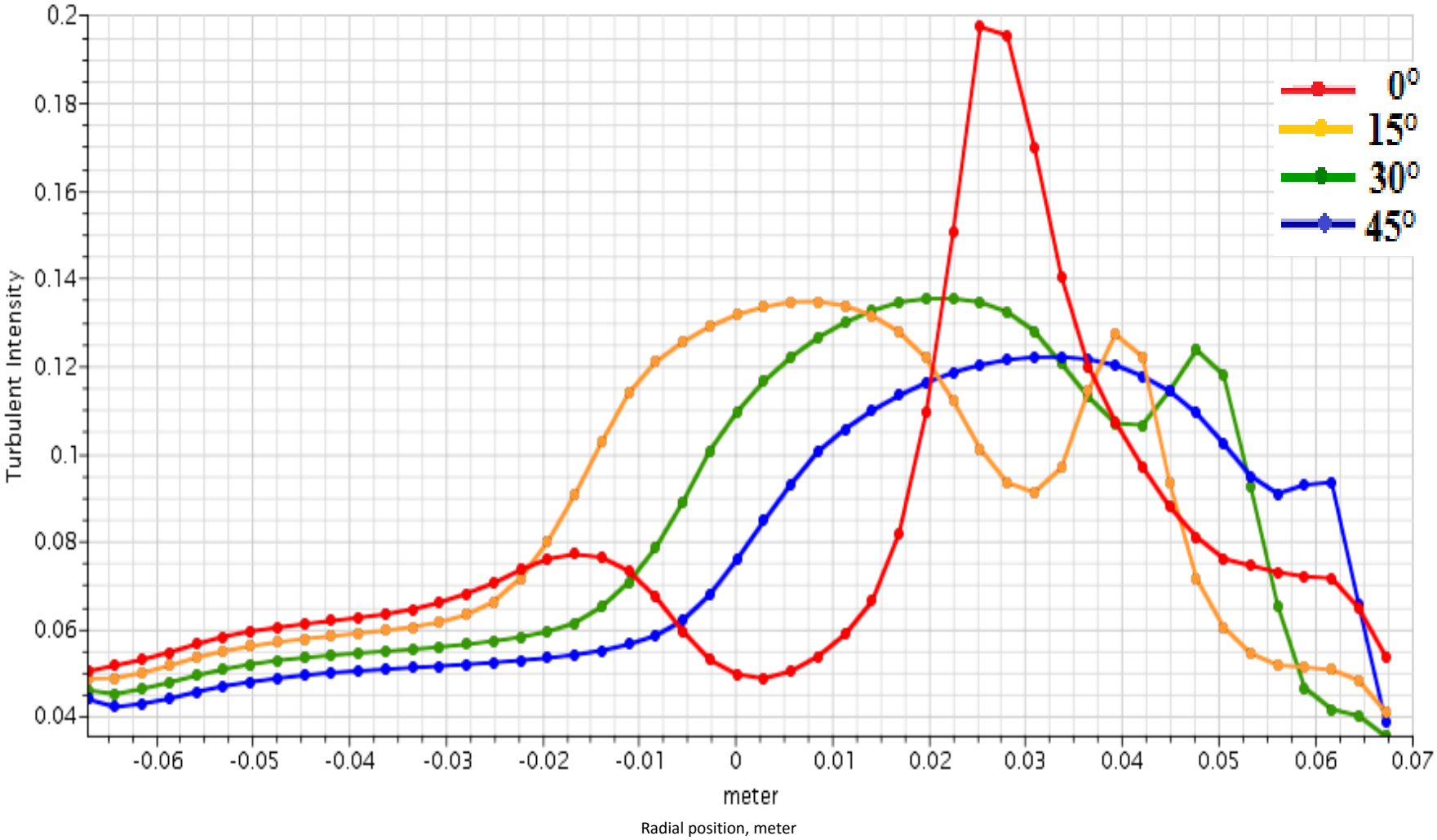

Figure 4.9: Turbulence Intensity distribution at 0.6D cold

It could be observed from figure 4.9 that the turbulence intensity was varying from the upper section to the lower section, and decays as it moves towards the upper wall. The highest turbulence intensity was recorded when the branch pipe was inclined at 0 degree to the vertical with the inclination at 45 degrees recording the lowest turbulence intensity. The highest peaks however, was recorded far away from the wall boundary (in the main flow).

For all four different angles of inclination, the turbulence intensity that was generated at the lower section remains nearly constant and is unaffected by the mean flow velocity; since the mean flow velocity is nearly constant in the lower section as well.

On the contrary, moving further downstream the mixing junction (for positions 0.6D, 1.6D, 2.6D and $3.5D_{cold}$) the peak value of turbulence intensity shifts towards the lower section. This is due to more disturbances propagating downstream which leads to uniform mixing in the bulk flow and not only in the upper section of the main pipe as shown in Figure 4.9.

An increase in turbulence intensity leads to an increase in the value of Nusselt number (Crowe, 2005), hence an increase in the heat transfer from the fluid to the structure. Therefore with 0 degree inclination recording the highest turbulence intensity at the wall boundary, it can be deduced that heat transfer from the hot fluid to the cold fluid will be effective leading to the attainment of thermal equilibrium and hence reduces the buildup of temperature at the wall boundary as compared to what prevails at the other angles of inclination. Increasing the angle of inclination of the branch pipe to the vertical from 0

degree to 45 degrees anticlockwise decreases the turbulence intensity and consequently decreasing the heat transfer from the hot fluid to the cold fluid. It can however be observed that, for the three different positions downstream the mixing junction (1.6D, 2.6D and $3.5D_{cold}$), that the highest peak of turbulence intensity which was recorded at 0 degree inclination occurred far from the wall boundary with the least peak occurring closer to the wall boundary as shown in Figure 4.10.

Moving, downstream the mixing junction, the magnitude of turbulence intensity decreases and the highest peak of turbulent intensity shifts from the wall boundary towards the main flow and there is a decay in turbulence in turbulence intensity as shown in *appendix II*.

Turbulence mixing is therefore more evident at 0 degree inclination angle in comparison to the other angles of inclination.

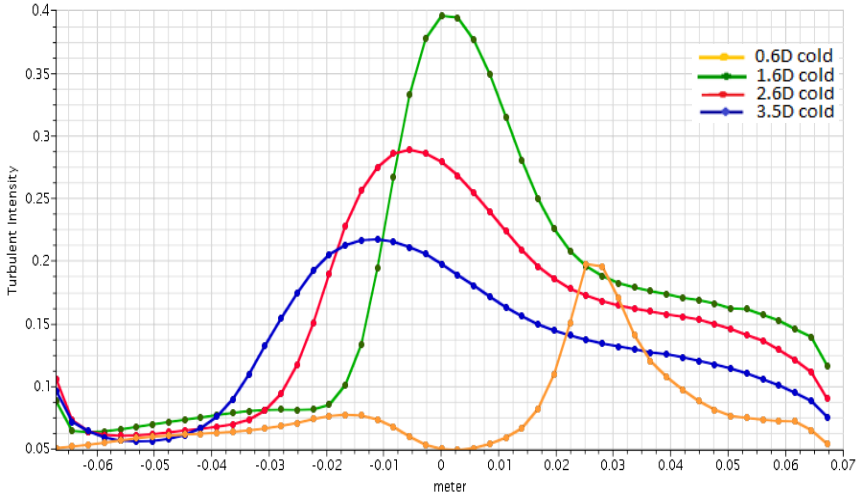

Fig.(a): 0 degree inclination

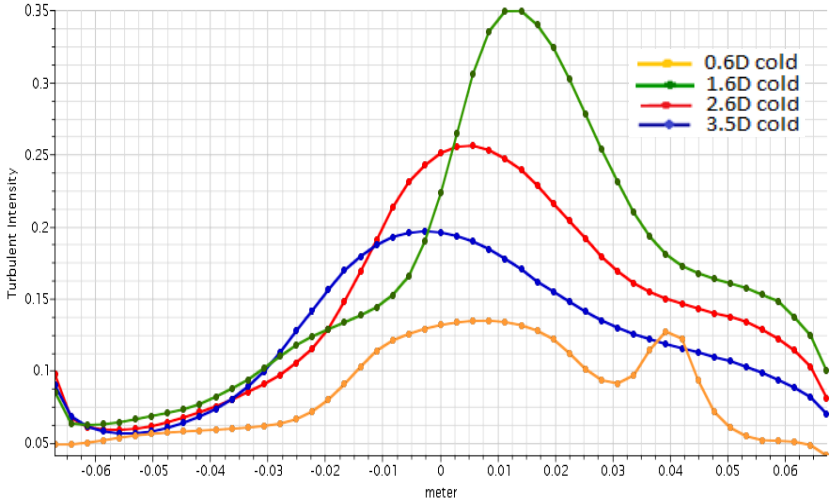

Fig.(b): 15 degree inclination

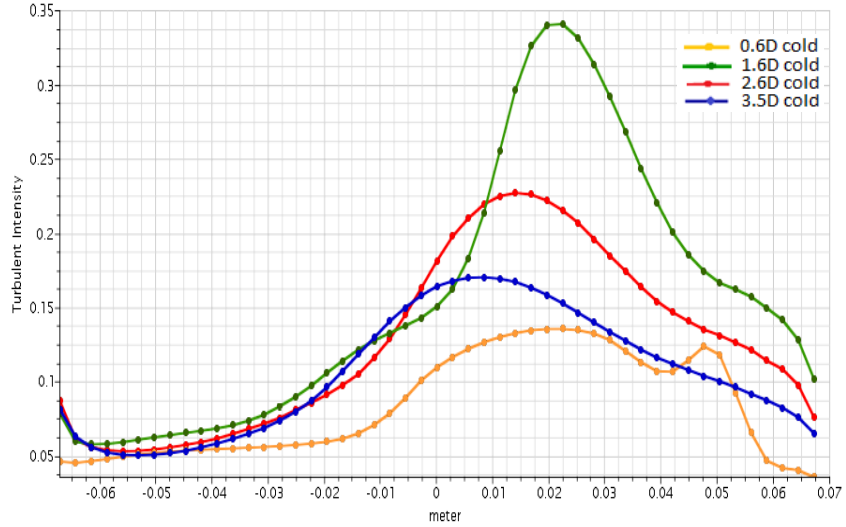

Fig.(c): 30 degree inclination

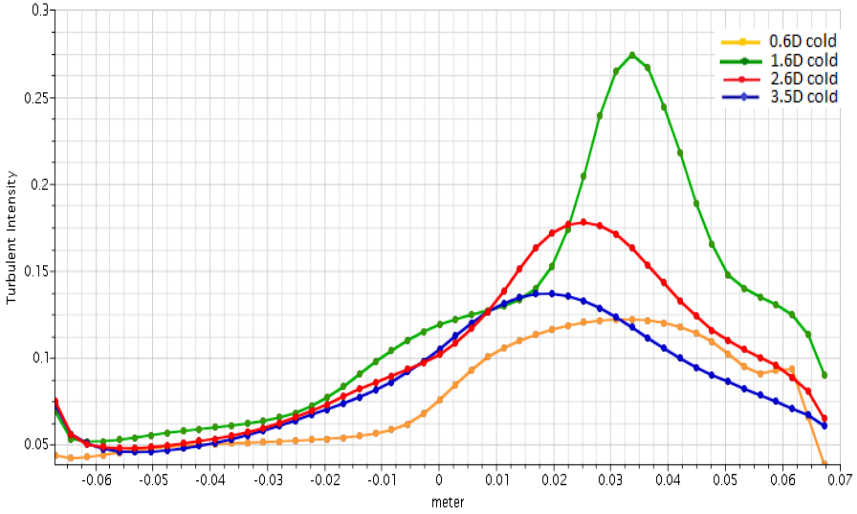

Fig.(d): 45 degree inclination

Figure 4.10: Decay of Turbulence Intensity for varying angles of inclination

4.3.3 Pressure Distribution

Pressure loss in a mixing channel is the effort required to achieve effective mixing as reported by Kockmann (2007). In order to analyze the mechanism of thermal fatigue, the pressure distributions downstream the mixing junction of the different inclinations were studied. Figure 4.11 is the comparison of pressure distributions along the centerline in the mean flow direction from the mixing junction to the outlet. The results were obtained for the 0, 15, 30 and 45 inclination angles.

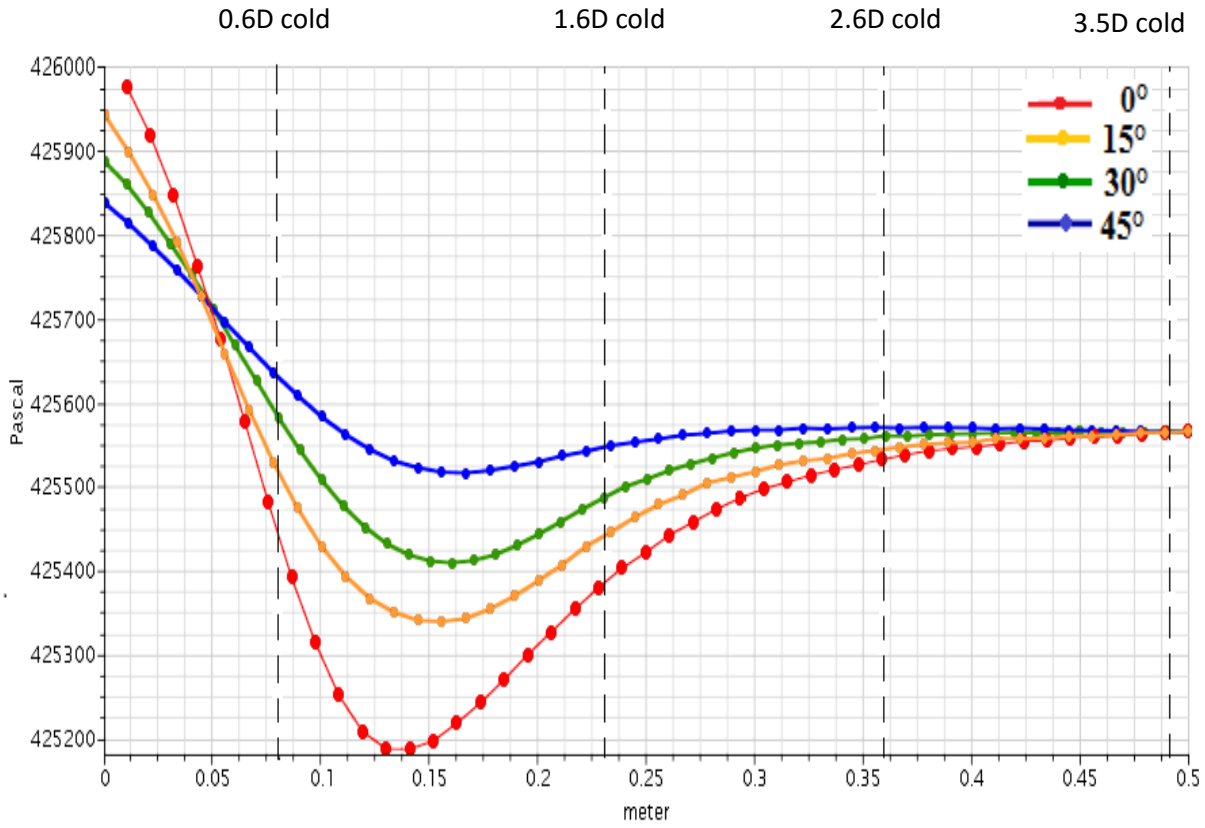

Figure 4.11: Pressure Distribution downstream the mixing junction for varying angles

The profile indicates that the pressure at all the various inclinations of the branch pipe dropped at the mixing junction and further downstream at an axial length of 0.15 m. The 0 degree inclination recorded the highest pressure drop with 45 degrees inclination recording the least pressure drop. The pressure drop in the mixing process are as a result of momentum exchange, friction and heat exchange. The quality of mixing reflects the interaction intensity between the two flows and is related to the pressure drop, the better the mixing effect, the higher the pressure drop because more energy is consumed in the process. It can be inferred that, the variation in the inclination angles caused differences in pressure and energy loss because the liquid velocities entering the main channel was constant for all inclinations and pressure drop decreases as the angle of inclination is increased hence less effective mixing.

The intensity of mixing decreases as the liquid flows downstream and the pressure along the centerline begins to stabilize.

4.3.4 Velocity Distribution

The simulation results were visualized and the fluid velocity distribution downstream the mixing junctions are shown in Figures 4.12. For position $0.6D_{cold}$, the influence of the mixing junction was still seen for all cases considered, the velocities were of a much higher magnitude compared to velocity magnitudes at positions further downstream the mixing junction.

Increasing the angle of inclination of the branch pipe to the vertical from 0 degree to 45 degrees anticlockwise can increase the range of the branch pipe to main pipe velocity (vb/vm). As a result, the velocity at 45 degree inclination propagates closer to the wall at all positions downstream the mixing junction in comparison to the other angles of inclination of branch pipe. This trend decreases with decreasing angle of inclination of the branch pipe and it can be observed in Figure 4.13. Other graphical illustrations of this trend are reported in *Appendix III.*

Higher velocities at the wall boundary means an increase in the heat transfer from the main fluid flow to the wall boundary, the flow streams will not have sufficient time to mix and there will be higher temperature buildup at the wall boundary. The highest velocity magnitude in the main flow was recorded when the branch pipe was inclined at 0 degree to the vertical with the inclination at 45 degrees recording the lowest. It can be deduced that, rapid mixing takes place in the main flow and heat transfer from the hot fluid to the

cold fluid will be effective leading to the attainment of thermal equilibrium and hence reduced buildup of temperature at the wall boundary.

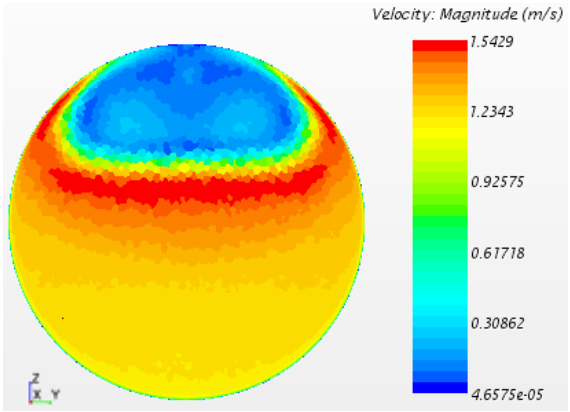

Fig.(a): 0 degree inclination

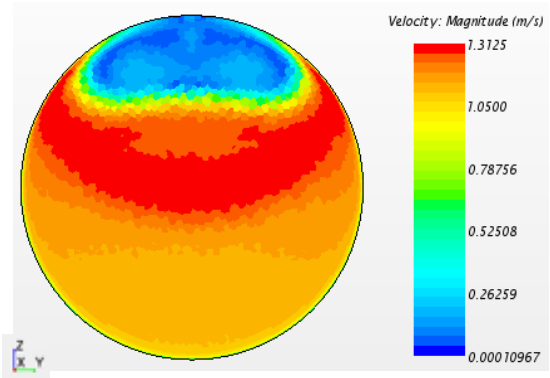

Fig.(b): 15 degree inclination

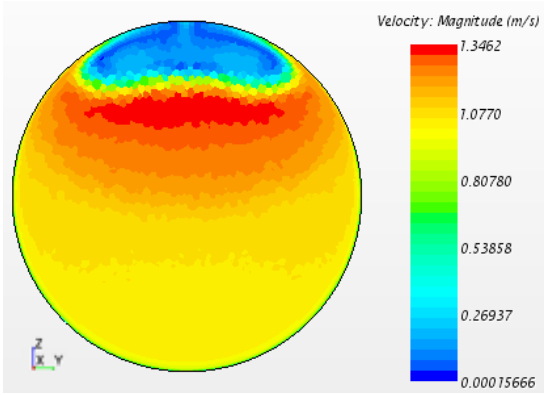

Fig.(c): 30 degree inclination

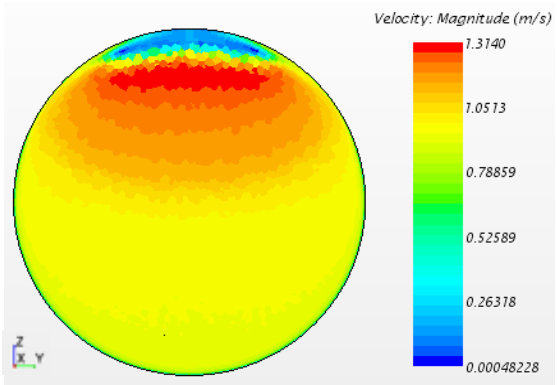

Fig.(d): 45 degree inclination

Figure 4.12: Velocity distribution at 0.6D cold

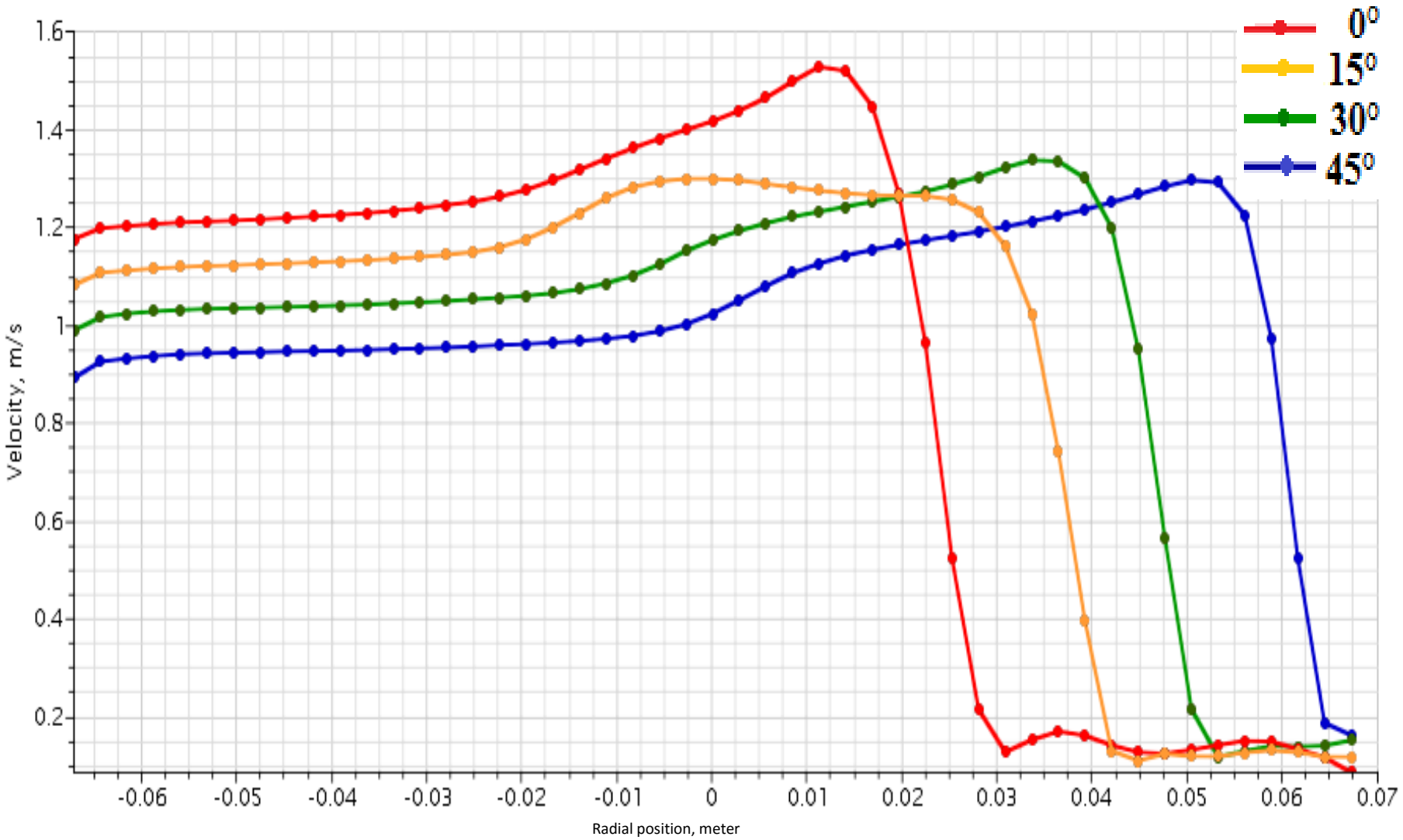

Figure 4.13: Velocity distribution at 0.6D cold

It is shown in figure 4.13 and (as well as *Appendix III*) that for all four different angles of inclination, moving downstream the mixing junction, the velocity magnitude decreased and the highest velocity shifted from the wall boundary towards the main flow thereby leading to uniform mixing in the bulk flow.

4.3.5 Mass Flow rate

Figures 4.14 and 4.15 show mass flow rate obtained at position 0.2 and 0.4 m respectively for varying angle of inclination of the branched pipe to the vertical axis. It could be observed that, the flow rate is maximum in the main flow for all angles of inclination of branch pipe. Both hot and cold fluid molecules flow possess kinetic energy, the turbulence created in the mixing junction increases the kinetic energy of the fluid. The cold water sweeps the hot water upwards causing stagnation in the upper section (lower mass flow rate).

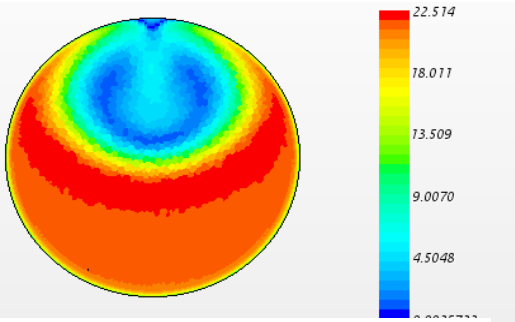

Fig.(a): 0 degree inclination

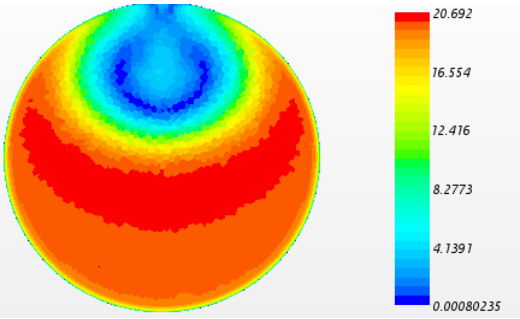

Fig.(b): 15 degree inclination

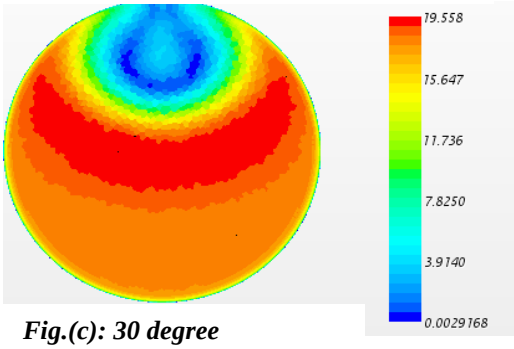

Fig.(c): 30 degree inclination

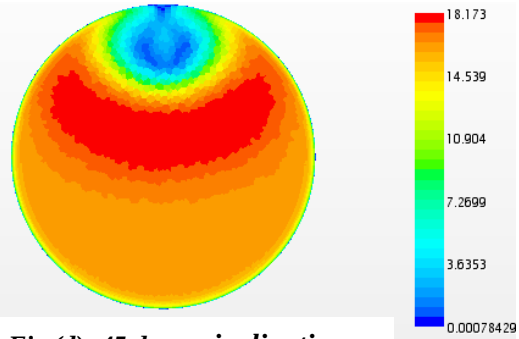

Fig.(d): 45 degree inclination

Figure 4.14: Mass Flow rate along main pipe at 0.2 m

Moving further downstream the mixing junction, there is bulk flow mixing. It can be deduced that, rapid mixing takes place in the main flow and heat transfer from the hot fluid to the cold fluid will be effective leading to the attainment of thermal equilibrium.

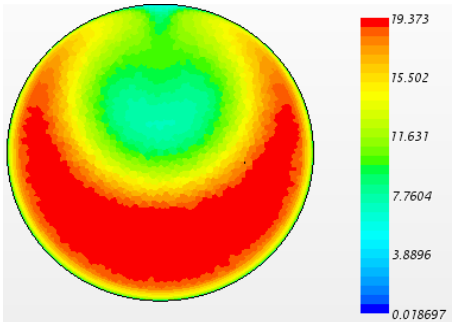

Fig.(a): 0 degree inclination

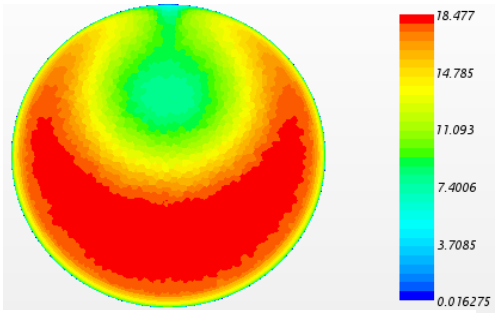

Fig.(b): 15 degree inclination

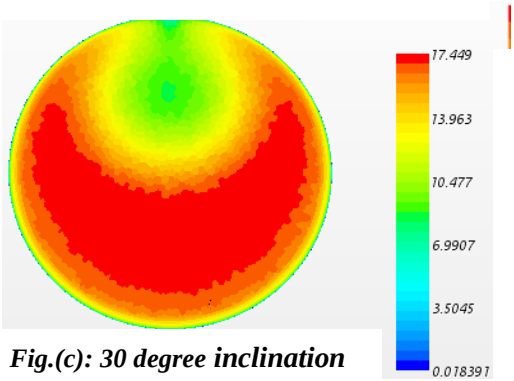

Fig.(c): 30 degree inclination

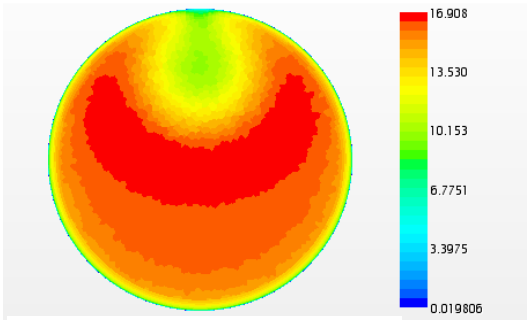

Fig.(d): 45 degree inclination

Figure 4.15: Mass Flow rate along main pipe at 0.4m

CHAPTER FIVE

CONCLUSIONS AND RECOMMENDAIONS

5.1 CONCLUSIONS

Numerical simulations of flow parameters contributing to thermal fatigue in a mixing junction with different angles of inclination of the branch pipe were conducted using k-omega turbulence model in STAR-CCM+. Comparison between dimensionless temperature, turbulence intensity, pressure and velocity distribution for the different types of branch pipe angles was carried out. The key findings are as follows:

- After the sensitivity analysis on the turbulence models were carried out, SST k- ω turbulent model was considered the suitable model and hence used for the solution of the physical problem under consideration.
- The dimensionless temperature registered in the 0 degree inclination of branch pipe were lower at the wall boundary at the upper boundary of the horizontal pipe than that observed in the 15, 30 and 45 degrees branch pipe inclination under the same boundary conditions. This implied that, effective mixing of cold and hot fluid which led to reduced and uniform temperature field at the pipe wall boundary, were achieved at 0 degree inclination of branch pipe; hence lower stress levels could be observed in the structural material of the pipe.

- The comparison of the velocity gradient near the wall indicates that the heat transfer from the main fluid flow to the wall boundary in the 45 degree inclination is much higher than that in 0, 15 and 30 degrees inclination of branch pipe, so the differences in angle of inclination of branch pipe accounts for the differences in the velocity distribution. The effect of higher velocity gradient near the upper wall boundary of the horizontal (main) pipe is temperature buildup at the wall boundary. This is due to insufficient time for the different flow streams to mix. 0 degree branch pipe inclination recorded the highest velocity magnitude in the main flow and lowest velocity magnitude near the wall boundary, indicating that, rapid mixing takes place in the main flow and heat transfer from the hot fluid to the cold fluid is effective thereby leading to the attainment of thermal equilibrium.

- Zero degree inclination recorded the highest turbulence intensity at the wall boundary, thus heat transfer from the hot to the cold fluid is considered effective thereby leading to the attainment of thermal equilibrium and hence reduced buildup of temperature at the wall boundary as compared to what was obtained at the other angles of inclination. Increasing the angle of inclination of the branch pipe to the vertical from 0 degree to 45 degrees anticlockwise decreases the turbulence intensity and consequently decreases the heat transfer from the hot fluid to the cold fluid. Turbulence mixing is therefore more evident at 0 degree inclination angle in comparison to the other angles of inclination.

- The pressure drop at 0 degree inclination (T-junction) were much higher than that in the 15, 30 and 45 degrees inclination of branched pipe under the same boundary conditions, effective mixing will therefore be achieved with 0 degree inclination and the least mixing effect with 45 degrees inclination. The quality of mixing reflects the interaction intensity between the two flows and is related to the pressure drop, the better the mixing effect, the higher the pressure drop because more energy is consumed in the process. It can be concluded that, the variation in the inclination angles caused differences in pressure and energy loss because, the liquid velocities entering the main channel was constant for all inclinations while pressure drop decreases as the angle of inclination is increased hence less effective mixing.

5.2 RECOMMENDATIONS

This research only considered fluid to fluid interaction hence further research should be conducted on Fluid Structure Interaction.

Lower temperatures were employed in this research based on the experimental facility used hence further work may be done with temperature scale up to the operating temperatures of PWR and BWR. Operating temperatures relating to proposed supercritical reactors can also be investigated.

In order to study the gradual degradation mechanism, The Department of Nuclear Engineering may acquire a structural mechanics code to enhance the determination of stresses induced in the pipe by the temperature fluctuations.

REFERENCES

Aulery, F., Toutant, A., Monot, R., Brillant, G., & Bataille, F. (2010). Numerical simulations of thermal fatigue due to turbulent fluctuations in a mixing tee. In Proc. 16th *International Solar Paces Concentrating Solar Power Symposium* (pp. 21-24).

Ayhan, H., & Sökmen, C. N. (2013). CFD Modeling of Thermal Mixing In T-junction: Effect of Branch Pipe Diameter Ratio. The 15th *International Topical Meeting on Nuclear Reactor Thermal - Hydraulics*, NURETH-15, Pisa, Italy.

Babiano, A., Boffetta, G., Provenzale, A., & Vulpiani, A. (1994). Chaotic advection in point vortex models and two-dimensional turbulence. *Physics of Fluids*, 6(7), 2465-2474.

Bardina, J.E., Huang, P.G., Coakley, T.J. (1997). Turbulence Modeling Validation, Testing, and Development. *NASA Technical Memorandum* 110446, California, U.S.A.

Chien, K. (1982). Predictions of Channel and Boundary-Layer Flows with a Low-Reynolds Number Turbulence Model, *AIAA Journal*, Vol. 20,No. 1, pp.33-38.

CD-adapco (2008). Computational Fluid Dynamics (CFD) Basics. *Americas Agency Training Document.*

Clayton T. Crowe (2005). *Multiphase Flow Handbook*. Technology and Engineering, CRC Press, pp. 1-64.

Egorov, Y., Menter, F. R., Lechner, R., & Cokljat, D. (2010). The Scale-Adaptive Simulation Method for Unsteady Turbulent Flow Predictions. Part 2: Application to Complex Flows. Flow, Turbulence and Combustion, 85(1), 139–165. doi:10.1007/s10494-010- 9265-4

Faidy, C., Chapuliot, S., & Mathet, E. (2005). Thermal fatigue of reactor components in OECD- NEA member countries: A threefold programme to enhance cooperation. In *Proceedings of 18th international conference* on structural mechanics in reactor technology.

Garlapati, P. (2012). Modeling and Analysis of Intake Manifold for a Compression Ignition engine using STAR CCM+ / Doctoral dissertation, California State University, Sacramento, USA.

Hannink, M. H. C., Kuczaj, A. K., Blom, F. J., Church, J. M., & Komen, E. M. J. (2008). A coupled CFD-FEM strategy to predict thermal fatigue in mixing tees of nuclear reactors. *In Proc. Of EUROSAFE Forum*, Paris, France.

Jayaraju, S. T., Komen, E. M. J., & Baglietto, E. (2010). Suitability of wall-functions in large eddy simulation for thermal fatigue in a T-junction. *Nuclear Engineering and Design*, 240(10), 2544-2554.

Jhung, M. J. (2013). Assessment of Thermal Fatigue in Mixing Tee by Fluid Structure Interaction Analysis. *Nuclear Engineering and Technology*, 45(1), 99-106.

Jones, W. P., and Launder, B. E. (1972). The prediction of Laminarization with a Two-Equation Model of Turbulence. *International Journal of Heat and Mass Transfer*, vol.15, pp.301-314

Jungclaus, D. (1998). "Common IPSN/GRS Safety Assessment of Primary Coolants Unisolable Leak Incidents caused by Stress Cycling", *NEA/CSNI Specialist Meeting* on Experience with Thermal Fatigue in LWR Piping caused by Mixing and Stratification, OECD/NEA, Paris France, 7-12.

Khinchin, A.I. (1949). Mathematical Foundation of Statistical Mechanics. *Dover Publications*. ISBN 0-486-60147-1.

Kockmann, N. (2007). Transport Phenomena in Micro Process Engineering. *Springer Publication*. ISBN 978-3-540-74616-4.

Kuczaj, A. K., Komen, E. M. J., & Loginov, M. S. (2010). Large-Eddy Simulation study of turbulent mixing in a T-junction. *Nuclear Engineering and Design*, 240(9), 2116-2122.

Launder, B. E., and Sharma, B. I. (1974). Application of the Energy Dissipation Model of Turbulence to the Calculation of flow Near a Spinning Disc, *Letters in Heat and Mass Transfer,* vol. 1, no. 2, pp. 131-138.

Manera, A., Prasser, H. M., Lechner, R., & Frank, T. (2009). Toward the prediction of temperature fluctuations by means of steady RANS for the estimation of thermal

fatigue. In Proc. *13th International Topical Meeting* on Nuclear Reactor Thermal Hydraulics (NURETH-13) (Vol. 27).

Menter, F. R. (1993). Zonal Two Equation k- Turbulence Model for Aerodynamic Flows. *AIAA Paper* 93-2906.

Menter, F. R. (1994). Two-Equation Eddy Viscosity Turbulence Models for Engineering Applications. *AIAA Journal*, vol. 32, no. 8, pp. 1598-1605.

Moin, P., & Mahesh, K. (1998). Direct numerical simulation: a tool in turbulence research. *Annual review of fluid mechanics*, 30(1), 539-578.

Nakamura, A., Utanohara, Y., Miyoshi, K., & Kasahara, N. (2015). A Review of Evaluation Methods Developed for Numerical Simulation of the Temperature Fluctuation Contributing to Thermal Fatigue of a T-junction Pipe, 6, 118–130.

Narasimhamurthy, V. D. (2004). Unsteady-RANS Simulation of Turbulent Trailing Edge Flow / Thesis for the Degree of Master of Science, Chalmers University of Technology G¨oteborg, Sweden.

Ndombo, J. M., & Howard, R. J. (2011). Large Eddy Simulation and the effect of the turbulent inlet conditions in the mixing Tee. *Nuclear Engineering and Design*, 241(6), 2172-2183.

Ohshima, H., Muramatsu, T., Kobayashi, J., & Yamaguchi, A. (1994). Current status of studies on temperature fluctuation phenomena in LMFBRs. *In Proc. of IAEA Specialist Meeting* on Correlation between Material Properties and Thermo hydraulics Conditions in Liquid Metal Cooled Fast Reactors (LMFRs).

Prasser, H.-M., Krepper, E., Lucas, D. (2002). Evolution of the Two-Phase Flow in a Vertical Tube - Decomposition of Gas Fraction Profiles according to Bubble Size Classes using Wire- Mesh Sensors*", International Journal of Thermal Sciences*, Vol. 41, pp. 17-28.

Pope, S. B. (2000). Turbulent flows. *Cambridge university press, Sussex*, U.K.

Prawoto, Y. (2013). *Solid Mechanics for Materials Engineers* - Principles and Applications of Mesomechanics. Lulu.com. Retrieved from https://books.google.com/books?id=Z98HBgAAQBAJ&pgis=1

Qian, S., Frith, J., & Kasahara, N. (2010). Classification of low patterns in angled T-junctions for the evaluation of high cycle thermal fatigue. In *ASME 2010 Pressure Vessels and Piping Division/K-PVP Conference* (pp.325-334). American Society of Mechanical Engineers.

Rodi, W. (1993). On the Simulation of Turbulent Flow Past Bluff Bodies. *Journal of wind engineering and industrial aerodynamics*, Vol. 46, pp. 3-19

Roos, E., Herter, K. H., & Schuler, X. (2006). Lifetime management for mechanical systems, structures and components in nuclear power plants. *International journal of pressure vessels and piping*, 83(10), 756-766.

Rumsey, C. L., & Gatski, T. B. (2003). Summary of EASM turbulence models in CFL3D with validation test cases, *NASA/TM-212431* Langley Research Gate, Hampton, Virginia, U.S.A.

Saito, M., & Sawada, T. (2002). Advanced Nuclear Energy Systems Toward Zero Release of Radioactive Wastes, *Gulf Professional Publishing* (Vol. 40, No. 3-4).

Salim, S. M., Ong, K. C., Cheah, S. C., (2011). Comparison of RANS, URANS and LES in the Prediction of Airflow and Pollutant Dispersion. *In Proc*. of *the World Congress on Engineering and Computer Science 2011*, vol. II WCECS 2011, San Francisco, USA

Schuler, X., Herter, K. H., Laurien, E., Klören, D., Kulenovic, R., & Kuschewski, M. (2012). Thermal fatigue. Fluid-structure interaction at thermal mixing events, *In Proc. of 38th M.P.A Seminar*, Stuggart, Germany.

Shah, V. N (1999). Assessment of Field Experience Related to Pressurized Water Reactor Primary System Leaks. *In Proc. ASME Pressure Vessel and piping Conf*. Boson, MA, USA, pp. 1-5.

Sheikh, M. H. (2014). Fatigue behavior and structural stress analysis of coach-peel and lap-shear friction stir welded joints of AZ31 magnesium alloy / Doctoral dissertation, The University of Alabama Tuscaloosa, U.S.A.

Sodja, J. (2007). Turbulence models in CFD/Doctoral dissertation University of Ljubljana, Slovenia, pp. 1-18.

Stigler J. (2014). CFD Analysis of the Flow field Sensitivity in Suction Pipe on the Test Well Configuration. *European Physical Journal Conference* 10.1051/epjconf/ 20147508001.

Tawade, S., & Suryavanshi, A. (2015). A Review on Thermal Stress in Mixing Tee Junction Using FSI, 2420–2427. doi:10.15680/IJIRSET.2015.0404043

Tijsseling, A. S. (1996). Fluid-structure interaction in liquid-filled pipe systems: a review. *Journal of Fluids and Structures*, 10(2), 109-146.

Timperi, Antti (2014). Conjugate heat transfer LES of thermal mixing in a T-junction. *Nuclear Engineering and Design*, 483-496. doi: 101016/jnucengdes201402031.

Tipping, P. (1996). Lifetime and ageing management of nuclear power plants: a brief overview of some light water reactor component ageing degradation problems and ways of mitigation. *International journal of pressure vessels and piping*, 66(1), 17-25.

User Guide STAR-CCM+ (2013). Version 8.06

Velusamy, K., Natesan, K., Selvaraj, P., Chellapandi, P., Chetal, S. C., Sundararajan, T., & Suyambazhahan, S. (2006). CFD Studies in the Prediction of Thermal Striping in an LMFBR. In Proc. *CFD4NRS Conference*, Garching, Munich, Germany.

Westin J., Alavyoon F, Andersson L., Veber P., Henriksson M., Andersson C. (2006). Experiments and Unsteady CFD-Calculations of Thermal Mixing in a T-Junction", OECD/NEA/IAEA In Proc. *Workshop on the Benchmarking of CFD Codes for Application to Nuclear Reactor Safety (CFD4NRS)*, Munich, Germany, pp. 1-15.

Westin J. (2007). "Thermal Mixing in a T-Junction. Model Tests at Vattenfall research and Development AB. *Boundary Conditions and List of Available Data for CFD Validation", Report Memo* U 07-26, Vattenfall R&D AB, Älvkarleby, Sweden, pp. 1-17.

Wilcox, David C. (1998). Turbulence Modeling for CFD. Second edition. *Anaheim: DCW Industries*, pp.174.

Wilcox, David C. (1998). Re-assessment of the scale-determining equation for advanced turbulence models. *AIAA Journal*, vol. 26, no. 11, pp. 1299-1310.

Zboray R., Manera A., Niceno B., Prasser H.-M. (2007). Investigations on Mixing Phenomena in Single-phase Flows in a T-Junction Geometry. *The 12th Int. Topical Meeting on Nuclear Reactor Thermal Hydraulics (NURETH-12),* Sheraton Station Square, Pittsburgh, Pennsylvania, U.S.A., Paper No. 71, pp. 1-20.

Huiren, Z. and Songling, L. (1991). Numerical Simulation of Traditional Flow and Heat Transfer in a Smooth Pipe. *Int. J. Heat Mass Transfer*, Vol.34, pp. 2475-2482.

APPENDIX I

Temperature Distribution at 1.6 Dcold

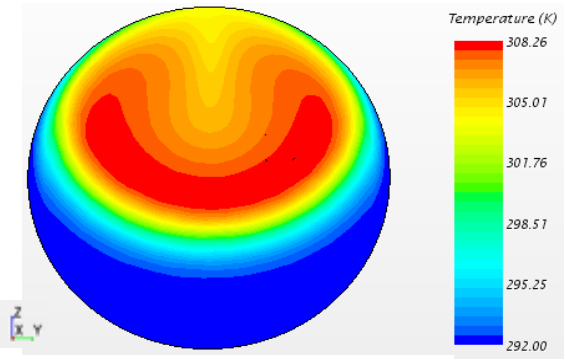

Fig. (a): 0 degree inclination

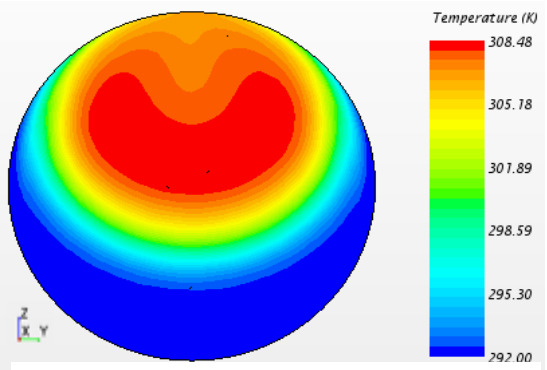

Fig. (b): 15 degree inclination

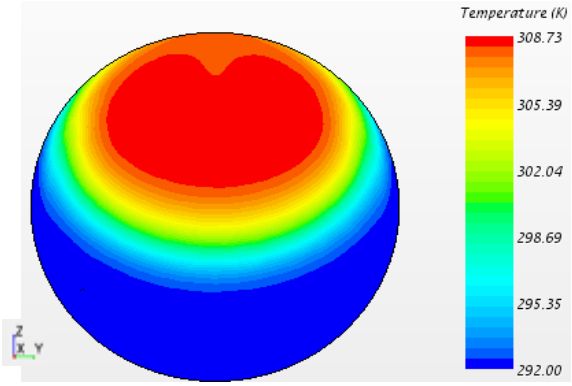

Fig. (c): 30 degree inclination

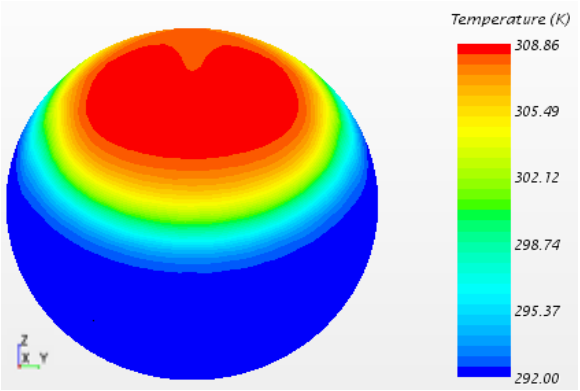

Fig. (d): 45 degree inclination

Dimensionless Temperature Distribution at 1.6 Dcold

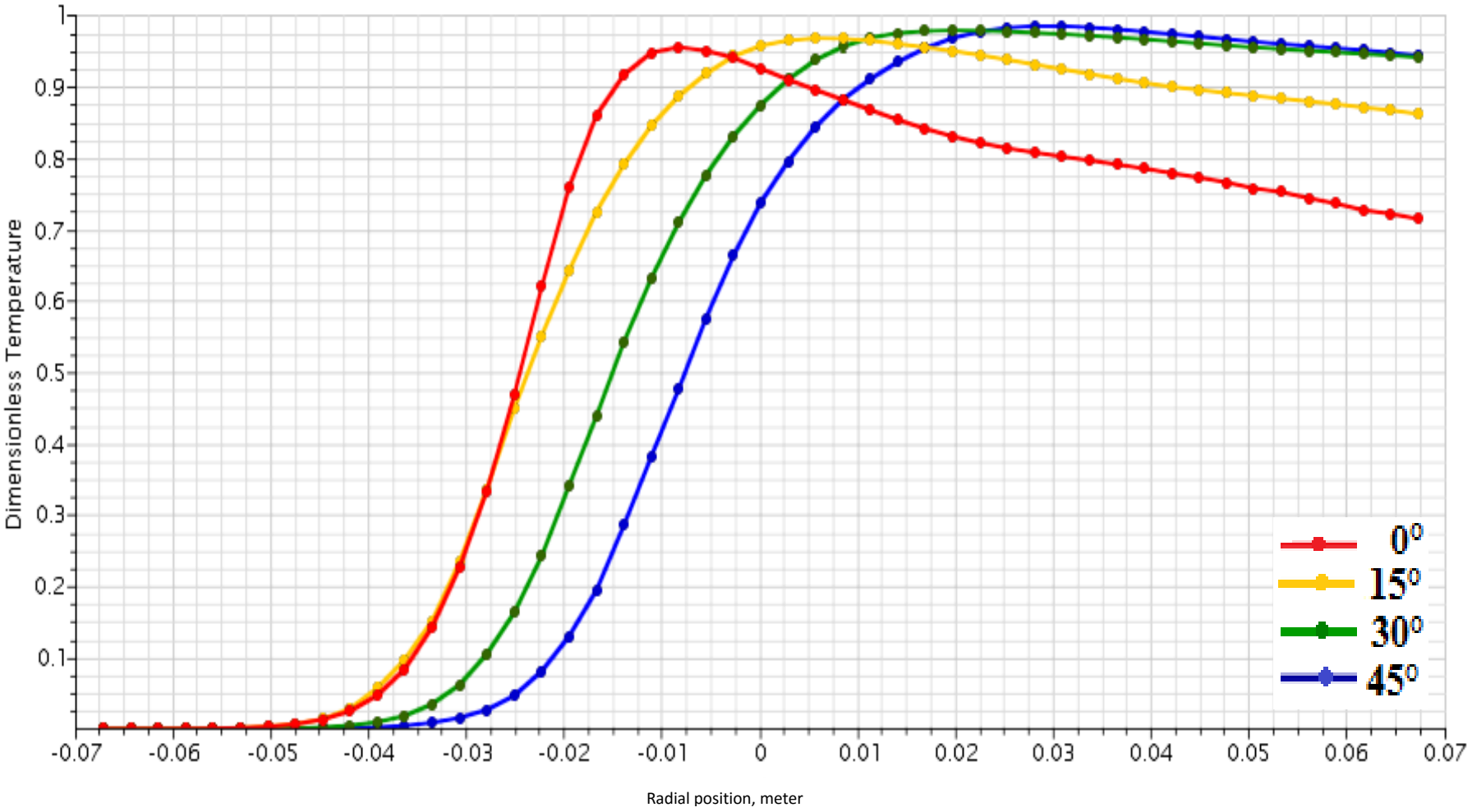

Temperature Distribution at 2.6 Dcold

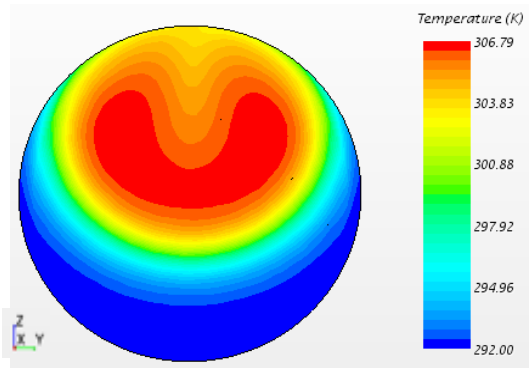

Fig.(a): 0 degree inclination

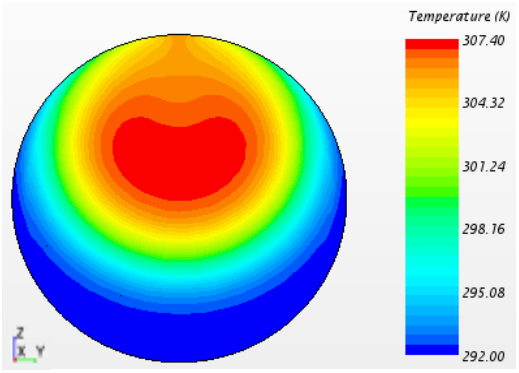

Fig.(b): 15 degree inclination

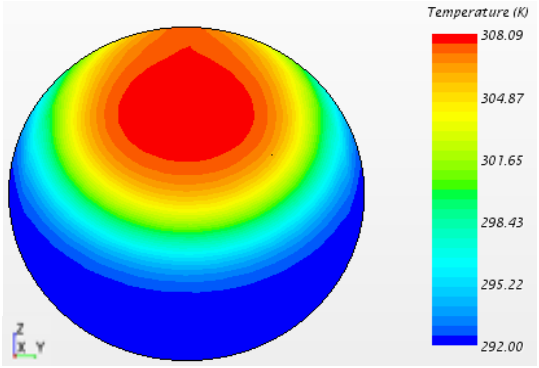

Fig.(c): 30 degree inclination

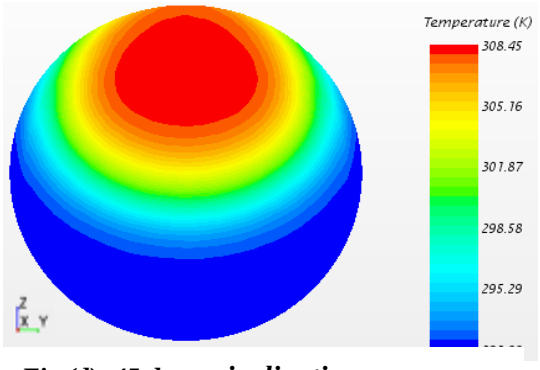

Fig.(d): 45 degree inclination

Dimensionless Temperature Distribution at 2.6 Dcold

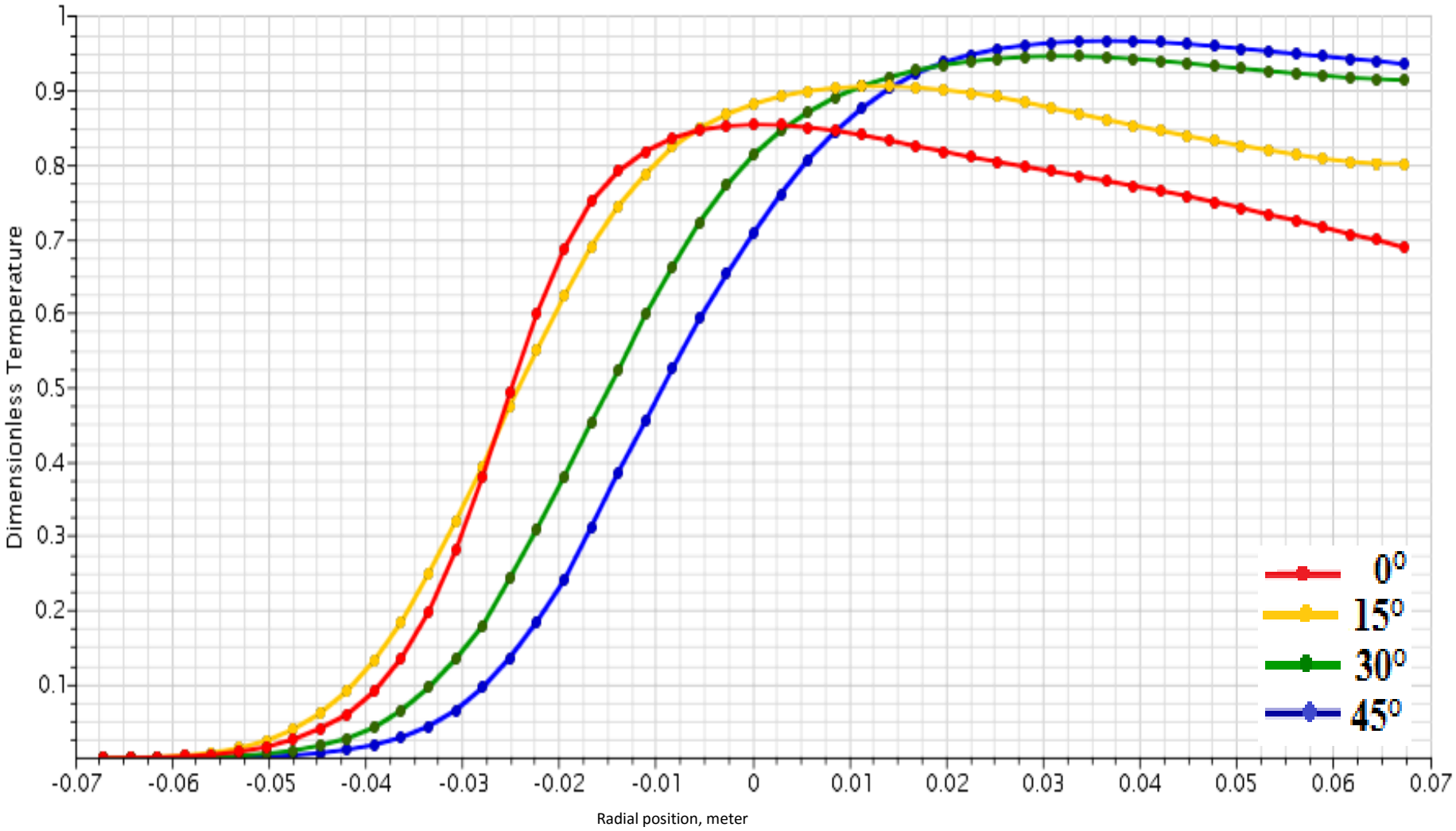

Temperature Distribution at 3.5 Dcold

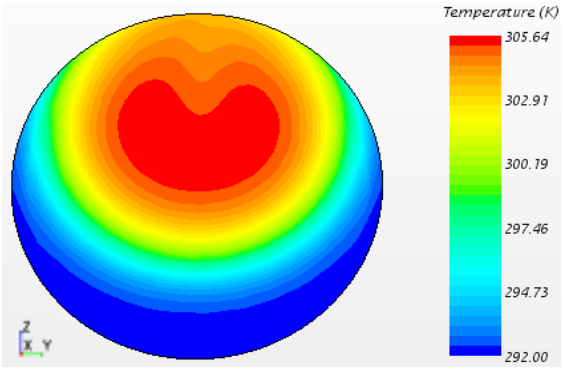

Fig.(a): 0 degree inclination

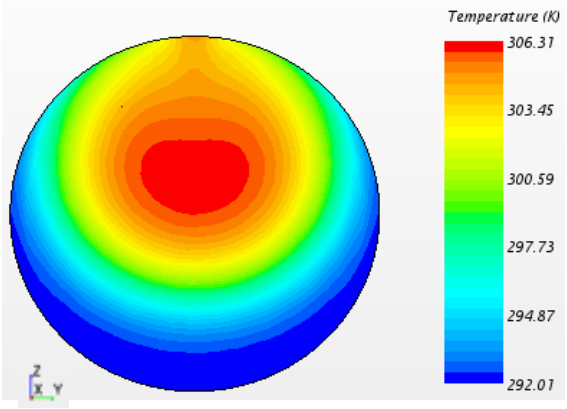

Fig.(b): 15 degree inclination

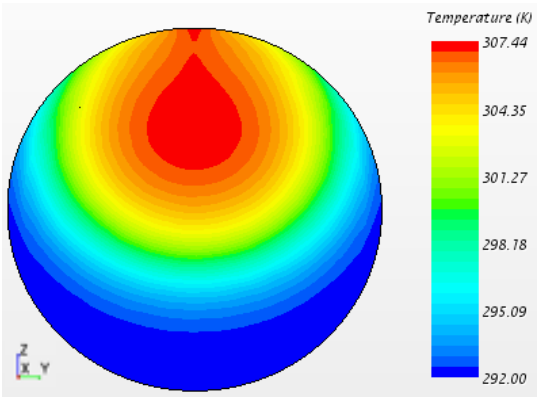

Fig.(c): 30 degree inclination

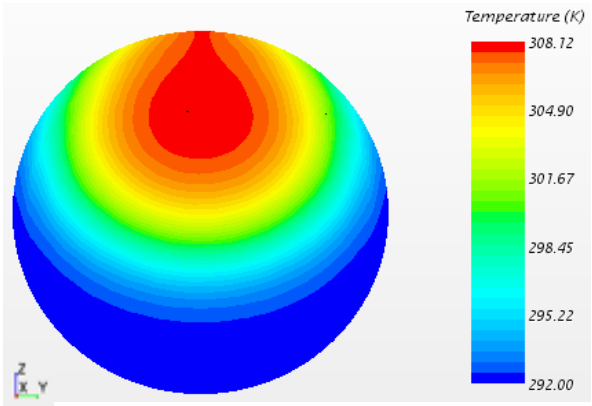

Fig.(d): 45 degree inclination

Dimensionless Temperature Distribution at 3.5 Dcold

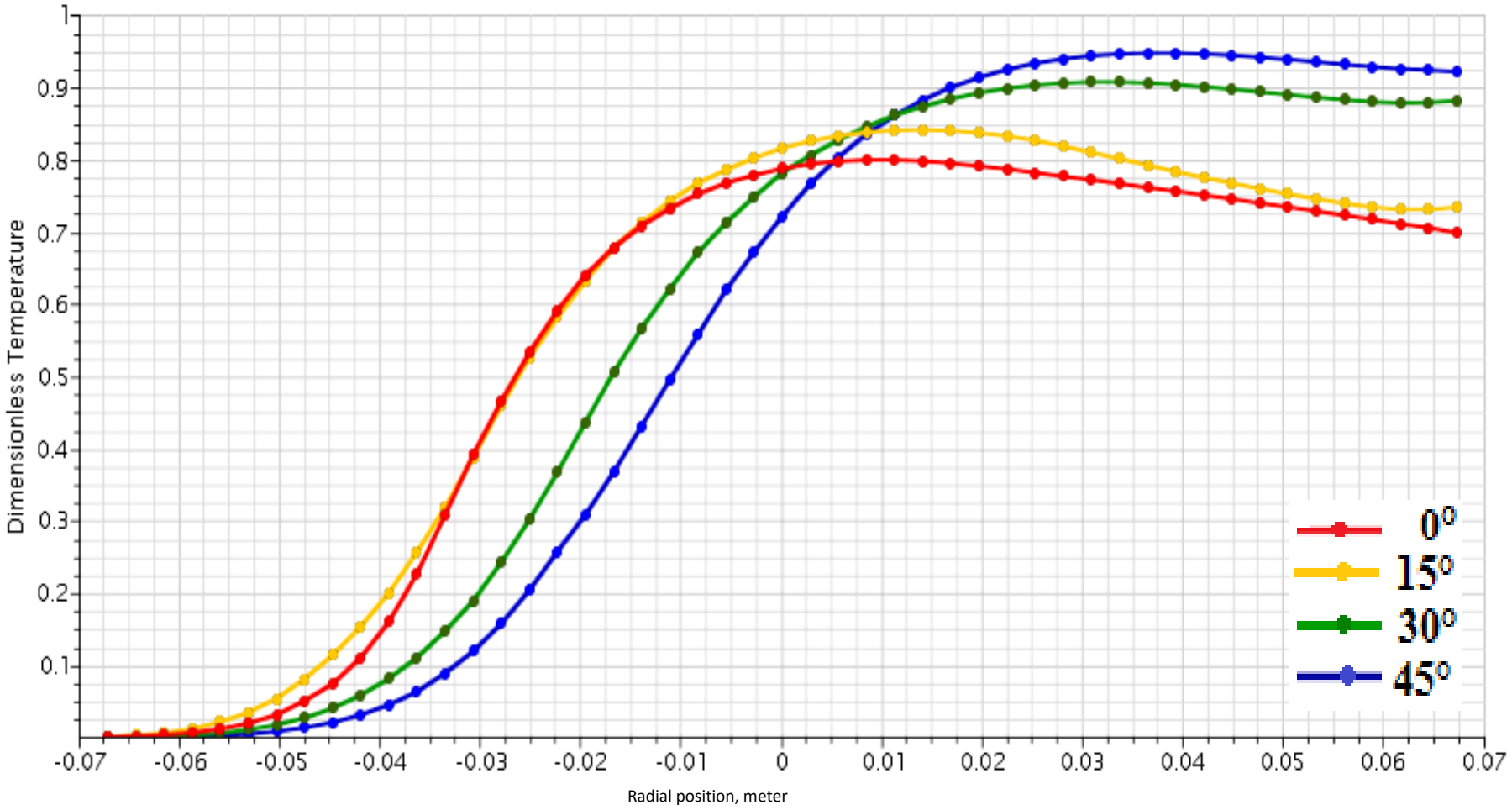

APPENDIX II

Scalar Scene of Turbulence Intensity Distribution at 1.6 Dcold

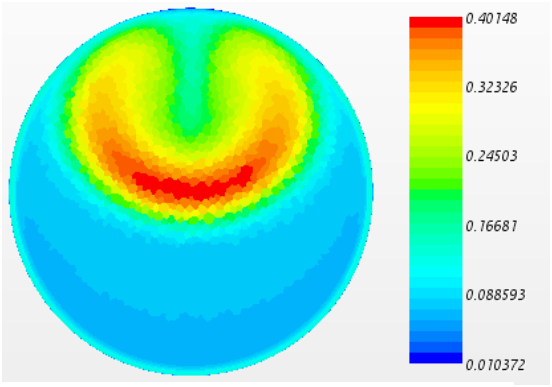

Fig.(a): 0 degree inclination

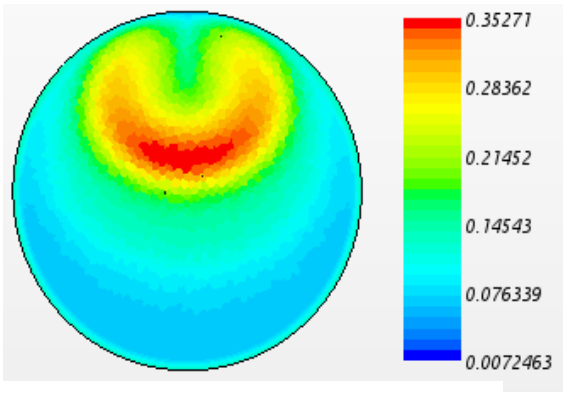

Fig.(b): 15 degree inclination

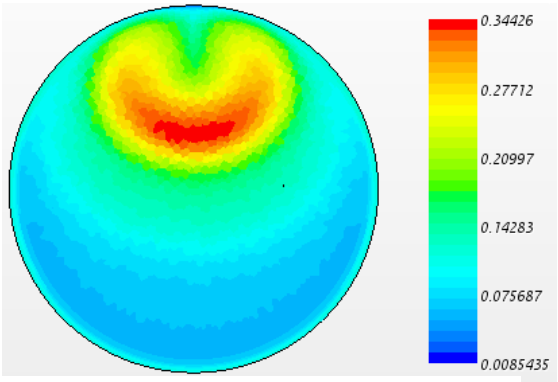

Fig.(c): 30 degree inclination

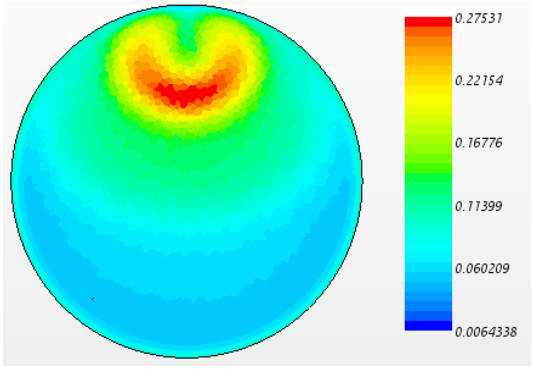

Fig.(d): 45 degree inclination

Turbulence Intensity Distribution at 1.6 Dcold

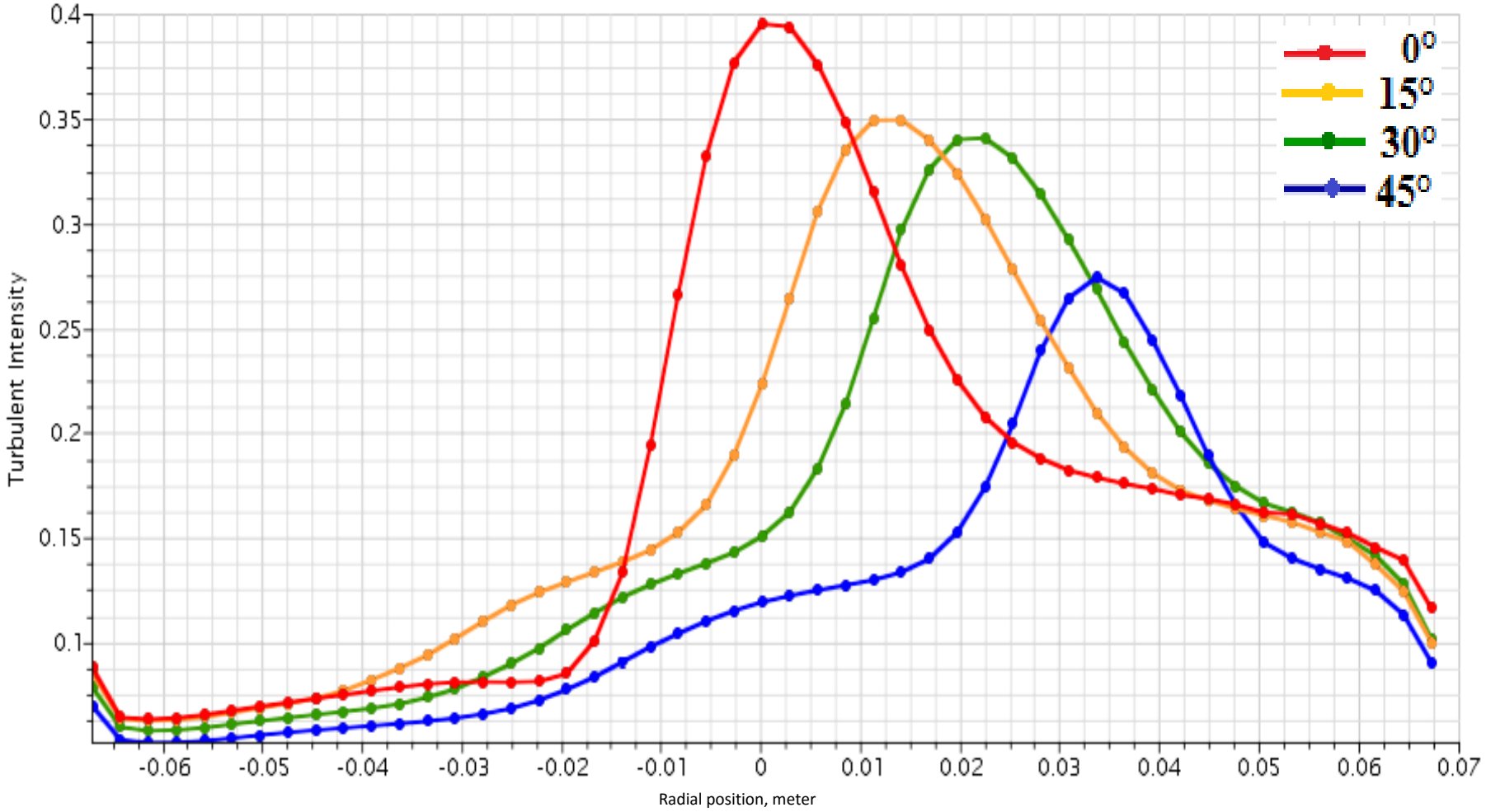

Scalar Scene of Turbulence Intensity Distribution at 2.6 Dcold

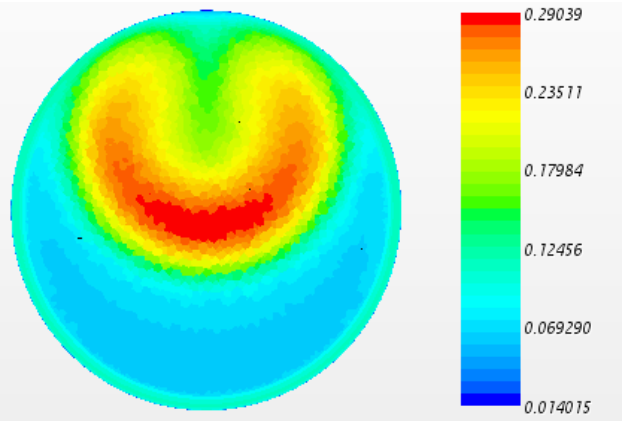

Fig.(a): 0 degree inclination

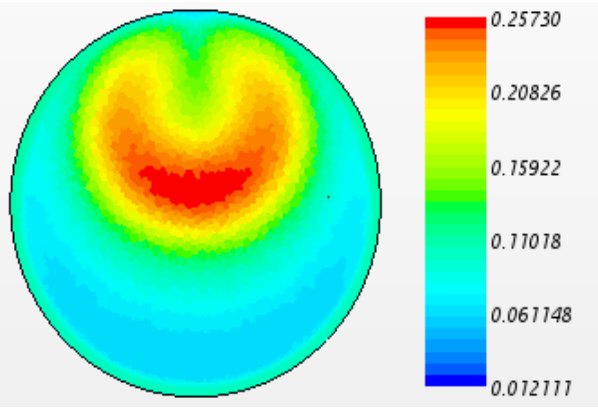

Fig.(b): 15 degree inclination

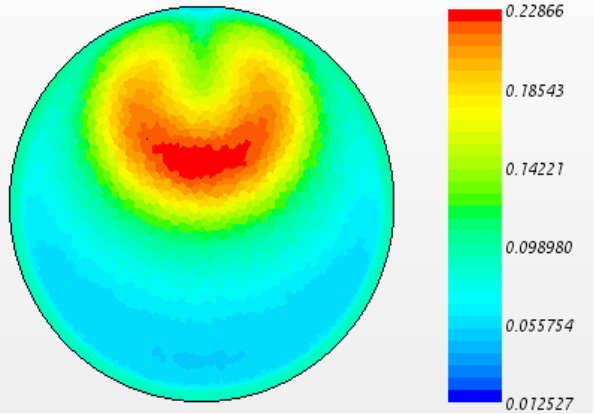

Fig.(c): 30 degree inclination

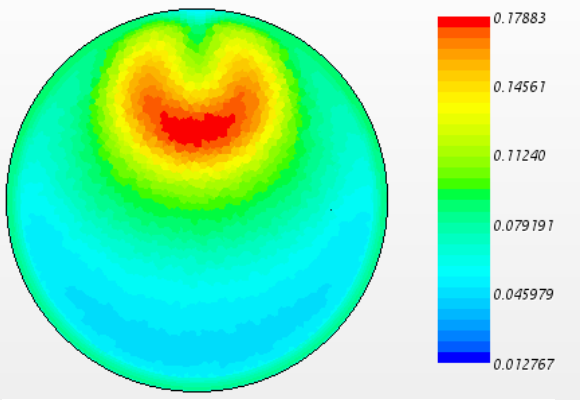

Fig.(d): 45 degree inclination

Turbulence Intensity Distribution at 2.6 Dcold

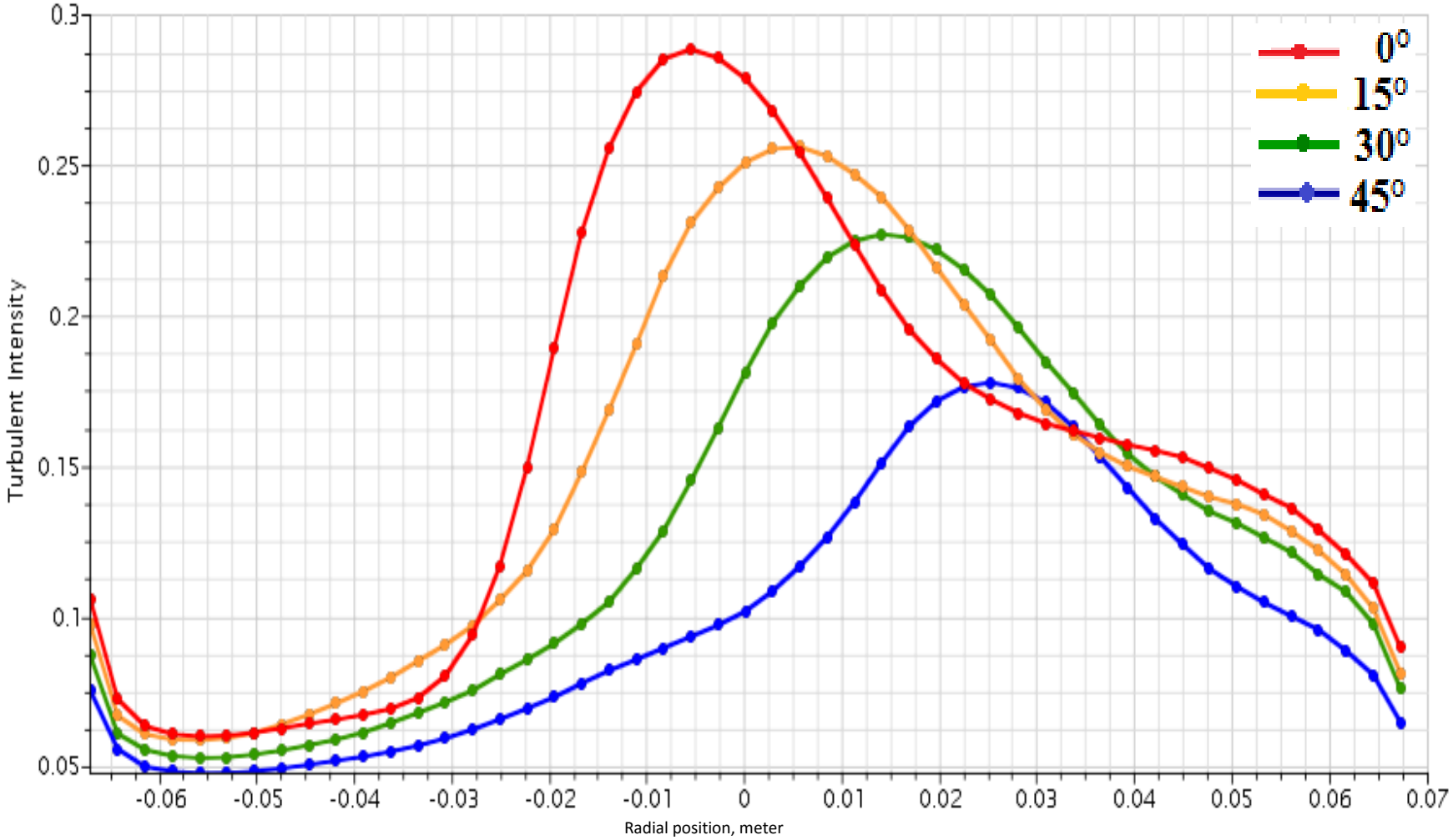

Scalar Scene of Turbulence Intensity Distribution at 3.5 Dcold

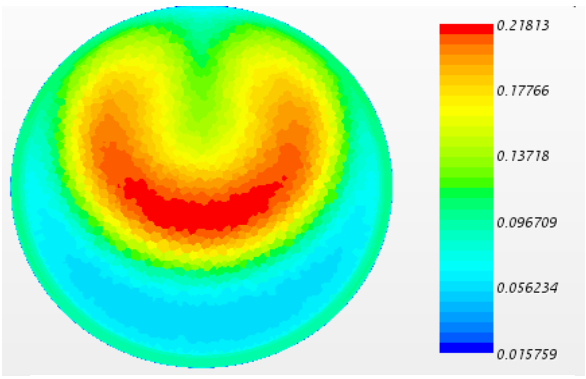

Fig.(a): 0 degree inclination

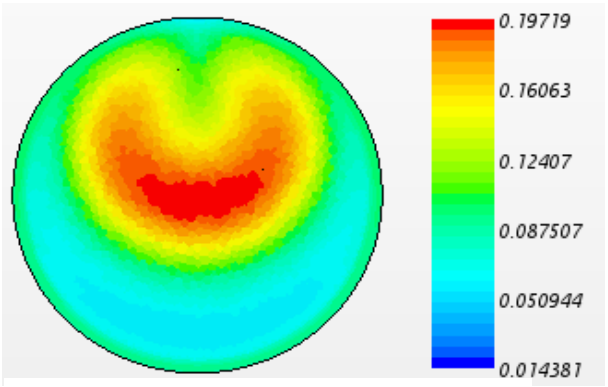

Fig.(b): 15 degree inclination

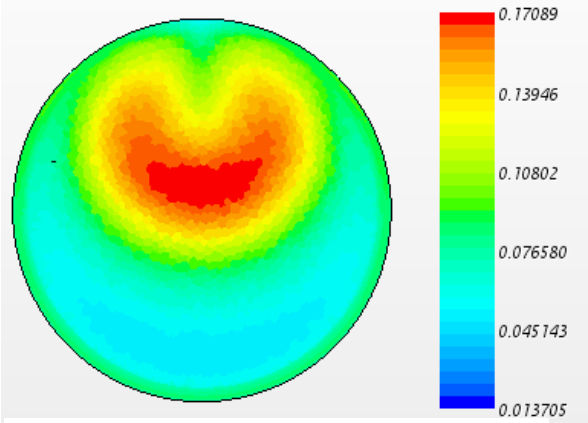

Fig.(c): 30 degree inclination

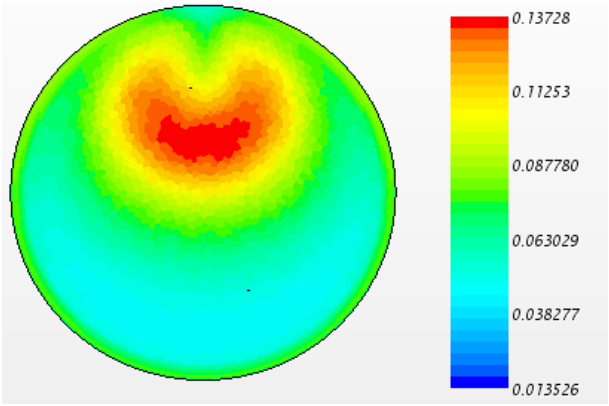

Fig.(d): 45 degree inclination

Turbulence Intensity Distribution at 3.5 Dcold

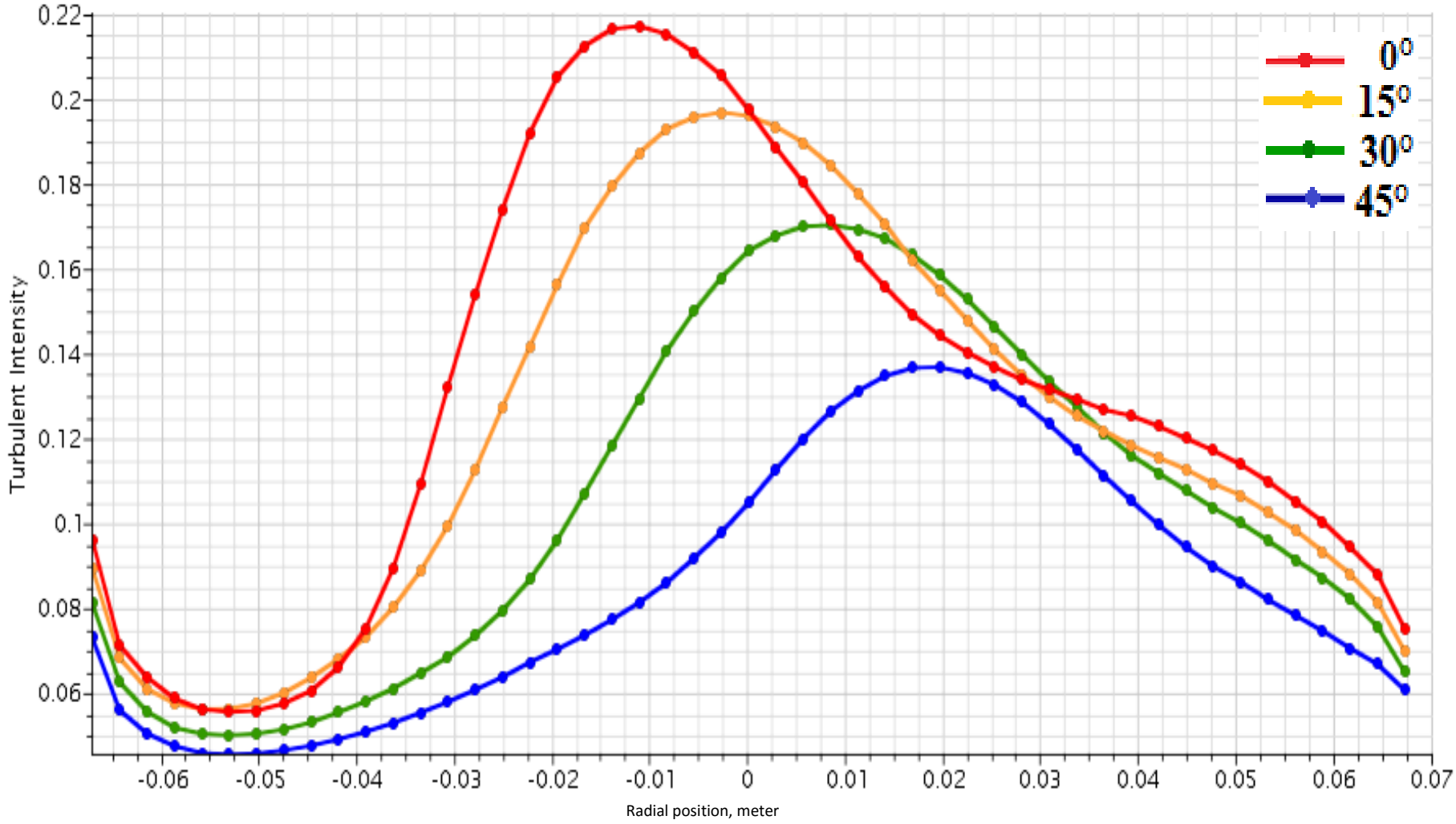

APPENDIX III

Scalar Scene of Velocity Distribution at 1.6 Dcold

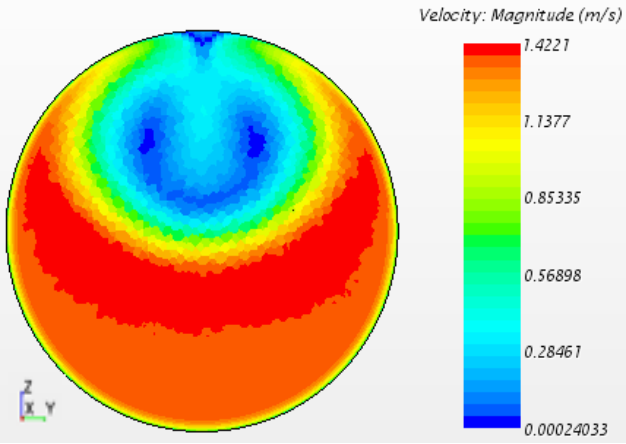

Fig.(a): 0 degree inclination

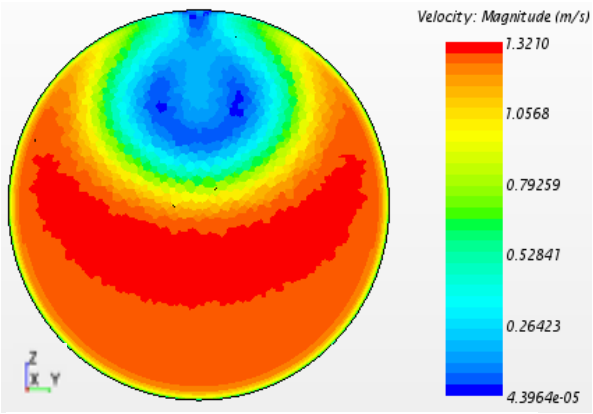

Fig.(b): 15 degree inclination

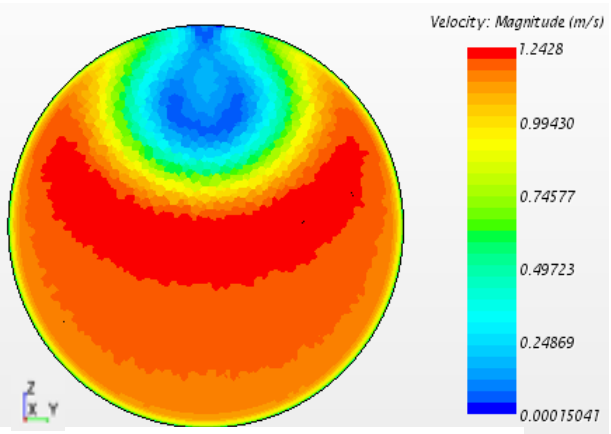

Fig.(c): 30 degree inclination

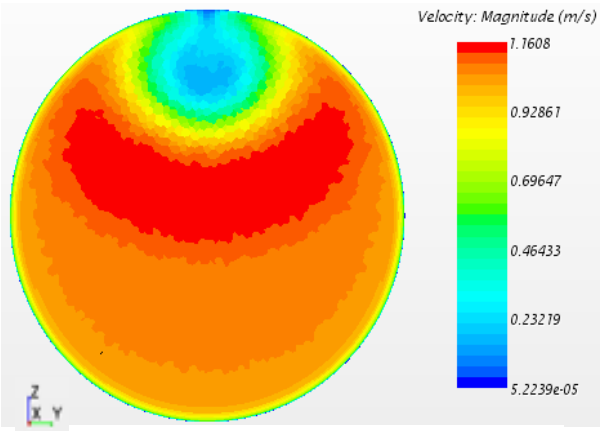

Fig.(c): 45 degree inclination

Velocity Distribution at 1.6 Dcold

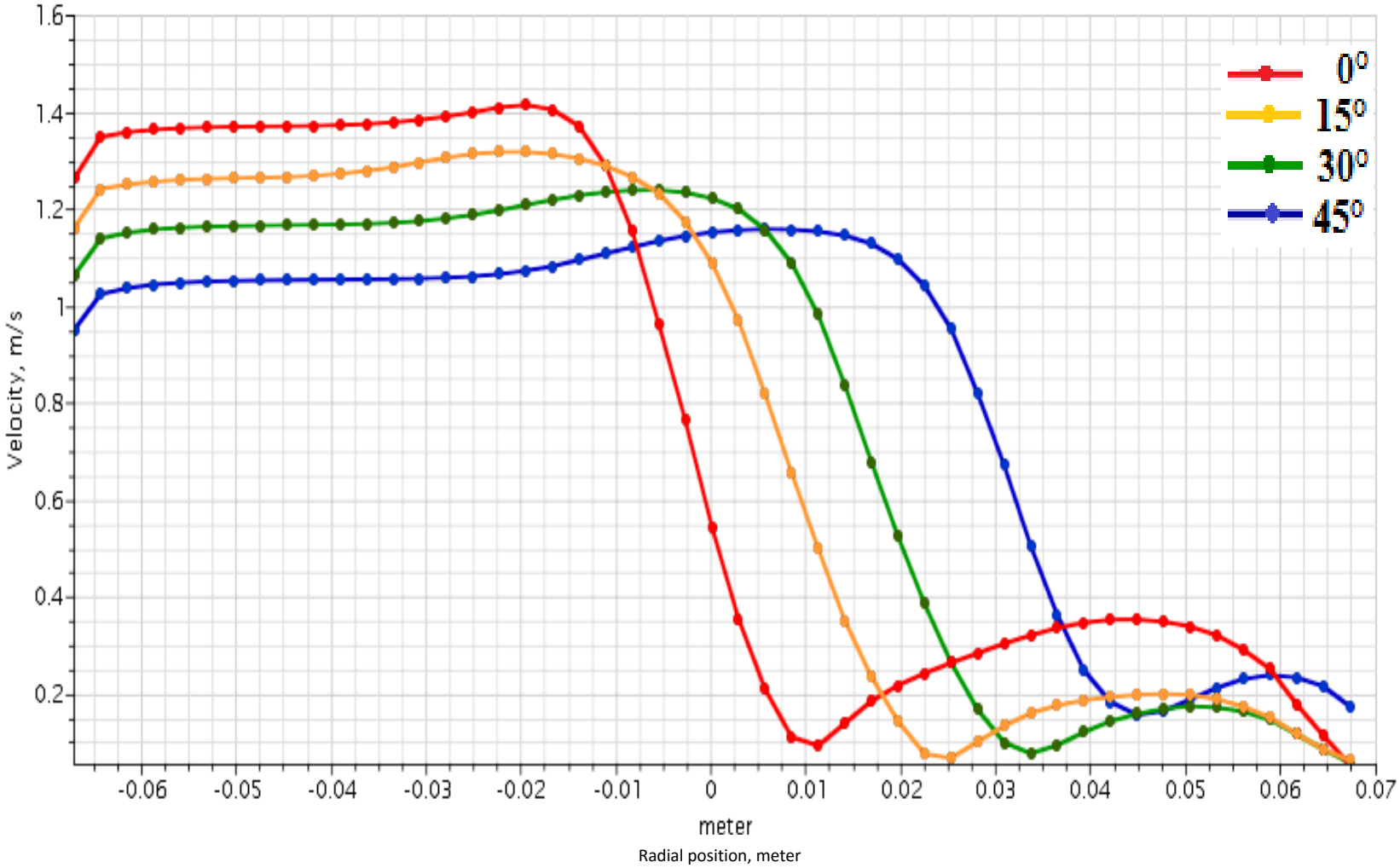

Scalar Scene of Velocity Distribution at 2.6 Dcold

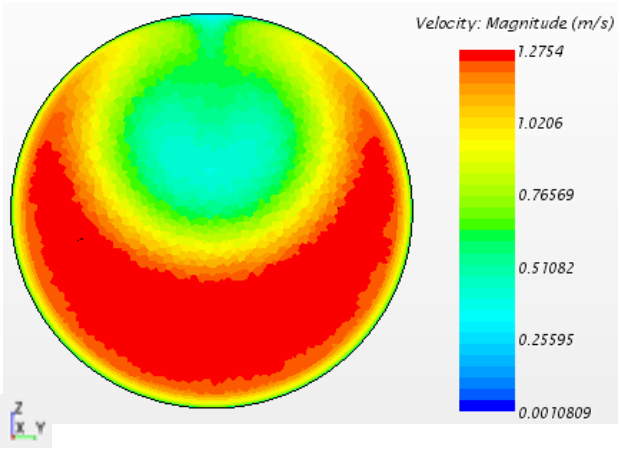

Fig.(a): 0 degree inclination

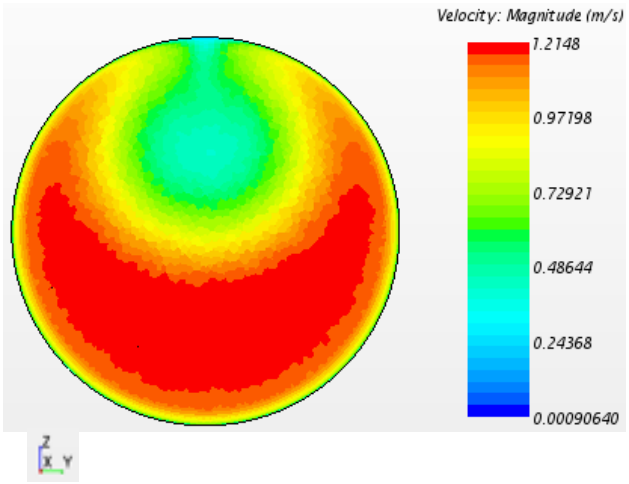

Fig.(b): 15 degree inclination

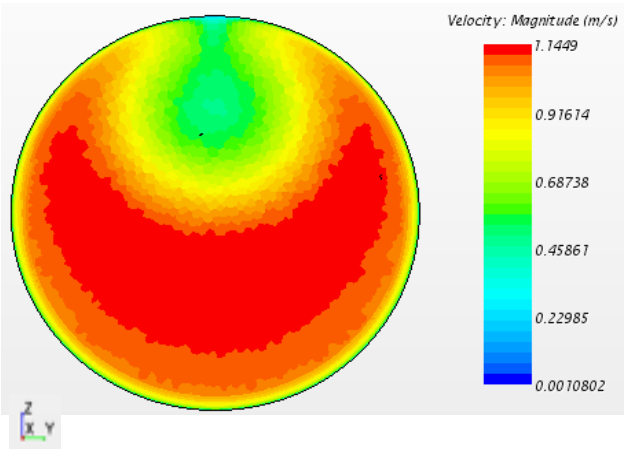

Fig.(c): 30 degree inclination

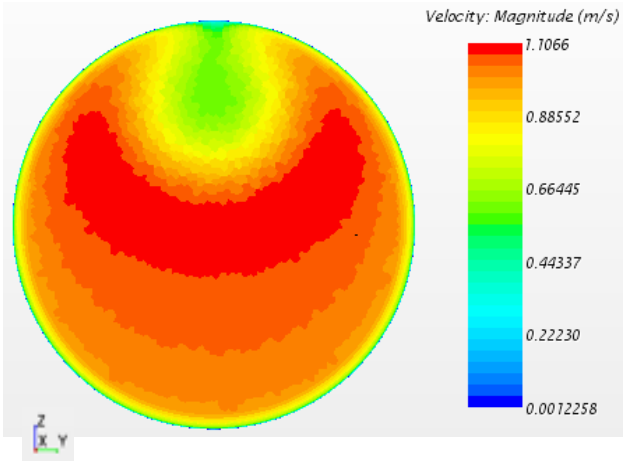

Fig.(d): 45 degree inclination

Velocity Distribution at 2.6 Dcold

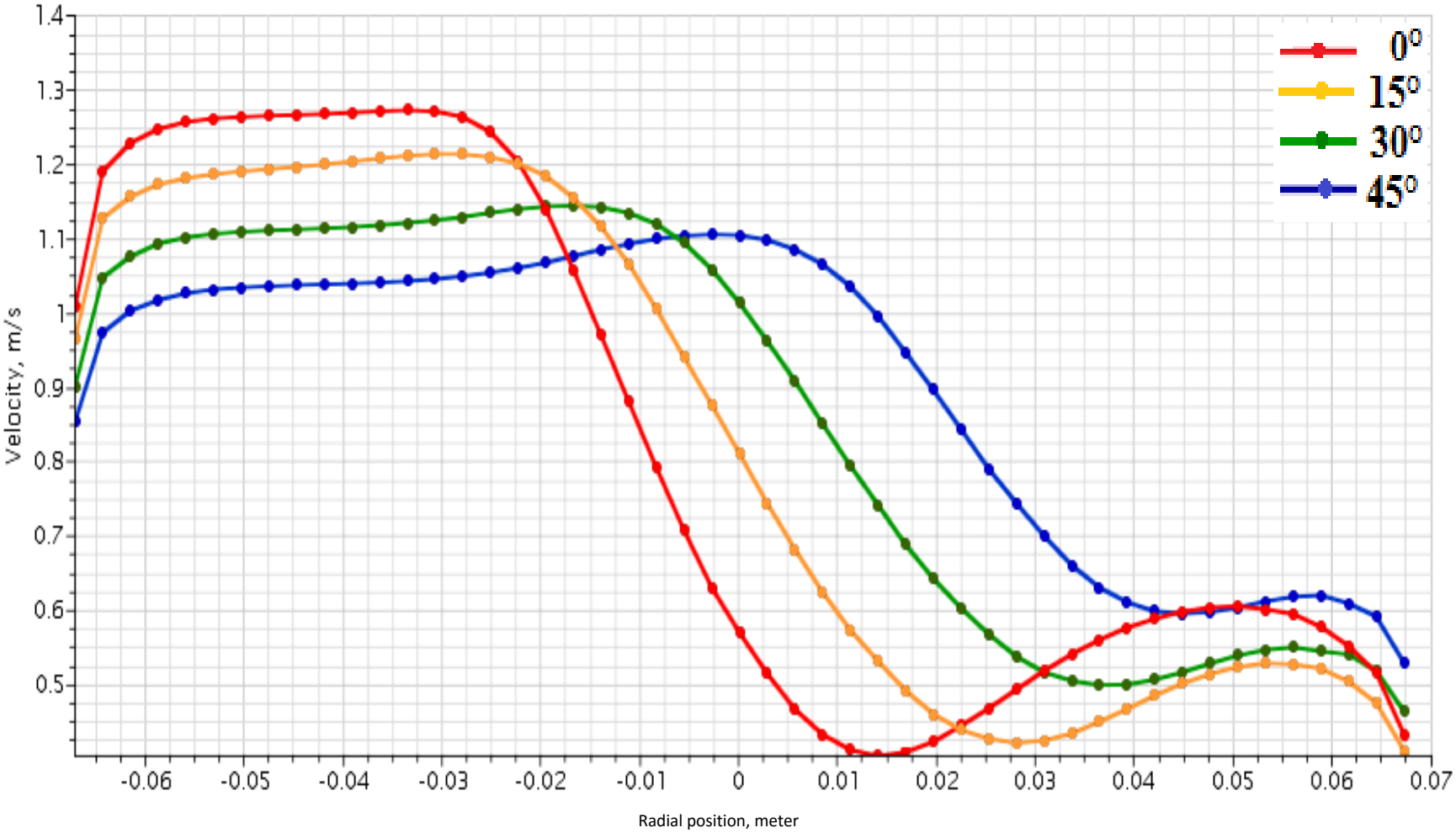

Scalar Scene of Velocity Distribution at 3.5 Dcold

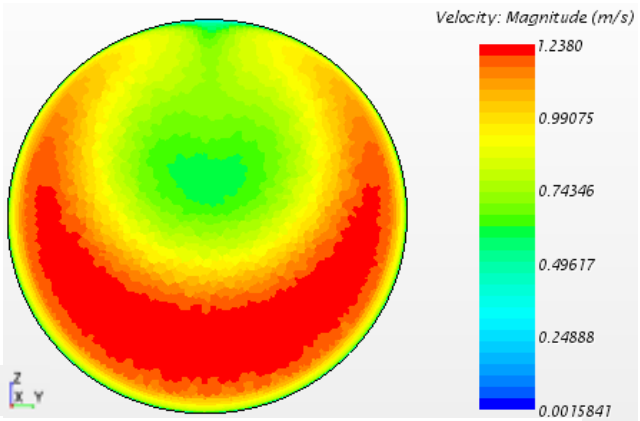

Fig.(a): 0 degree inclination

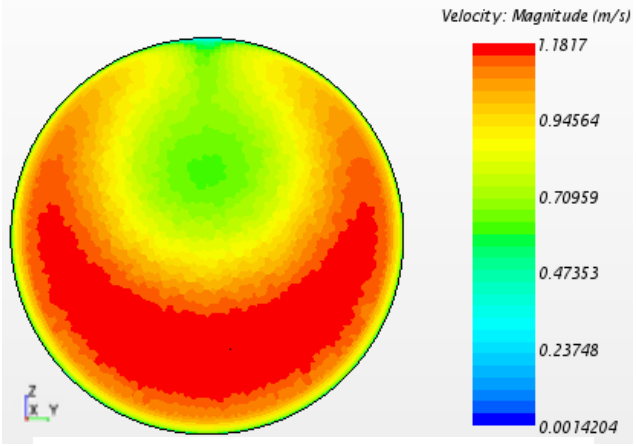

Fig.(b): 15 degree inclination

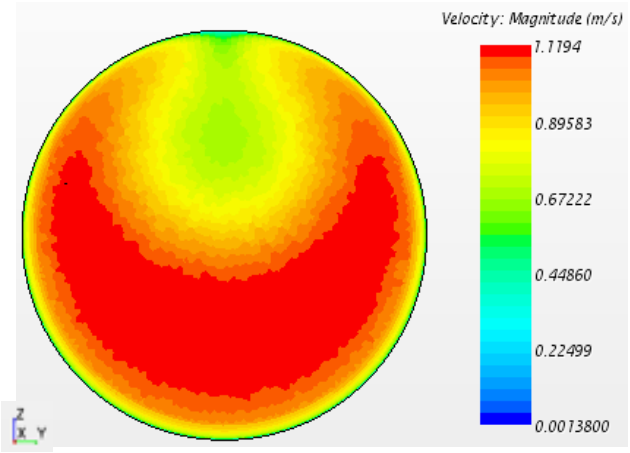

Fig.(c): 30 degree inclination

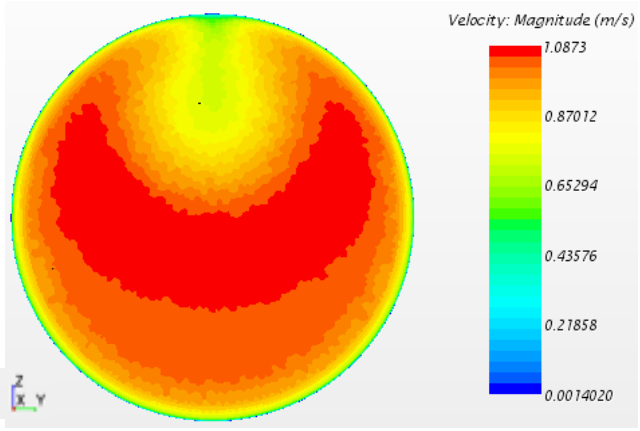

Fig.(d): 45 degree inclination

Velocity Distribution at 3.5 Dcold